I&EC research
Industrial & Engineering Chemistry Research

pubs.acs.org/IECR

Review

Review of the Decomposition of Ammonia to Generate Hydrogen

Ilaria Lucentini, Xènia Garcia, Xavier Vendrell, and Jordi Llorca*

Cite This: *Ind. Eng. Chem. Res.* 2021, 60, 18560−18611

Read Online

ACCESS | Metrics & More | Article Recommendations

ABSTRACT: Because of the problems associated with the generation and storage of hydrogen in portable applications, the use of ammonia has been proposed for on-site production of hydrogen through ammonia decomposition. First, an analysis of the existing systems for ammonia decomposition and the challenges for this technology are presented. Then, the state of the art of the catalysts used to date for ammonia decomposition is described considering the catalysts composed of noble and non-noble metals and their combinations, as well as novel materials such as alkali metal amides and imides. The effect of the supports and promoters used is analyzed in detail, and the catalytic activity obtained is compared. An analysis of the kinetics of the reaction obtained with different catalysts is also presented and discussed, including the reaction mechanism, the determining step of the reaction, and the apparent activation energy. Finally, the structured reactors used to date for the decomposition reaction of ammonia are explored, as well as the possibilities offered by catalytic membrane reactors, which allow the on-site simultaneous production and separation of hydrogen.

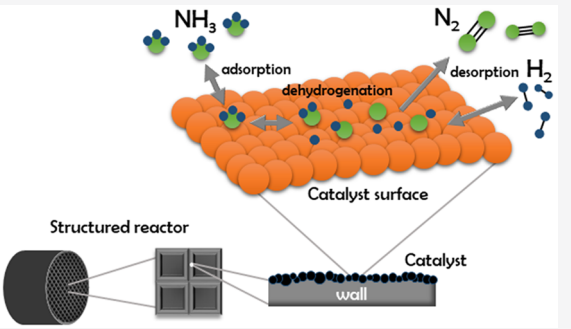

1. INTRODUCTION

The fundamental problem of the current energy system is the great negative environmental impact of energy production using fossil fuels.[1] Alternative technologies to fossil fuels have been added over time and existing technologies have been improved; however, a radical change in the energy system, the so-called "energy transition", has yet to take place. In the framework of the energy transition toward a new clean and efficient system, the dramatic decrease in costs in solar and wind technologies, and now in energy storage technologies, is a strong impulse toward the radical change that is proposed.[2] It should be pointed out that the energy transition is not only technological, but also a combination of economic, political, institutional, and socio-cultural changes, and it must be based on ethics and sustainability.[3]

1.1. Hydrogen as an Energy Vector.

The "hydrogen economy" is a concept introduced a long time ago. This term was used by John Bockris in 1972, and proposes to base the energy transition on the use of hydrogen as a vector for the generation of clean and environmentally sustainable energy.[4] In recent decades, the production of hydrogen from various sources, its transport and storage, and finally its use to provide energy with low emissions have been extensively investigated.[5] Hydrogen is taking one of the leading positions in the energy sector for stationary and transport applications, including vehicles and other means of transport, auxiliary power units, stationary power generation in domestic and industrial applications, and as an energy vector to store the excess of electrical energy generated off-peak.[6]

Nowadays almost all the hydrogen produced comes from catalytic steam reforming of fossil fuels, mainly from natural gas,[7,8] which is currently a well-established commercial technology and is the least expensive way to produce hydrogen on a large scale. Although the electrolysis of water is a well-known and established technology to produce clean and high purity hydrogen,[9] it comprises high energy losses.[10] Nevertheless, a large reduction in the cost of electricity from renewable sources and electrolyzers is needed to allow the hydrogen produced by electrolysis to compete with conventional sources of energy on a large scale.[11] Currently, most of the hydrogen is produced and used on-site in industry, principally for ammonia production and petroleum refining, which together account for two-thirds of the total hydrogen use.[12] Hydrogen represents an effective and clean alternative to the use of fossils fuels, which have a high carbon footprint, to produce energy by using fuel cells, since water is the only product generated in the process, apart from heat. Moreover, fuel cells have the ability to continuously produce electricity while fueling them, which is a significant advantage compared to batteries. Currently, there are several commercialized fuel cell-based technologies that differ mainly in the electrolyte, fuel and/or working temperature. The

Special Issue: José Luis García Fierro Festschrift

Received: March 2, 2021
Revised: May 10, 2021
Accepted: May 11, 2021
Published: May 21, 2021

most common fuel cells are solid oxide fuel cells (SOFC), proton exchange membrane (PEMFC), direct methanol (DMFC), alkaline (AFC), phosphoric acid (PAFC), and molten carbonate (MCFC) fuel cells. PEMFCs are the most widely used for mobility and small applications.[13]

Another of the current challenges in hydrogen technologies is its storage and transport. Hydrogen has a very high energy density by mass (119.7 MJ kg^{-1} of lower heating value at 25 °C and 1 bar[14]), but it has a very low energy density by volume (8.96 GJ m^{-3}, referred to as liquid fuel[15]). Furthermore, hydrogen tends to diffuse through the materials, leading to embrittlement or weakening of the storage material.[16] Nowadays, hydrogen is commonly stored as compressed gas at pressures up to 700 bar at 25 °C.[17] It can be also stored as a liquid with a higher volumetric energy density at much lower temperatures (−253 °C at 1 bar).[18] The cryo-compression, where hydrogen is cooled down until the pressure required for its compression drops to 350 bar,[19] offers an alternative to store hydrogen, although the energy needed is very high.[20] Alternatively, hydrogen can be adsorbed on materials with a large surface area and pores of adequate size (such as carbonaceous materials or carbon nanotubes),[21,22] metal hydrides,[23] and structures based on metal−organic frameworks (MOFs).[24,25] However, the adsorption/absorption of hydrogen leads to an increase in its transportation weight and volume[26] and there are difficulties in the regeneration processes of the materials.[23] A different approach is the chemical storage in the form of another hydrogen-containing compound that can be easily transported, and hydrogen is generated on-site through a chemical reaction.[27] In this sense, the chemical storage can be in the form of simple hydrides like LiH, NaH, KH, or CaH_2, and also as binary hydrides such as $LiBH_4$, $NaBH_4$, KBH_4, $LiAlH_4$, or $NaAlH_4$.[28] However, these compounds must be synthesized from the respective metals and hydrogen, which involves a high loss of energy.[29,30] For example, in the case of calcium hydride, losses are at least 60%, and for other compounds the losses can be even higher.[28] For this reason, up to date, the chemical storage of hydrogen in these types of compounds has a limited practical application. Nevertheless, other interesting compounds for chemical storage are synthetic fuels that are easy to synthesize and can be stored in a liquid form at ambient or near-ambient conditions; one of the most promising compounds is ammonia.[31]

1.2. Ammonia as a Source of Hydrogen. Ammonia has a high hydrogen content (17.8% by weight and a volumetric density of 121 kg H_2 m^{-3} at 10 bar)[32] and can liquefy at low pressure, 8.6 bar at 20 °C,[33] so its transport and storage are relatively easy and require a low amount of energy.[34,35] The decomposition reaction of ammonia is endothermic ($2NH_{3(g)} \leftrightarrows N_{2(g)} + 3H_{2(g)}$; $\Delta H° = 92$ kJ mol^{-1}) and reaches 99.99% ammonia conversion at 400 °C and 1 atm according to thermodynamics, considering an inlet flow composed only of ammonia. This means that a moderately high operating temperature is required to drive the ammonia decomposition reaction to completion and thus produce very high purity hydrogen. This purity is compulsory if the hydrogen produced is used in fuel cells such as PEMFCs, which are irreparably degraded at very low concentrations of ammonia (ca. 0.1 ppm).[32] Alternatively, hydrogen-selective membrane systems can be used, such as catalytic membrane reactors.[36]

Ammonia is the second most widely produced chemical, after sulfuric acid,[37] and is mainly used in fertilizer manufacturing, which is the largest source of demand (88% of the total ammonia produced).[38] More than 90% of the total production of ammonia is carried out by the inverse reaction of decomposition, which is the so-called Haber-Bosch process, originally developed by Fritz Haber and Carl Bosch. Iron catalysts with promoters, temperatures around 400−600 °C, and pressures between 100 and 400 bar are typically used. Starting in 1990, ruthenium was introduced as a catalyst, which has allowed the reaction pressure to be lowered, but due to its high cost, it is only used in a few plants.[39] In the synthesis of ammonia, the production of the mixture of H_2 and N_2 has the greatest contribution to the total cost of the process; moreover, energy from fossil fuels is used almost exclusively for the production of H_2 (steam reforming of natural gas) and the separation of N_2 from air.[38] Ammonia production consumes about 2% of the world's energy supply and its production releases more than 400 Mt of CO_2, which represents 1.6% of the total global emissions.[40] Therefore, several attempts have been made to decarbonize the NH_3 production process through the concepts of "blue ammonia" production using carbon capture systems, and "green ammonia" using hydrogen produced from electrolysis of water.[41]

Currently, the ammonia decomposition reaction is applied industrially mainly for annealing metals and galvanizing. The ammonia crackers use external energy sources, nickel supported on aluminum oxide as catalyst, and operate at a temperature of about 850−950 °C.[42] To apply ammonia decomposition in power generation (ammonia-to-power) and to minimize the presence of ammonia in the outlet gas, several solutions have been proposed:

- First, the ammonia can be separated from the stream by cooling. The fraction of condensed ammonia depends on the pressure of the gas stream, and at low pressures, such as atmospheric pressure, the required temperature is below zero.[43] To avoid lowering the gas temperature, ammonia capture materials, such as $CaCl_2$, $MgCl_2$, $MgBr_2$, or $CaBr_2$ have been used on porous supports, silica or zeolite, which can remove ammonia at high temperatures (typically 100−250 °C and 5−30 bar). These materials can emit less than 0.1 ppm of ammonia from an input concentration greater than 10 000 ppm. The main disadvantage of using these materials is that the ammonia cannot be directly recirculated in the process, but has to be desorbed from the material at temperatures around 300−400 °C. Furthermore, these materials do not adsorb nitrogen, and if the output gas is used to supply H_2 to a PEM-type fuel cell in mobile applications, such as in a vehicle, the requirement of maximum 100 ppmv N_2 has to be met, necessary so that the inlet stream to the PEMFC has a purity of H_2 greater than 99.97% (ISO 14687-2:2012).[44] Currently these technologies are on a laboratory scale or are used in pilot plants.[43]
- Second, alternative fuel cells that are not affected by high levels of ammonia in the hydrogen stream could be used. In this sense AFCs can tolerate ammonia concentrations of up to 9%.[45] However, the main limitation to the direct use of ammonia is that at the low operation temperatures of AFCs, ammonia does not decompose easily, and therefore an external reformer is necessary. Recently, high temperature PEMFCs have shown a greater capacity to resist poisoning by other compounds such as CO, and they have also the potential to resist higher concentrations of ammonia.[46] In SOFCs, ammonia can be used directly

https://doi.org/10.1021/acs.iecr.1c00843
Ind. Eng. Chem. Res. 2021, 60, 18560−18611

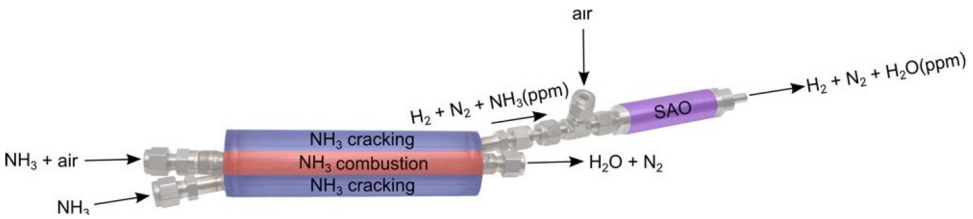

Figure 1. Scheme of the system used by Rencat.[65] Reprinted with permission from RenCat (https://rencat.net/).

as fuel at high temperatures, at which the decomposition occurs directly at the anode.[36] Ammonia-fed SOFCs have been tested at pilot scale at Kyoto University, Japan, in 1 kW applications.[47]

- Third, ammonia can be used directly as a fuel in gas turbines or engines, exploiting its high octane number (110−130).[48] The main obstacle of these technologies is the emission of NO_x associated with the combustion of ammonia. Ammonia in a gas turbine has initially been used in the form of mixtures with air[47] or with water steam,[49] as well as coupled with other fossil fuels, which leads to a reduction in carbon emissions without losing energy efficiency. Gas turbines fired directly with ammonia have been tested in pilot plants in Japan (IHI Corporation).[50] However, the application of ammonia as an engine fuel in a vehicle is still in the prototype stage. In this sense, two options have been examined: the direct combustion of ammonia alone or in mixtures, or the decomposition and use of the H_2 produced on-board as fuel. In 1905, the first ammonia combustion engine was developed by Ammonia Casale Ltd.., which was patented in Italy in 1935−36.[51] Later on, in 1933, Norsk Hydro built a prototype vehicle with a hydrogen combustion engine, produced from the decomposition of ammonia.[52] Another approach for using ammonia in a combustion engine is mixing it with hydrogen; ammonia mixtures containing a minimum of 10% by volume hydrogen have been shown to be very effective.[32] In 2013, a hybrid car prototype was presented, the Marangoni Toyota GT86-R Eco Explorer, which worked with a mixture of NH_3−H_2, for which the H_2 came from the decomposition of the same NH_3 in a separate catalytic reactor using the heat of the exhaust gases.[53] Apollo Energy Systems (AES)[54] and Intelligent Energy Corporation (IE)[55] have patented ammonia decomposition systems to supply hydrogen at a PEMFC of ∼10 kW for vehicle applications.[37] Pochari Technologies has designed a system to decompose ammonia in a microchannel reactor to supply H_2 to a PEMFC in vehicles.[56]

Concerning medium-sized systems for stationary power generation applications, different companies have designed systems that use ammonia for power generation. In this sense, Tower Power uses the generated energy to power cell phone towers in locations that lack a consolidated electricity service. In 1999 they built the first prototype and in 2012 the first equipment was installed in Namibia to generate a power of 1.2 kW. Currently, eight different updated models of ammonia crackers (ToWER/CuBE) with an output power between 1.3 and 10 kW are available.[57] Another company, GenCell, has recently developed a system (GenCell A5) that can produce electricity (4 kW) from the decomposition of ammonia continuously for a year disconnected from the electricity grid. The system is already in the commercial phase and has a lower cost than a diesel system of the same dimensions.[58] In a different way, the company AFC Energy has tested an ammonia decomposition system connected to an AFC of 240 kW, which has successfully completed an 18-month field test.[59] In United Kingdom, the Science and Technology Installations Council (STFC), which had already developed a prototype for the generation of energy in vehicles from the decomposition of ammonia contained in amides,[60] together with Siemens, Ecuity, and Engie, has started a project to supply low-cost stationary energy from H_2 produced from the decomposition of NH_3.[61,62]

Regarding portable applications of very small dimensions (between 50 and 150 W) there are projects at prototype scale or in the first steps for their commercialization. The compact system developed by Meso Systems Technology, Inc. (MTI) uses a microchannel reactor (MesoChannel) to decompose ammonia and produce 50 W integrating it to a PEMFC.[63] In a similar way, Analytic Power Corporation uses ammonia decomposition (A-Cracker) to provide hydrogen for small power supplies using 150 W fuel cells.[64] A new company in Denmark (Rencat) commercializes a technology to generate low-cost, high-purity hydrogen from ammonia for use in fuel cells (Figure 1, RenGen) that uses catalytic decomposition and oxidation of ammonia simultaneously.[65] Other organizations such as CSIRO in Australia[66] and Bettergy Corp. in the USA[67] develop ammonia decomposition systems to generate energy using hydrogen-selective membrane reactors.

2. HYDROGEN GENERATION FROM AMMONIA

The decomposition of ammonia occurs at high temperature in the presence or absence of a catalyst. One of the first works about the decomposition of ammonia reaction was carried out in 1904 by Perman and Atkinson.[68] The effect of temperature and pressure on the decomposition rate was evaluated, as well as the catalytic activity of elements such as Hg, Fe, and Pt. Over time, the decomposition of ammonia has proven to be an interesting reaction for different industrial applications; in 1934 Tyler[69] proposed the use of the hydrogen produced through the decomposition of ammonia at high pressures (7−14 bar) coupled with a residual ammonia scrubber to harden oils. It is important to mention that the technology of ammonia crackers at ambient pressure was already established in the metallurgical industry to reduce and temper metals. Regarding the effect of pressure, the decomposition of ammonia is favored at low pressures, for this reason many studies have focused on investigating the reaction rate at low pressures up to ultrahigh vacuum in the presence of platinum,[70] nickel, rhodium, tantalum, tungsten,[71] and iridium[72] catalysts. More recently, the effect of high pressures on the reaction rate was examined, considering that generally the hydrogen produced has to be compressed for its supply, for example, to a fuel cell.[73] In this sense, in order to avoid compressing the hydrogen generated, the decomposition of ammonia has been evaluated directly at high pressures, up to 40 bar, in the presence of a Ru/CaO

https://doi.org/10.1021/acs.iecr.1c00843
Ind. Eng. Chem. Res. 2021, 60, 18560−18611

catalyst promoted with K.[73] Di Carlo et al.[74] tested a Ru/Al_2O_3 catalyst at pressures between 1 and 10 bar, evaluating the decrease in conversion with increasing pressure.

As a result of the first studies and applications, and in parallel with the research of catalysts for thermal decomposition, alternative methods have been proposed to provide the activation energy necessary for the reaction, among which is the application of electric current, electron beams or ions, microwave, plasma, or solar energy. Integrated systems have also been studied in which the ammonia decomposition has been coupled with other parallel exothermic reactions, such as the combustion of propane or butane. These technologies can be applied with or without the presence of catalysts. The production of hydrogen from the electrolysis of liquid ammonia has also been studied, by photocatalysis, mechanochemical methods, or the decomposition of ammonia in the presence of other compounds such as hydrocarbons, H_2S, oxygen or water. Some of these methods have been proposed to avoid unwanted ammonia emissions. The different technologies that have been proposed in the literature are listed in Table 1.

Table 1. Technologies Used to Decompose Ammonia for Removal or for the Production of Hydrogen

technology	year	ref
thermal decomposition	1904, 1934	68,69
decomposition at pressures other than 1 bar	1967, 1968, 2001, 2020, 2014	70−74
decomposition with electric current	1997, 2000, 2002, 1938, 2013	75−79
decomposition with an electron beam	1928, 1980, 1970, 2013	80−83
decomposition with an ion beam	2016	84
microwave decomposition	2017, 2017, 1972	85−87
decomposition with plasma technologies	1967, 2013, 2019, 2019, 2014, 2017, 2018, 2015	88−95
decomposition with solar energy	2020, 2019	96,97
decomposition coupled with other reactions	2017, 2018, 2017, 2012, 2011, 2003, 2009, 2013, 2005	98−106
electrolysis of liquid NH_3	2010, 2016	107,108
photocatalysis in gaseous or aqueous medium	2015, 2018, 1932, 1983, 2012	109−113
decomposition with mechanochemical methods	2010	114
reaction of NH_3 with hydrides	2007	115
decomposition in gasification atmospheres	1905, 1996, 1999, 1995, 1997, 2008, 2008, 2004, 1993, 1995, 2002, 2002	116−127
decomposition in the presence of H_2S	2008, 2005, 2000, 2002	128−131
decomposition in the presence of oxygen	2012, 2008, 2015, 2002, 2017	132−136
decomposition in wastewater	1999	137
decomposition in the presence of water vapor	1977, 2014	138,139

2.1. Energy Supply Methods. The first experiments related to the decomposition of ammonia using electric current were focused on studying the decomposition as the inverse reaction of ammonia synthesis. The first tests were carried out in one or two chamber cell reactors made up of ceramic materials with Fe/K^+,[75] Pd[76], and Ag[77] electrodes, obtaining ammonia conversions between 25 and 35% at temperatures of 500−600 °C. In the case of Fe/K^+ electrodes, poisoning by ammonia was observed.[75] In these cells, the temperature at which ammonia begins to decompose remains very high, while if a strong electric field is coupled with alpha particles, the reaction temperature can be significantly lowered. In the experiments reported by Smith and Essex in 1938,[78] Pt electrodes were used, and it was demonstrated that the decomposition of ammonia was mainly due to alpha particles. After these first works, the studies were extended until reaching conversions of ammonia comparable to those obtained with thermal decomposition. In this sense, Zhao et al.[79] analyzed the results in an alternating current discharge reactor testing three types of electrodes (Cu, stainless steel, and Ni), obtaining an almost complete conversion with Ni electrodes. Other attempts to decompose ammonia by eliminating the effect of temperature was carried out in 1928 by McLennan and Greenwood,[80] who investigated the ammonia decomposition in a cathode ray tube. In their study, it was initially determined that the electric discharge generated in the reactor completely decomposed the ammonia in a very short time, and that the chamber composed of glass had an initial catalytic effect. By eliminating the generation of electric current, they analyzed the decomposition due only to the high-speed electron beam, reaching a decomposition of up to 30% with pure ammonia. They also analyzed the influence of the gases generated on the reaction rate, determining a favorable effect of the dilution of ammonia with N_2 and an inhibition by H_2. With the objective of generating hydrogen, McLennan and Greenwood[80] and Seabury et al.[81] analyzed the decomposition of ammonia using electron beams on a Ni(111) catalyst. In a similar way, Hirabayashi and Ichihashi[84] evaluated the decomposition reaction of ammonia through an ion beam using various vanadium and niobium nitrides, determining that some of them were promising for the generation of hydrogen. In another sense, and due to the corrosive characteristics of ammonia, Dawson and Peng,[82] among others, sought to eliminate ammonia by exposing the corrosive gas to a tungsten surface in the presence of a low-energy electron beam, detecting ammonia conversion at temperatures as low as 27 °C. At present, the decomposition of ammonia through an electron beam has also been proposed to eliminate its strong odor from industrial gas streams.[83] For this, the decomposition in the presence of different types of substances such as helium, nitrogen, oxygen, or water has been evaluated, showing that the maximum efficiency of ammonia removal takes place in the presence of O_2.

To provide heat to the reactor instead of using a conventional oven, the use of microwaves has been proposed, which allows reaching the desired temperature in a shorter time. In the work of Guler et al.,[85] mesoporous carbon was used as support for a catalyst composed of molybdenum. The ammonia conversion obtained in the microwave reactor was complete at 400 °C, while using the same catalyst in a conventional oven under the same reaction conditions an ammonia conversion of only 49% at 600 °C was obtained. Similar results were obtained by Varışlı et al.[86] using an iron catalyst supported on mesoporous carbon, which was shown to completely convert ammonia in a microwave reactor at 450 °C, while in a conventional reactor the complete conversion was reached at 600 °C. In a previous work (1971) developed by Barker,[87] the decomposition of ammonia through microwave discharges was examined, and the effect of adding scavengers of H atoms such as allyl alcohol and propylene promoted also the formation of hydrazine (N_2H_4).

https://doi.org/10.1021/acs.iecr.1c00843
Ind. Eng. Chem. Res. 2021, 60, 18560−18611

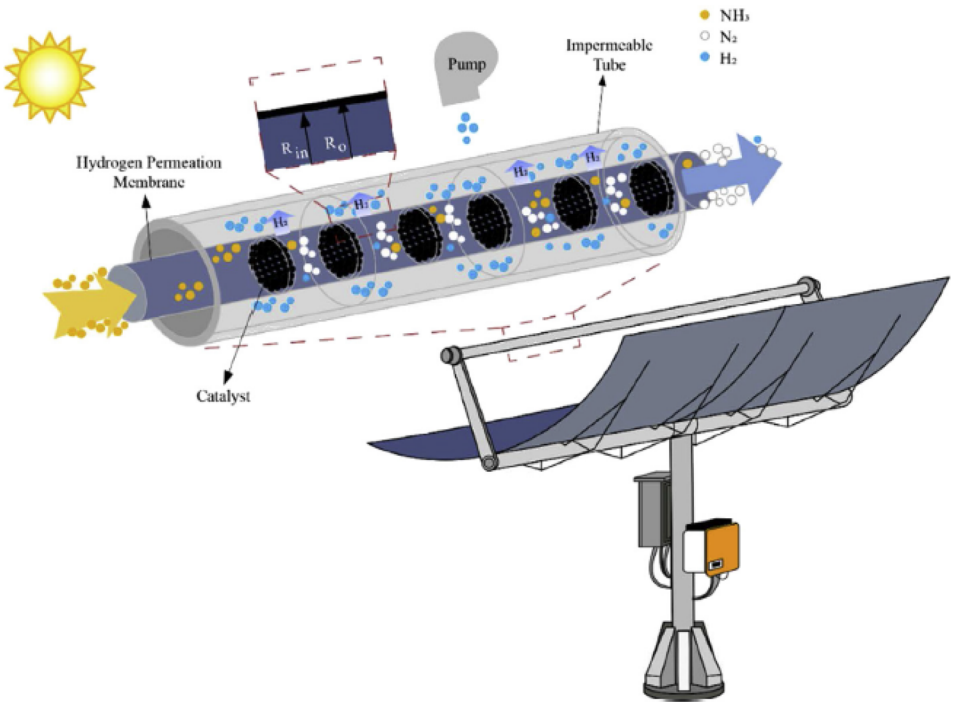

Figure 2. Conceptual diagram of the reactor equipment proposed by Wang et al. Reprinted with permission from ref 97. Copyright 2019 Elsevier.

Another widely studied method to supply energy to the system is plasma technology. In the case of ammonia decomposition, the first work that proposed the use of plasma generated in an incandescent discharge tube of alternating voltage at low pressure was carried out by Carbaugh et al.[88] in 1967, also targeting the generation of hydrazine. Very low conversions were obtained, but no catalyst was used. More recently, the decomposition of ammonia through pulsed plasma or plasma generated by dielectric barrier discharges (DBD) in the presence of a catalyst (Fe[89] and Fe−Ni[90]) or coupling plasma with a membrane reactor[91] reached higher conversions. In a similar way, the work of Inoue et al.[92] showed that complete conversion could be achieved at low temperatures with atmospheric pulsed plasma in the absence of catalysts by controlling the reaction conditions and dilution of ammonia with argon. However, the use of a stream of pure ammonia and DBD plasma resulted in lower conversions (19%), according to Goto et al.[93]

As shown by Akiyama et al.,[94] the type of electrodes used to produce the plasma does not interfere significantly in the decomposition of ammonia, whereas the applied power and the residence time of the gas shows a strong dependence on the conversion rate. Moreover, applying plasma technology at higher temperatures and in the presence of a low-cost catalyst results in a complete conversion at low temperatures.[89,90] Different metals such as Ni, Co, Fe, and Mo and their bimetallic forms Fe−Co, Mo−Co, Fe−Ni, and Mo−Ni have been tested, and the catalyst composed of Fe−Ni is the most active.[90] Following the catalytic test performed by Yi et al., Wang et al.[95] analyzed various elements and various supports as catalysts, among which Co/SiO_2 showed the strongest synergy with plasma, giving higher NH_3 conversion. Finally, it is possible to use a combined system composed of a catalytic reactor and a plasma reactor with a hydrogen-selective membrane (Pd−Cu alloy) to decrease the energy input necessary to decompose ammonia and obtain high energy efficiency.[91] The results show a total hydrogen energy efficiency of about 30%.

Within the framework of energy efficiency and to limit carbon emissions into the atmosphere, the production of hydrogen from ammonia using solar concentrators to convert renewable solar energy into chemical energy is currently being studied. In this sense, Hu et al.[96] and Wang et al.[97] are heading in this direction. At first, a catalyst composed of nickel supported on Al_2O_3 was used in a tubular reactor, in which the ammonia conversion was evaluated by changing its geometric characteristics and the reaction conditions, simulating through a model and obtaining an optimized reactor geometry, reaching conversions around 70% at a reactor wall temperature of 650 °C. Subsequently, it was proposed to couple the solar concentrator with a catalytic membrane reactor (Pd−Ag alloy), reaching almost complete conversion (99%) at only 200 °C at a pressure of 0.1 bar (Figure 2). The low reaction temperatures lead to very high total energy efficiency.

Another method proposed in the literature to provide the necessary heat to the catalytic reactor is to couple the ammonia decomposition reaction with an exothermic reaction. This is the case proposed by Chen et al.,[98] who designed a microreactor where channels with a platinum catalyst were used for the combustion of a methane−air mixture. The gases are alternated with other channels for the decomposition of ammonia in the presence of ruthenium, obtaining a compact reactor of reduced size. Also Engelbrecht et al.[99] and Chiuta et al.[100] designed an autothermal microchannel reactor in which the decomposition of ammonia and its oxidation takes place in stainless steel plates alternated in parallel with Ru (decomposition) and Pt (oxidation) supported on alumina catalysts. Another application to couple ammonia decomposition with another exothermic reaction was proposed by Kim et al.,[101] where a microcombustor burns a mixture of H_2, NH_3, and air, and a microreformer converts NH_3 to hydrogen using a ruthenium catalyst. The reformer is placed around the combustor to facilitate the transfer

https://doi.org/10.1021/acs.iecr.1c00843
Ind. Eng. Chem. Res. 2021, 60, 18560−18611

of heat. The ruthenium catalyst showed higher conversion rates compared to Ni/SiO_2−Al_2O_3 and Ir catalysts.[102] Finally, Arana et al.[103] coupled the combustion of butane with the decomposition of ammonia, and Kaisare et al.[104,105] and Deshmukh and Vlachos[106] used a similar microreactor using propane/air and ammonia.

The production of hydrogen in an aqueous medium from ammonia has also been considered, such as by alkaline electrolysis[107,108] or photocatalysis.[109,110] Hanada et al.[107] proposed the alkali metal amides $LiNH_2$, $NaNH_2$, and KNH_2 as electrolytes. The results showed that KNH_2 is the best compound among the three proposed for generating a high current density. The results showed that the electrolysis of ammonia is a valuable technology for the on-site generation of H_2, also considering that it requires 94% less energy than the electrolysis of water. In the study by Modisha and Bessarabov,[108] KOH was used as the electrolyte and platinum−iridium was used as the electrocatalyst. The influence of temperature and ammonia concentration on the conversion was studied, obtaining an output flow with an ammonia concentration less than 0.1 ppm, which allows its direct use in a PEMFC. In relation to the photocatalysis of ammonia in aqueous medium, different photocatalysts have been proposed, such as those based on titania, a widely studied photocatalyst, alone or doped with ceria,[109] or Ru/ZnS.[110] In the work by Reli et al.[109] it was shown that doping titania with ceria increases ammonia conversion compared to undoped titania, whereas in the work of Iwase, Li, and Kudo[110] Ru/ZnS was active for the photocatalysis of ammonia under both ultraviolet and sunlight conditions. The photolysis of ammonia has also been tested in the gas phase. One of the first works on the photolysis of gaseous ammonia without a catalyst was carried out in 1932 by Wiig and Kistiakowsky.[111] Later on, in 1983, Li et al.[112] tested several photocatalysts to convert ammonia, obtaining the best results with Ru−Ni supported on $BaTiO_3$. Importantly, they demonstrated that the photocatalytic decomposition of pure ammonia was almost zero, but in the presence of water vapor it increased to reach considerable H_2 production values. More recently, Yuzawa et al.[113] compared the photocatalytic results obtained in the presence of water vapor with those obtained with ammonia in an aqueous medium. The results showed that platinum supported on titania was the most active photocatalyst compared to Cu, Ni, Au, Rh, and Pd for gaseous ammonia photocatalysis in the presence of steam. Furthermore, comparing the conversion of ammonia in the presence and that in the absence of water vapor, it was concluded that the production of hydrogen in the first case was more than three times higher. In the case of aqueous photocatalysis, it was determined that the production of hydrogen increased considerably using hydrazine instead of ammonia. $SrTiO_3$ and $BaTiO_3$ prepared by mechanochemical methods have been tested at room temperature, and a conversion of 2.5 and 4.5% has been obtained, respectively.[114]

2.2. Decomposition in the Presence of Other Substances. The study of the decomposition of ammonia in the presence of other substances has had several objectives, among which the main ones are to increase the conversion of ammonia or to eliminate it from a gas flow. In the first case, the possibility of the generation of hydrogen from ammonia through other routes, such as the reaction between ammonia and metal hydrides as magnesium hydride MgH_2, has also been investigated.[115] The experiments in this case were carried out in a discontinuous reactor in the temperature range of 75−150 °C in the presence of catalysts, obtaining good results of H_2 production using Pd−Cl compounds. In another direction, White and Melville[116] investigated in 1905 the decomposition of ammonia in the gas produced during the destructive distillation of coal. For this, the experiments focused on decomposition in the presence of combinations of various gases, CO, H_2O, H_2, and N_2, determining that H_2 and N_2 could be considered inert, while CO and water vapor increased the decomposition reaction rate.

The presence of NH_3 in a gas stream can also be undesirable, as for example in the gas produced by the gasification of coal, and high NO_x emissions can occur when the gas is burned in a gas turbine. In this sense, Chambers et al.[117] studied the use of CaO to clean the hot gas stream produced in the gasification of coal by decomposing the NH_3 present. The same phenomenon occurs in biomass gasification; Wang et al.[118] studied nickel as catalyst for the decomposition reaction of ammonia for its removal in a wide range of temperatures (between 200 and 1000 °C) at a pressure of 21 bar. The main difficulty of ammonia removal in the presence of gas from the gasification of hydrocarbons is the possible poisoning of the catalyst by carbon deposition. Nickel has shown a greater capacity to be regenerated, removing carbon through oxygen treatment, compared to catalysts composed of Ru.[119] Other materials such as dolomite[120] have also been tested, but dolomite deactivates in the presence of carbon and water vapor. In this regard, a long-term (6 years) lifetime experiment of Ni-based catalysts in the presence of carbon and/or water compounds was proposed by Platonov and Stepanov,[121] showing a constant deactivation. Pansare and Goodwin[122] determined that tungsten-based catalysts, in particular WZ, showed a constant long-term conversion in the presence of syngas (CO + H_2) after an initial period of induction. Ohtsuka et al.,[123] studying a catalyst composed of Fe supported on carbon, determined that in the presence of syngas the catalytic activity decreased dramatically due to the deposition of carbon in the catalyst. However, the introduction of CO_2 into the inlet gas stream showed a recovery of the conversion. In a later work, Ohtuska et al.[128] studied the tolerance of FeOOH (limonite) to the presence of H_2S, a product of gasification, obtaining that in the presence of ca. 500 ppm of H_2S the conversion remained constant, while at 2000 ppm the catalyst suffered a reversible deactivation. In an opposite way, Uemiya et al.[129] showed that Fe-based catalysts can convert ammonia in the presence of 5000 ppm of H_2S without being deactivated. Furthermore, when Ni was used as a catalyst, a deactivation of the catalyst was not detected in the presence of gas streams containing up to 150 ppm of H_2S.[130] Additionally, the catalyst did not show deactivation by carbon deposition in the presence of tar. It is important to mention that the degree of sulfur poisoning during ammonia decomposition is related to the number of active sites of a catalyst.[131] The removal of ammonia by decomposition from gas flows generated from coal gasification has also been coupled to membrane reactors,[124−127] with which it was possible to achieve the complete destruction of ammonia in the presence of the low-cost catalysts Ni/Al_2O_3 at relatively low temperatures (400 °C).[125]

In the presence of oxygen, the decomposition of ammonia follows a different route, and depending on the amount of oxygen present in the reagent stream, it can decompose and generate N_2 or nitrogen oxides, NO_x. The oxidation of ammonia was studied for its elimination from gas streams when a selective catalyst toward the generation of N_2 that prevents the formation of nitrogen oxides was sought. Theoretically, catalysts based on

https://doi.org/10.1021/acs.iecr.1c00843
Ind. Eng. Chem. Res. 2021, 60, 18560−18611

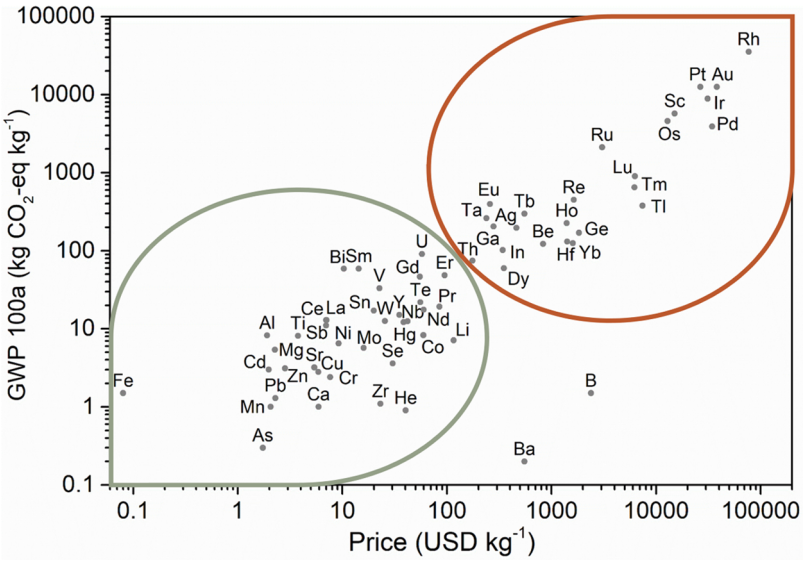

Figure 3. Comparison of the price (USD kg^{-1})[146] and the global warming power on a 100-year basis (kg CO_2−equiv kg^{-1})[147] of the elements.

Ir can achieve 100% selectivity toward N_2.[132] Hung[133,140] proposed a catalyst formed by Cu and ceria oxide, obtaining a selectivity toward the production of N_2 up to 85% with an ammonia conversion of up to 98%. Other studies on the selective oxidation of ammonia were carried out by Lee et al.[134] using a bimetallic catalyst formed by Ag and Cu supported on alumina, and by Bera and Hedge,[135] who tested different active phases supported on alumina or ceria, obtaining the best results with Pt. The oxidation of ammonia in the presence of oxygen has been also proposed for ammonia decomposition to generate H_2 in the presence of a RuO_2/Al_2O_3 catalyst.[136] In this case, the as-developed process does not need an external source of heat to initiate or maintain the reaction due to the exothermicity of the ammonia oxidation reaction.

The decomposition of ammonia has also been studied as an intermediate reaction of the supercritical oxidation of water from organic waste.[137] Supercritical oxidation is applied to destroy excess sludge from sewage treatment plants, and the reaction is performed with an oxidant such as hydrogen peroxide at temperatures between 450 and 550 °C. The decomposition of ammonia is one of the slowest stages in the supercritical oxidation process of sludge. The decomposition of ammonia into N_2 and H_2 in the presence of water vapor was studied using Ni-based catalysts supported on alumina;[138,139] water vapor inhibited the conversion of ammonia and initially deactivated the catalyst until a constant conversion was reached.

3. CATALYSTS FOR THE THERMAL DECOMPOSITION OF AMMONIA

Thermal decomposition or catalytic cracking is the most common technique used for the generation of hydrogen from ammonia. It can be carried out with or without the presence of a catalyst, as the presence of a catalyst allows the decrease of the temperature necessary for the decomposition. For this reason, it is important to study the catalysts involved as well as different reactor configurations in order to decrease the supply of energy, in this case in the form of heat, to the system.

3.1. Catalysts. Since the decomposition of ammonia is the inverse reaction of the Haber-Bosh process for the synthesis of ammonia, initially the same catalysts used for the synthesis, Ru and Fe,[141] were considered for the thermal decomposition of ammonia assuming the principle of microreversibility in heterogeneous catalysis. Afterward, Cu-based catalysts were studied[142] as well as other metals, including Ni, Ir, Mo, Co, Pt, Pd, and Rh,[143] and different combinations of metals, such as Co−Mo, Ni−Mo, Fe−Mo, Ni−Co, Co−Mo−Fe−Ni−Cu, Mg−Fe, Fe−Co, Ni−Fe, Mg−Co−Fe, Ni−Pt, Ni−Pd, Ir−Ni, Cu−Zn, and bimetallic compositions with Ru.[144] Nowadays, the catalyst used commercially for the decomposition of ammonia is nickel supported on alumina, due to its mechanical properties and heat resistance.[34] Among the catalysts studied in the literature, the highest catalytic activity for the decomposition of ammonia has been found with ruthenium supported on different oxides or structured and unstructured carbon,[145] with the main problem being deactivation.[44] However, ruthenium is a noble metal, rare in nature, and consequently an expensive element. For this reason, low-cost catalytic compositions with a catalytic activity comparable to that of ruthenium have been actively sought.[143] In addition to the price of the metal on which the catalyst is based, within the framework of environmental sustainability it is recommended to also take into account the environmental impact of the material used, such as its global warming power or the energy demand of its extraction and refining. Figure 3 shows the relationship between the price of the different elements of the periodic table and their global warming power (GWP) over a period of 100 years.[146,147] Generally, the price and the GWP have a linear relationship, since both are related to the abundance of an element on earth; the scarcer is the element, the higher is its price and the energy necessary for its availability. For this reason, noble metals, such as Ru, are at the top of the chart, having a high price and high environmental impact. If possible, the use of the elements that are located in the lower part should be preferred, such as the transition metals Fe, Ni, Mo, or Co, among others.

The catalytic activity in the decomposition of ammonia depends not only on the active phase used, but also on the support and promoters. In general, the catalytic activity improves with supports that exhibit high surface area, with high dispersion and reduced particle size of the metal, and in the presence of electrodonating promoters such as K, Cs, or Ba.[148] The support can stabilize the size and/or morphology of the metal particles and increase the exposure of their active sites and,

https://doi.org/10.1021/acs.iecr.1c00843
Ind. Eng. Chem. Res. 2021, 60, 18560−18611

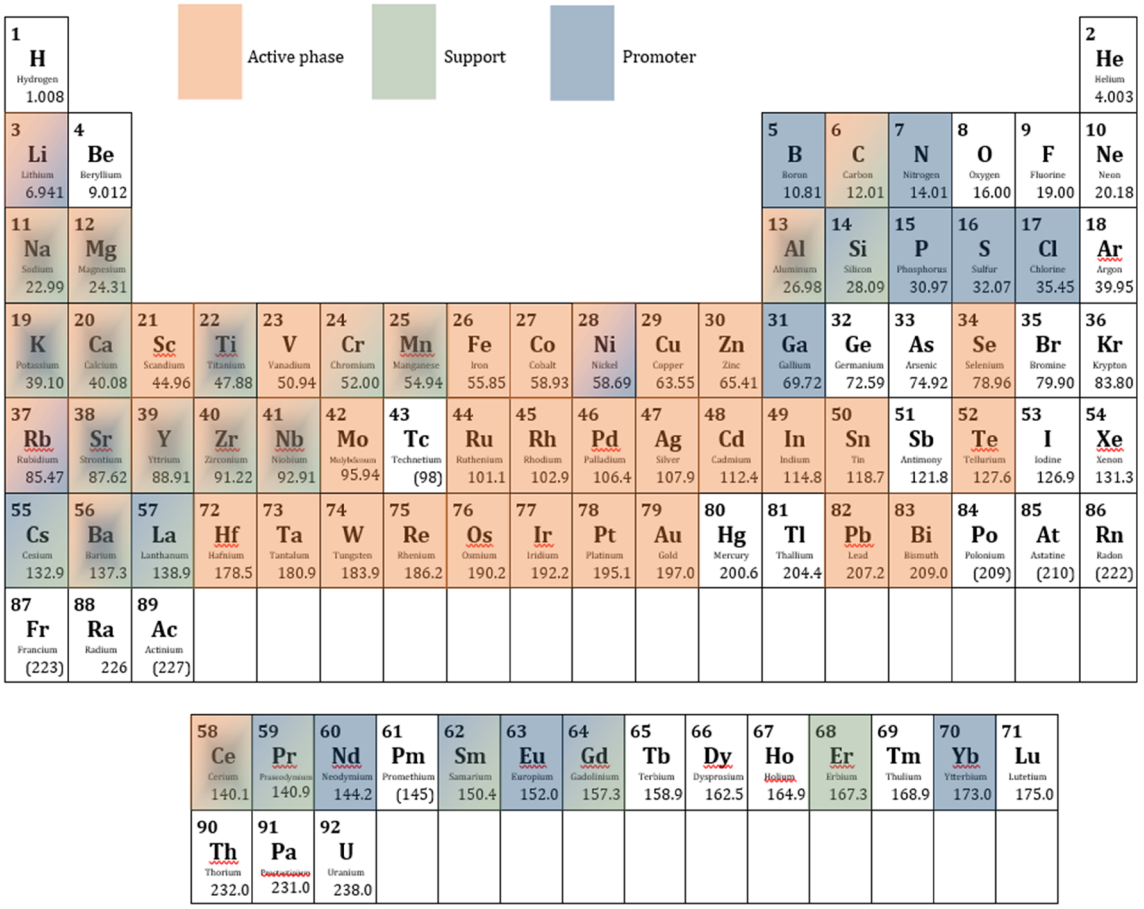

Figure 4. Simplified periodic table of the elements used in the formulation of catalysts for the decomposition of ammonia.

at the same time, it can affect the electronic structure of the supported metals.[143] In particular, it has been determined that the basicity of the catalyst increases the catalytic activity[149] as well as the ability to generate bonds with nitrogen atoms with a given energy.[145] On the other hand, it must be considered that the composition of the reaction gas also influences the catalytic performance, being that the composition of the gas varies across the catalytic bed, which means that an optimal catalyst in the inlet conditions may not be optimal in the outlet, where there is a higher concentration of H_2 and N_2 and a lower concentration of NH_3.[148] In Figure 4, the elements reported in the literature involved in the catalysts for the decomposition of ammonia are indicated, divided by active phase, support, and promoters. Some elements such as Mg, Al, or Ce are used for the three components, while others such as noble metals are used only as the active phase of the catalyst, or the alkali metals, that are used mainly as promoters.

The different catalysts reported in the literature for the decomposition of ammonia are presented according to their active phase in Tables 2−10 (section 3.1.1). The results reported correspond to those obtained at atmospheric pressure and in the presence of pure ammonia or diluted with an inert gas, assuming a pressure of 1 atm when not specified. The values of the conversion of ammonia, H_2 formation rate, TOF, and apparent activation energy at the temperatures specified in the text are included in the tables. When not present in the text, the values were estimated by extrapolation, reporting representative values between 350 and 500 °C. In the case that different methods were used for the synthesis of catalysts with the same composition, or that they had different relative amounts of the components, it was chosen to report only the results of the catalyst for which the higher catalytic activity was obtained. The reaction conditions are reported or calculated from the data provided in the different studies (if they are not indicated it is because they have not been specified by the authors). The works related to reaction kinetics studies are compiled in Table 11 (section 3.2), including results obtained at pressures other than atmospheric. Apparent activation energy values have been obtained from experiments as well as theoretical studies.

As far as review articles on the catalytic decomposition of ammonia are concerned, works that consider decomposition in the framework of hydrogen production as well as works that focus on the type of catalyst or structured support used have been found in the literature. The first are the works of Klerke et al. (2008),[34] Zamfirescu and Dincer (2008−2009),[35,48] Cheddie (2012),[149] Lan et al. (2012),[33] Giddey et al. (2017),[36] Abd Ali et al. (2018),[150] and Makepeace et al. (2019).[141] Among those that analyze the catalysts, supports and types of reactor used are the works of Yin et al. (2004),[151] Schüth et al. (2012),[145] Chiuta et al. (2013),[46] Duan et al. (2013),[152] García-Bordejé et al. (2014),[148] Bell and Torrente-Murciano (2016),[144] Mukherjee et al. (2018),[143] and Lamb et al. (2019).[44]

3.1.1. Importance of the Active Phase. There are several works focusing on a comparison of the catalytic activity of different metals supported on the same support for ammonia decomposition. Boisen et al.[153] in 2005 carried out a decisive study; they compared different active phases (Fe, Co, Ni, Cu and

https://doi.org/10.1021/acs.iecr.1c00843
Ind. Eng. Chem. Res. 2021, 60, 18560−18611

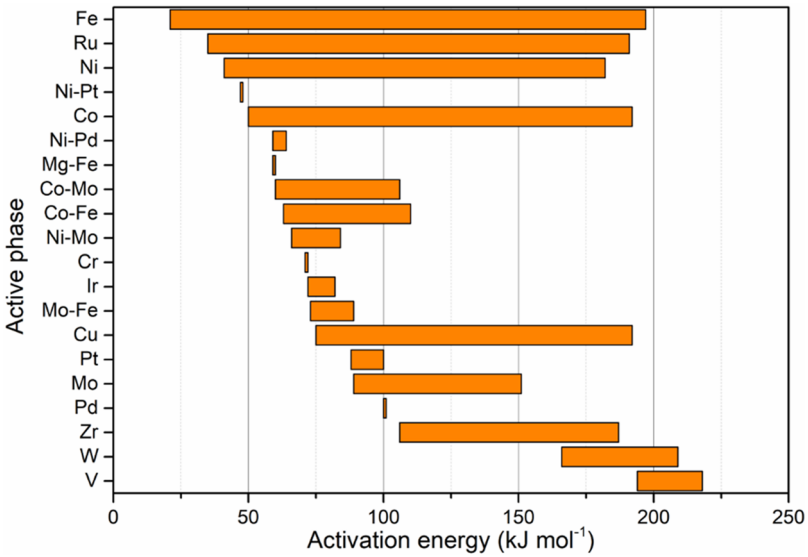

Figure 5. Apparent activation energy values for the decomposition of ammonia recorded on different metal-based catalysts.

Ru) supported on $MgAl_2O_4$ spinel and observed that the best catalysts for the synthesis of ammonia are not good catalysts for its decomposition. They evaluated it by calculating the TOF values and comparing them with the dissociation energy of the nitrogen bond at the active sites, obtaining a volcano-shaped curve, with the optimum in the case of metals that can generate the less strong N bond. They also observed that the position of the maximum of the curve varied according to the reaction conditions, such as the concentration of ammonia. Through an interpolation in the periodic table, they proposed the catalyst composed of Co_3Mo_3N as a good candidate for the decomposition of ammonia.[154] This model, which focuses on the energy of nitrogen chemisorption, is the one that predicts more precisely the catalytic activity of metals. However, it cannot foresee the higher activity of rhodium compared to cobalt.[155] Ganley et al. proposed that this occurs because the determining step of the decomposition reaction mechanism changes according to the catalyst.[155] They compared the results of several monometallic catalysts supported on alumina and were able to define the following relative activity relationship for decomposition: Ru > Ni > Rh > Co > Ir > Fe ≫ Pt > Cr > Pd > Cu ≫ Te, Se, Pb. However, since the support has an important influence on the catalytic activity, the relationship between the catalytic activities of the catalysts can vary considerably depending on the support considered. For example, in the study by Yin et al. at a reaction temperature of 400 °C, the TOF as well as the ammonia conversion of the catalysts supported on carbon nanotubes can be arranged in the order: Ru > Rh ≈ Ni > Pt ≈ Pd > Fe,[156] different from the catalysts supported on alumina prepared by Ganley et al.[155]

Using a high-throughput method, Liu et al.[157] tested a high number of transition metals supported on SiO_2, verifying that the activity of the catalysts at 570 °C is Ru > Ni > Co > Ir > Ag > Mo > Pd > Gd, while the other metals showed a catalytic activity equal to or less than that obtained without a catalyst. They also determined that a nitriding pretreatment with H_2/N_2 can change the catalytic activity of the catalysts, as in the case of Fe, Co, and Mo, which presented a much higher catalytic activity after pretreatment due to the formation of the respective nitrides. Also V, W, and Ti showed an increase in their activity after the pretreatment. Therefore, not only does the support but also the reaction conditions and the preparation method influence the activity of a catalyst. In this sense, Choudhary et al.[158,159] using SiO_2 as a support, determined the order of catalytic activity Ru > Ir > Ni at various temperatures using pure ammonia. By testing the Ru and Ir catalysts supported on Al_2O_3, they concluded that both metals present lower catalytic activity compared to when supported on SiO_2,[158] but they follow the same relative trend. Comparing the active phases of Fe, Ni, and Ru with their encapsulated forms in SiO_2 (@SiO_2) under the same reaction conditions, a significant increase in catalytic activity resulting from encapsulation was observed in all three cases (in the case of Ru the increase was the highest, ammonia conversion increased by 62% at a temperature of 500 °C).[160,161] The encapsulated catalysts showed the order of catalytic activity: Ru > Ni ≈ Fe. However, a Co catalyst prepared following the same technique presented lower activity than the other three formulations.[162] On the contrary, when they were supported on carbon nanotubes, Co showed a higher catalytic activity with respect to Fe.[163] Finally, promoters can also have a positive effect on one type of catalyst, while they decrease the activity of another type. Li et al.[164] investigated different forms of SiO_2 (fumed SiO_2, MCM-41, and SBA-15) as supports for Ni and Ru catalysts, showing that the catalysts supported on these materials are more active than those supported on conventional SiO_2. In general, supported Ru catalysts are more active than supported Ni catalysts (a conversion about 20% higher under the same conditions and considering the same support), and MCM-41 is the best support for both metals. The modification of the Ru catalysts with KOH contributes to a significant increase of the catalytic activity, while in the case of Ni the promoter effect is minimal.

The apparent activation energy values for the different catalysts have been analyzed with respect to the active phase used, obtaining the graph presented in Figure 5. The apparent activation energy is very different depending on the metal used and the support. In general, it is possible to conclude that the lowest apparent activation energy values are found for iron, ruthenium, and nickel catalysts, which are also the most studied catalysts in the literature. It can be concluded that the catalytic activity has a strong dependence with the type of support and

https://doi.org/10.1021/acs.iecr.1c00843
Ind. Eng. Chem. Res. 2021, 60, 18560−18611

promoter. The lowest catalytic activity is obtained with the nitrides and carbides of V and W.

3.1.2. Noble Metals. The noble metals are grouped by their resistance to oxidation and corrosion. There is no strict definition for them, and Ru, Rh, Pd, Ag, Re, Os, Ir, Pt, and Au are usually considered.[165] Papapolymerou and Bontozoglou[166] tested different noble metals in the form of wires or polycrystalline foils at low reaction pressures between 225 and 925 °C and determined that the reaction rate for the decomposition of ammonia followed the order Ir > Rh > Pt > Pd. However, among the noble metals, ruthenium is the element most studied as a catalyst for the decomposition of ammonia.

3.1.2.1. Ruthenium. Hill and Torrente-Murciano[167] reported the catalyst considered as the most active up to date in the decomposition of ammonia: Ru/CNTs (ruthenium supported on carbon nanotubes) promoted with Cs (20 wt %). In a follow-up study, they prepared the same catalyst with a graphitization treatment of the carbon nanotubes and a lower Cs content (4 wt %), obtaining a significant increase in the conversion compared to the catalyst with the support without graphitization under the same reaction conditions.[168] Wang et al.[169] tested other types of promoters for the Ru/CNTs catalyst, obtaining the following order of promotion at 400 °C: K > Na > Li > Ce > Ba > La > Ca; all promoted catalysts showed a higher catalytic activity with respect to the unpromoted ones. In general, various types of carbon show very good results as supports of Ru catalysts, in their unpromoted or alkali metal-promoted form. For example, a very high TOF of about 35 s^{-1} was obtained at 400 °C with a Ru catalyst supported on carbon and promoted with K.[170] It is worth mentioning that nitrogen doping changes the properties of carbon and further increases the catalytic activity of the catalyst. Ru supported on ordered mesoporous carbon (OMC) doped with nitrogen presented a high catalytic activity, compared to other forms of carbon (CNTs, activated carbon or undoped OMC).[171] Nitrogen-doping has also a positive effect on Ru catalysts supported on carbon nanotubes.[172,173] Chen et al.[174] showed that doping carbon nanotubes with nitrogen increases the metal dispersion. Using carbon nanofibers (CNFs) as a support for Ru, Marco et al.[175] showed that doping with N leads to an increase of the catalytic activity compared to the support without doping, and that if oxygen is introduced into the structure of the nanofibers instead of nitrogen, the activity does not increase. In general, carbon nanofibers are proven to be an optimal support for Ru, presenting similar catalytic activity with respect to Ru/CNTs. Another important aspect to take into account is the Ru particle size. By varying the size of the Ru particles the ammonia conversion has been optimized, obtaining the best results with a Ru particle size of about 2 nm.[176] On the contrary, activated carbon (AC) did not show to have superior activity with respect to carbon nanotubes, even if promoting a Ru catalyst supported on activated carbon with Na.[177,178] Yin et al. tested the catalysts Ru/MgO and Ru/AC promoted with K, obtaining an increase in the conversion in both cases, particularly with the catalyst supported on activated carbon.[179]

Yin et al.[156] carried out an analysis of the catalytic activity of Ru supported on various oxides and forms of carbon and obtained the order: CNTs > MgO > TiO_2 > Al_2O_3 > ZrO_2 > AC. They attributed the superior catalytic activity of the CNTs to a greater dispersion of Ru and to its high electronic conductivity, which allows a greater transfer of electrons and, consequently, facilitates the desorption of N_2 from the catalyst. They also tested the same catalysts prepared with acetone as solvent, instead of water, obtaining an increase in the ammonia conversion, which highlights the importance of the catalyst preparation method.[180] Petrunin et al. analyzed the best ratio between K and Ru on mesoporous carbon (Sibunit) and obtained an increase in ammonia conversion of around 10% with respect to the catalyst without promoter at 450 °C with a K/Ru molar ratio of 0.5. Nevertheless, further increase of the amount of K produced a strong decrease in conversion.[181] By changing the carbonaceous support, Li et al.[182] tested a catalyst composed of Ru supported on graphene, which resulted in a high conversion of ammonia (91% at 450 °C) using pure ammonia. In another work, Li et al. also tested other types of carbon as support for Ru,[183] obtaining that the catalytic activity of the supports follows the order: graphitic carbon > CNTs > black carbon > mesoporous carbon CMK-3 > activated carbon. They also tested Cr_2O_3 as a support for a Ru catalyst[184] and analyzed the relationship between Ru particle size and conversion, obtaining the maximum of activity with 4 nm particles. The catalytic activity of chromium oxide without ruthenium was also studied, and it was observed that the catalytic activity increased by increasing the size of the Cr_2O_3 particles.[184] Raróg-Pilecka et al.[185] tested a catalyst composed of Ru supported on carbon modified with Cs and Ba, determining that for the whole range of concentrations of ammonia tested (5−50%), Cs has a promoting effect greater than Ba. Also Huang et al.[186] obtained that Cs is an optimal promoter for the Ru/C catalyst, obtaining an increase in conversion of 48% at 400 °C with respect to the unmodified catalyst using pure ammonia. Not only have alkali metals showed a promoting effect on carbon supported ruthenium catalysts, but also other elements. For example, Li et al.[187] tested a catalyst composed of Ru supported on ordered mesoporous carbon (CMK-3) and evaluated different materials as promoters for the catalyst, obtaining a relative activity of K > Na > Ca > Cl > SO_4 > PO_4 > Li. The Li-modified catalyst showed lower activity with respect to the unpromoted catalyst.

Various forms of carbon mixed with other compounds, mainly oxides, were also tested as Ru supports. For example, Yin et al.[188] compared the activity of Ru catalysts supported on CNTs, MgO and a mixture of the two, and they verified a synergy between the supports, especially when the catalyst is promoted with K. Under the same conditions, the conversion of ammonia at 400 °C reached 80% while the nonpromoted Ru/CNTs-MgO catalyst reached a conversion of only 13%. In a similar manner, Bajus et al.[189] verified whether the same alkali metals that showed a promoting effect on the catalytic activity of Ru supported on carbon could be used to promote Ru/Al_2O_3. They reported that the three metals Li, Na, and Cs do indeed have the ability to promote the catalyst. With Na and Cs, TOF was approximately twice that of the unpromoted catalyst, while Li presented the highest increase (0.26 vs 0.05 s^{-1} at 350 °C). Moreover, Pyrz et al.[190] identified Ba, Cs, and K as more promising with respect to Sr, Rb, Ca, Na, and Li when used as promoters of ruthenium supported on alumina. They also prepared catalysts using a combination of promoters, such as Ru/Al_2O_3 promoted with Ba and K or Cs and K. They found that the use of double promoted catalysts did not increase catalytic activity.

Moving on to a different type of supports, Klerke et al.[191] compared TiO_2 with three types of titanates ($Na_2Ti_3O_7$, $K_2Ti_6O_{13}$ and $Cs_2Ti_6O_{13}$) as support for Ru, obtaining the same general trend to promote ruthenium catalysts with alkali metals: Cs > K > Na. Comparing Ru supported on Al_2O_3 and La-doped Al_2O_3, Chung et al.[192] obtained a higher catalytic activity in the second case; at a temperature of 600 °C the conversion increased from 4 to 98% by adding 50 mol % La to the support,

https://doi.org/10.1021/acs.iecr.1c00843
Ind. Eng. Chem. Res. 2021, 60, 18560−18611

and the catalyst showed high stability in a 120 h test. Lanthanum has been used not only as a promoter, but also as a support; Huang et al.[193] determined that the activity of Ru catalysts supported on La_2O_3 is higher than Ru supported on Al_2O_3, Er_2O_3, SiO_2,and TiO_2, and that the addition of KOH can effectively improve the catalytic activity of the catalysts. Szmigiel et al.[194] tested a Ru catalyst deposited on a magnesium−aluminum spinel and compared its activity with the same catalyst doped with Ba and Cs. Also in the case of $MgAl_2O_4$ the two alkali metals are good promoters and the activity increased about 10 times compared to the unpromoted catalyst, although it is still lower than that obtained with the Ru/C catalyst promoted with Cs and Ba. A similar composition was tested by Su et al.,[195] who prepared a Ru catalyst supported on a double layer oxide composed of Mg and Al, obtaining a higher activity with respect to the Ru supported on the corresponding MgO and Al_2O_3 oxides separately. A Ru catalyst supported on MgO and Al_2O_3 was also tested by Tan et al.,[196] obtaining an increase of ammonia conversion of 44% at 500 °C with respect to the catalyst supported only on alumina.

Also zirconium oxide has proven to be a good support for ruthenium. Using a Ru/ZrO_2 catalyst, Wang et al.[197] tested different zirconia supports modified with Ba. As a promoter of the active phase, it presented a lower conversion of ammonia compared to the unpromoted catalyst, whereas when it was used as a promoter of the zirconia support a spectacular increase in activity was achieved. The conversion was further increased by adding K and Cs as promoters, obtaining the best results with Cs. By incorporating Ru nanoparticles into a La-doped ZrO_2 support, Lorenzut et al.[198] obtained a significantly higher activity with respect to the reference catalysts prepared by impregnation using ZrO_2−La_2O_3 as support (81 vs 4% at 450 °C). In a similar way, Miyamoto et al.[199] modified a Ru/ZrO_2 catalyst with different amounts of La, Ca, and Sr obtaining a higher catalytic activity with respect to the unmodified catalyst in all three cases. Also, the subsequent promotion of Ru−La/ZrO_2 with Mg, Ca, and Sr did not allow an increase in the conversion of ammonia; nevertheless, the catalyst promoted with La and Sr presented the highest TOF value. Differently, Yin et al.[200] modified a Ru catalyst supported on ZrO_2 with KOH to increase the basicity of the catalyst, obtaining a better ammonia conversion than the catalyst further promoted with K (KOH-Ru/KOH-ZrO_2). On the contrary, Zhang et al.[201] modified a Ru catalyst supported on MgO with K and Cs and obtained a higher ammonia conversion. The promoter effect using K with a catalyst composed of Ru supported on MgO was confirmed by Ju et al.[202]

Other less conventional supports have been proposed for Ru catalysts, for example an organic−metal chromium terephthalate structure (MIL-101) mixed with MgO.[203] The catalyst presented a similar catalytic activity with respect to when the support is not mixed with magnesia. However, after doping the two catalysts with Cs, the activity showed a significant increase, and the catalyst supported on MgO-MIL-101 presented the greatest increase. To lower the cost of the catalyst made up of Ru, red mud was tested as support.[204] Red mud is composed mainly of the oxides of Al, Si, Ca, and Fe and it is a residual material from the alumina production process. High ammonia conversion was obtained, comparable with other configurations of Ru catalysts, and stable over 170 h. Another waste material that has been tested as Ru support for the ammonia decomposition reaction is fly ash, composed mainly of SiO_2 and Al_2O_3 with the presence of Fe, but the results are not as good as with red mud.[205,206]

Silica is another support that has been extensively tested as a catalytic support, alone or mixed with other materials, and also as a natural mineral. A catalyst composed of Ru on SiO_2 showed high catalytic activity, reaching a conversion of 86% at 500 °C with a high space velocity of pure ammonia. The catalytic activity is also promoted by K, and the ammonia conversion increases by 50% at 600 °C with respect to nonpromoted catalysts.[207,208] A natural material, halloysite nanotubes (HNTs), composed mainly of SiO_2, Al_2O_3, and other impurities, was used as a support for Ru and tested in the decomposition of ammonia.[209] Although the catalytic performance of Ru/HNTs is not comparable to that of Ru/CNTs, the former has the advantages of using a low cost and highly abundant support.

Cerium oxide is a material that allows easy control of the shape of its particles by varying the synthesis conditions. A low amount of Ru (1 wt %) supported on two types of CeO_2 nanoshapes, nanorods, and nanospheres, showed high catalytic activity (32 and 25% at 350 °C, respectively) compared to the catalyst supported on Al_2O_3 and MgO, with a conversion of only 5 and 11% under the same reaction conditions.[210] Comparing different 1D nanoshapes of ceria, alumina, titanate, and carbon, Hu et al.[211] found that CeO_2 nanorods were the best support for Ru catalyst compared to CNTs and Al_2O_3, particularly at low temperatures. This result is attributed to the strong metal−support interaction and the electronic modification of Ru by ceria. The addition of Na to the catalyst improved the activity when CNTs and Al_2O_3 were used as supports, but had a negligible effect on CeO_2-based catalysts.

The basicity of Ru-based catalyst was proven to be important. Comparing catalysts based on Ru promoted with K supported on different materials (CNTs, MgO, sepiolite, and CaO), Sayas et al.[73] obtained the highest catalytic activity with CaO, which is the most basic support of those used. The Ru supported on a layered oxide composed of Ca and Al ($CaAlO_x$) was compared with other types of supports widely used in the literature, carbon nanotubes and SiO_2, obtaining a higher conversion (78 vs 21 and 62% at 450 °C, respectively).[212] In a similar way, Hayashi et al.[213] tested as supports an electride, $[Ca_{24}Al_{28}O_{64}]^{4+}(e^-)_4$, where electrons work as anions, and mayenite oxide $[Ca_{24}Al_{28}O_{64}]^{4+}(O^{2-})_2$, and compared the results with conventional catalysts of Ru supported on CaO, Al_2O_3, MgO. They also prepared a K-promoted Ru/MgO and Cs-promoted Ru/C catalyst. At relatively low temperatures (400 °C) the catalyst supported on $[Ca_{24}Al_{28}O_{64}]^{4+}(e^-)_4$ showed the highest conversion. Barium has also shown to be a catalyst promoter when used to modify an alumina support. For instance, Ru supported on barium hexaaluminate (BHA) shows superior catalytic activity compared to traditional supports such as MgO, Al_2O_3, and CNTs; around 4 times higher compared to MgO and Al_2O_3 supports, and more than double compared to carbon nanotubes. A very good stability for 60 h was reported using pure ammonia at 450 °C.[214]

An intensive analysis of the catalytic activities of Ru supported on Pr_6O_{11} was carried out by Nagaoka et al.[215] The ammonia conversion on promoted Pr_6O_{11} followed the trend Cs_2O > Rb_2O > K_2O > Na_2O, where Cs_2O is the most basic oxide. Ru/Pr_6O_{11} promoted with Cs_2O showed a very high ammonia conversion. Comparing the nonpromoted Ru/Pr_6O_{11} catalyst with Ru supported on other oxides, they obtained a similar catalytic activity with Ru/La_2O_3. Moreover, when Ru/La_2O_3 is promoted with Cs, the activity increases, but to a lesser extent with respect to the promoted Ru/Pr_6O_{11} catalyst.[216] Ru supported on MgO, Al_2O_3, and SiO_2/Al_2O_3 showed a low

https://doi.org/10.1021/acs.iecr.1c00843
Ind. Eng. Chem. Res. 2021, 60, 18560−18611

Table 2. Catalysts Based on Ruthenium Used to Decompose Ammonia and Their Catalytic Performances at 1 atm

active phase	wt %	support	promoter	WHSV (mL g^{-1} h^{-1})	GHSV (h^{-1})	% NH_3 inlet flow	T (°C)	conv (%)	H_2 rate (mmol g^{-1} s^{-1})	E_a (kJ mol^{-1})	TOF (s^{-1})	ref
Ru				30000		100	500	34	0.34			161
Ru	3	@La_2O_3−ZrO_2		4000		100	450	81				198
Ru	3	@La_2O_3−ZrO_2	$NaBH_4$	4000		100	450	63				198
Ru		@SiO_2		30000		100	500	96	0.50	41	18.1	161
Ru		@SiO_2		360000		100	600	23				207
Ru		@SiO_2		30000		100	500	84				208
Ru		@SiO_2	K	360000		100	600	73				207
Ru	2.0	$[Ca_{24}Al_{28}O_{64}]^{4+}(O^{2-})_2$		15000		30	400	42		69	1.0	213
Ru	2.2	$[Ca_{24}Al_{28}O_{64}]^{4+}(e^-)_4$		15000		30	400	70		55	6.9	213
Ru	2	AC		20000		10	350	25			0.07	178
Ru	4.8	AC		30000		100	450		0.16	75	1.7	180
Ru	5.0	AC		6000		100	450	9				171
Ru	5	AC		150000		100	500	9	0.29	76		156
Ru	5	AC		30000		100	550	14	0.07			183
Ru	5	AC		15000		100	400	4				203
Ru	5	AC	K	30000		100	450	40				179
Ru	2	AC	Na	20000		10	350	46			0.14	178
Ru	0.5	Al_2O_3				100	580				6.85	155
Ru	0.7	Al_2O_3		2300		10	500	4				192
Ru	1	Al_2O_3		22000		100	350	5			0.2	210
Ru	1	Al_2O_3		3000		100	350	7				216
Ru	1.9	Al_2O_3		30000		100	500	85		80		217
Ru	2	Al_2O_3		30000		100	500	42				196
Ru	2.0	Al_2O_3		15000		30	400	13		86	1.0	213
Ru	2	Al_2O_3		240000	80000	50	500	98				218
Ru	2	Al_2O_3		13800	3067	57	400	37			1.0	219
Ru	2.1	Al_2O_3		30000		100	450	7		122	0.6	214
Ru	4	Al_2O_3				10	400	28				190
Ru	4	Al_2O_3		125000		100	450	33		95		220
Ru	4	Al_2O_3		120000		10	350	24		130	1.5	221
Ru	4	Al_2O_3		5400		100	400			125	0.14	222
Ru	4.7	Al_2O_3		4160		67	350				0.05	189
Ru	4.8	Al_2O_3		30000		100	450		0.13	61	2.5	180
Ru	4.8	Al_2O_3		18000		100	350	13				193
Ru	5	Al_2O_3		150000		100	500	11	0.30	65		156
Ru	5	Al_2O_3		30000		100	550	78				223
Ru	5	Al_2O_3		7200		100	450	54			0.093	32
Ru	5	Al_2O_3			13000	10	400	79				224
Ru	8.5	Al_2O_3			1200	100	400	99		117		74
Ru	10	Al_2O_3		30000		100	450			80	6.5	158
Ru	4	Al_2O_3	Ba			10	400	37				190
Ru	4	Al_2O_3	Ba, K			10	400	95				190
Ru	4	Al_2O_3	Cs			10	400	47				190
Ru	4.7	Al_2O_3	Cs			67	350				0.10	189
Ru	4	Al_2O_3	K			10	400	96				190
Ru	4	Al_2O_3	K	5400		100	400			66	0.33	222
Ru	4.6	Al_2O_3	K	30000		100	400	12	0.07		0.19	195
Ru	4.7	Al_2O_3	K			67	350				0.12	189
Ru	5	Al_2O_3	K	30000		100	550	86				223
Ru	4.7	Al_2O_3	Li	3700		67	350				0.26	189
Ru	1	Al_2O_3	LiOH			100	350				1.6	225
Ru	7	Al_2O_3 rods		6000		29	350	4		111	0.006	211
Ru	7	Al_2O_3 rods	Na	6000		29	350	21		95	0.031	211
Ru	7.0	AX-21		5200	33	100	450	24				226
Ru	3	Ba-ZrO_2		30000		100	500	24	0.13	92		197
Ru	3	Ba-ZrO_2	Cs	30000		100	500	38	0.21	64		197
Ru	3	Ba-ZrO_2	K	30000		100	500	33	0.18	71		197
Ru	2.7	BHA		30000		100	450	42		65	2.9	214
Ru	5	black carbon		30000		100	550	56	0.27			183
Ru	9.1	C		1500000		5.7	400			191		185

https://doi.org/10.1021/acs.iecr.1c00843
Ind. Eng. Chem. Res. 2021, 60, 18560−18611

Table 2. continued

active phase	wt %	support	promoter	WHSV (mL g^{-1} h^{-1})	GHSV (h^{-1})	% NH_3 inlet flow	T (°C)	conv (%)	H_2 rate (mmol g^{-1} s^{-1})	E_a (kJ mol^{-1})	TOF (s^{-1})	ref
Ru	9.1	C				50	400				0.5	227
Ru	25	C		30000		100	400	42	0.23	54		186
Ru	4.6	C	Ba			20	400			158	1.64	194
Ru	9.1	C	Ba	1500000		5.7	400			158	0.56	185
Ru		C	Cs	30000		100	400	90	0.50			186
Ru	4.6	C	Cs			20	400			134	5.10	194
Ru	9.1	C	Cs	1500000		5.7	400			134	1.48	185
Ru	2.7	C	K	15000		30	400	56		57	2.9	213
Ru	9.1	C	K			50	400			139	34.7	170
Ru	3.5	$CaAlO_x$		6000		100	450	78				212
Ru	1.8	CaO		15000		30	400	15		84	2.6	213
Ru	2.9	CaO		9000		100	400	7		96	0.20	73
Ru	2.8	CaO	K	9000		100	400	60		75	1.25	73
Ru	2	CeO_2		13800	3067	57	400	77			1.8	219
Ru	1	CeO_2 rods		22000		100	350	32		151	3.2	210
Ru	7	CeO_2 rods		6000		29	350	23		83	0.034	211
Ru	7	CeO_2 rods	Na	6000		29	350	25		86	0.046	211
Ru	1	CeO_2 spheres		22000		100	350	25				210
Ru	5	CMK-3		30000		100	550	23	0.12			183
Ru	5	CMK-3		30000		100	550	23	0.12			187
Ru	5	CMK-3	Ca	30000		100	550	49	0.25			187
Ru	5	CMK-3	Cl	30000		100	550	37	0.19			187
Ru	5	CMK-3	K	30000		100	550	79	0.40			187
Ru	5	CMK-3	Li	30000		100	550	15	0.08			187
Ru	5	CMK-3	Na	30000		100	550	51	0.26			187
Ru	5	CMK-3	PO_4	30000		100	550	34	0.17			187
Ru	5	CMK-3	SO_4	30000		100	550	36	0.18			187
Ru	3.9	CNFs		9900		5	450	72				175
Ru	7.9	CNFs		6500		100	400	55		183	0.05	176
Ru	10	CNFs		36000		100	500				0.2	228
Ru	0.8	CNTs		42000		100	550	44			22.5	174
Ru	1.7	CNTs		25200		100	500	17				229
Ru	2	CNTs		20000		10	400	18				173
Ru	2	CNTs		36000		100	450		0.18			230
Ru	2	CNTs		6000		100	450	82				231
Ru	2.5	CNTs		30000		100	450	18		87	1.1	214
Ru	3.2	CNTs		6500		100	400	8				176
Ru	3.5	CNTs		6000		100	450	21				212
Ru	4.8	CNTs		60000		100	400	12		71		169
Ru	4.8	CNTs		30000		100	450		0.24	69	2.3	180
Ru	4.85	CNTs		60000		100	400	9	0.08			188
Ru	5	CNTs		30000		100	500	88	0.47	69		156
Ru	5.0	CNTs		6000		100	450	69				171
Ru	5	CNTs		30000		100	550	85	0.43			183
Ru	5	CNTs		60000		5	400	84		89		232
Ru	5	CNTs										233
Ru	7	CNTs		5200		100	327	2		97	0.002	168
Ru	7	CNTs		20000		29	400	34		81	0.05	172
Ru	7	CNTs		6000		29	350	2		104	0.004	211
Ru	7.0	CNTs		5200	33	100	450	50				226
Ru	4.8	CNTs	Ba	60000		100	400	20		65		169
Ru	4.8	CNTs	Ca	60000		100	400	15		70		169
Ru	4.8	CNTs	Ce	60000		100	400	26		63		169
Ru	7	CNTs	Cs	5200			327	46		60	0.04	167
Ru	7	CNTs	Cs	5200		100	327	14		59	0.04	168
Ru	4.8	CNTs	K	60000		100	400	63		54	4.8	169
Ru	4.8	CNTs	K	30000		100	450		0.54	56	5.1	180
Ru	4.85	CNTs	K	60000		100	400	62	0.70			188
Ru	5	CNTs	K	150000		100	500	28	0.80	56		156
Ru	4.8	CNTs	La	60000		100	400	17		67		169

https://doi.org/10.1021/acs.iecr.1c00843
Ind. Eng. Chem. Res. 2021, 60, 18560−18611

Table 2. continued

active phase	wt %	support	promoter	WHSV (mL g^{-1} h^{-1})	GHSV (h^{-1})	% NH_3 inlet flow	T (° C)	conv (%)	H_2 rate (mmol g^{-1} s^{-1})	E_a (kJ mol^{-1})	TOF (s^{-1})	ref
Ru	4.8	CNTs	Li	60000		100	400	33		64		169
Ru	4.8	CNTs	Na	60000		100	400	41		61		169
Ru	7	CNTs	Na	6000		29	350	58		85	0.088	211
Ru	4.85	CNTs-MgO		60000		100	400	13	0.10			188
Ru	4.85	CNTs-MgO	K	60000		100	400	80	0.88			188
Ru	5	Cr_2O_3		30000		100	450	11		76	3.5	234
Ru	3	$Cs_2Ti_6O_{13}$		42000		29						191
Ru	4.8	Er_2O_3		18000		100	350	11				193
Ru	5	fly ashes		60000		100	550	7	0.07			205
Ru	5	fumed SiO_2		30000		100	500	26				164
Ru	5	fumed SiO_2	K	30000		100	500	28				164
Ru	5	GC		30000		100	550	95	0.49			183
Ru	5	GNP		15000	12000	10	375	35		73		235
Ru	5	GNP	K	15000	12000	10	375	62				235
Ru	5	GNP	Na	15000	12000	10	375	44				235
Ru		graphene		20000		100	450	91	0.35			182
Ru	2	graphite		36000		100	600	93				236
Ru	7	graphitized CNTs		5200		100	327	14		68	0.01	168
Ru	7	graphitized CNTs	Cs	5200		100	327	72		54	0.07	168
Ru	2.6	HNTs		12600		100	525	81			8.75	209
Ru	3	$K_2Ti_6O_{13}$		42000		29						191
Ru	4.8	La_2O_3		18000		100	350	19		42	0.43	193
Ru	5	La_2O_3		3000		100	350	40				216
Ru	5	La_2O_3	Cs_2O	3000		100	350	73				216
Ru	4.8	La_2O_3	K	18000		100	350	33		35	3.66	193
Ru	3	La_2O_3−ZrO_2		4000		100	450	4				198
Ru	3	La_2O_3−ZrO_2	$NaBH_4$	4000		100	450	7				198
Ru	0.7	La−Al_2O_3		2300		10	500	98		72		192
Ru	5	MCM-41		30000		100	500	24				164
Ru	5	MCM-41	K	30000		100	500	29		50	7.2	164
Ru	4.6	$MgAl_2O_4$	Ba			20	400			124	0.46	194
Ru	4.6	$MgAl_2O_4$	Cs			20	400			105	0.54	194
Ru	1	MgO		22000		100	350	11			0.6	210
Ru	1	MgO		3000		100	350	11				216
Ru	2.0	MgO		15000		30	400	33		82	1.5	213
Ru	2.8	MgO		30000		100	450	41			7	201
Ru	2.9	MgO		30000		100	450	12		103	1.6	214
Ru	3.5	MgO		36000		100	450	53	0.35	83	3	202
Ru	4.7	MgO		60000		100	400	6	0.07	99	0.33	237
Ru	4.8	MgO		30000		100	450		0.17	62	4.0	180
Ru	4.85	MgO		60000		100	400	7	0.07			188
Ru	5	MgO			15000	100	450	16		124		238
Ru	5	MgO		150000		100	500	13	0.37	62		156
Ru	5	MgO		60000		5	400	47		86		232
Ru	2.0	MgO	Cs	15000		30	400	53		68	2.5	213
Ru	2.8	MgO	Cs	30000		100	450	61				201
Ru	2.8	MgO	K	30000		100	450	57				201
Ru	3.5	MgO	K	36000		100	450	87	0.47	58		202
Ru	4.6	MgO	K	30000		100	400	11	0.06		0.31	195
Ru	4.8	MgO	K	9000		100	400	39	0.11			73
Ru	4.85	MgO	K	60000		100	400	22	0.25			188
Ru	5	MgO	K	30000		100	450	29				179
Ru	5	MgO	K	60000		5	400	76		51		232
Ru	2	MgO-Al_2O_3		30000		100	500	86				196
Ru		MgO-MIL-101		15000		100	400	45				203
Ru		MgO-MIL-101	Cs	15000		100	400	88				203
Ru	4.6	$Mg_yAl_zO_n$	K	30000		100	400	17	0.10		0.61	195
Ru		MIL-101		15000		100	400	42				203
Ru		MIL-101	Cs	15000		100	400	66				203
Ru	4.7	MWCNT	K	9000		100	400	31	0.09			73

https://doi.org/10.1021/acs.iecr.1c00843
Ind. Eng. Chem. Res. 2021, 60, 18560−18611

Table 2. continued

active phase	wt %	support	promoter	WHSV (mL g^{-1} h^{-1})	GHSV (h^{-1})	% NH_3 inlet flow	T (°C)	conv (%)	H_2 rate (mmol g^{-1} s^{-1})	E_a (kJ mol^{-1})	TOF (s^{-1})	ref
Ru	3	$Na_2Ti_3O_7$		42000		29						191
Ru	5.1	N-CNFs		9900		5	450	86				175
Ru	0.8	N-CNTs		42000		100	550	61			18.8	174
Ru	2	N-CNTs		20000		10	400	37				173
Ru	7	N-CNTs		20000		29	400	48		85	0.07	172
Ru	5.0	N-OMC		6000		100	450	85		37		171
Ru	3.7	O-CNFs		9900		5	450	69				175
Ru	5.0	OMC		6000		100	450	59				171
Ru	5	Pr_6O_{11}		3000		100	350	41				215
Ru	5	Pr_6O_{11}	BaO	3000		100	350	20				215
Ru	5	Pr_6O_{11}	CaO	3000		100	350	19				215
Ru	5	Pr_6O_{11}	Cs_2O	3000		100	350	93			0.3	215
Ru	5	Pr_6O_{11}	Gd_2O_3	3000		100	350	25				215
Ru	5	Pr_6O_{11}	K_2O	3000		100	350	61				215
Ru	5	Pr_6O_{11}	La_2O_3	3000		100	350	22				215
Ru	5	Pr_6O_{11}	Li_2O	3000		100	350	36				215
Ru	5	Pr_6O_{11}	MgO	3000		100	350	25				215
Ru	5	Pr_6O_{11}	Na_2O	3000		100	350	49				215
Ru	5	Pr_6O_{11}	Pr_6O_{11}	3000		100	350	27				215
Ru	5	Pr_6O_{11}	Rb_2O	3000		100	350	66				215
Ru	5	Pr_6O_{11}	Sm_2O_3	3000		100	350	21				215
Ru	5	Pr_6O_{11}	SrO	3000		100	350	21				215
Ru	5	Pr_6O_{11}	Yb_2O_3	3000		100	350	20				215
Ru	5	red mud		60000		100	550	17	0.19			205
Ru	5.5	red mud		240000		100	550	24		92		204
Ru	5	SBA-15		30000		100	500	25				164
Ru	5	SBA-15	K	30000		100	500	27				164
Ru	4.9	Sepiolite	K	9000		100	400	47	0.13			73
Ru		Sibunit		34200	17100	100	450	13				181
Ru		Sibunit	K	34200	17100	100	450	23				181
Ru	4.8	SiO_2		18000		100	350	4				193
Ru	5	SiO_2		6000		100	450	62				212
Ru	10	SiO_2		30000		100	450	36	0.19	82	10.5	158
Ru	1	SiO_2–Al_2O_3		3000		100	350	3				216
Ru	3	TiO_2		42000		29						191
Ru	4.8	TiO_2		30000		100	450		0.15	61	3.1	180
Ru	4.8	TiO_2		18000		100	350	1				193
Ru	5	TiO_2		150000		100	500	12	0.32	63		156
Ru	7	titanate NTs	Na	6000		29	350	6		96	0.009	211
Ru	0.5	ZrO_2		4600		100	500	60			0.025	199
Ru	3	ZrO_2		3000		100	500	43				197
Ru	5	ZrO_2		150000		100	500	10	0.27	66		156
Ru	3	ZrO_2	Ba	3000		100	500	29				197
Ru	0.5	ZrO_2	Ca, La	4600		100	500	87			0.038	199
Ru	5	ZrO_2	K	150000		100	500	19	0.53	57		156
Ru	0.5	ZrO_2	La	4600		100	500	86			0.039	199
Ru	0.5	ZrO_2	Mg, La	4600		100	500	84			0.031	199
Ru	0.5	ZrO_2	Sr, La	4600		100	500	76			0.046	199
Ru	4.85	ZrO_2–KOH		150000		100	350	18	0.49	47	4.9	200
Ru	4.85	ZrO_2–KOH	K	150000		100	350	15	0.41	48	4.7	200

catalytic activity compared to Ru/Pr_6O_{11} and Ru/La_2O_3.[216] Catalysts based on ruthenium that are used to decompose ammonia and their catalytic performances are reported in Table 2.

3.1.2.2. Other Noble Metals. Other noble metals tested in the decomposition of ammonia are rhodium and platinum. For example, using Rh/SiO_2 promoted with Nb, Maeda et al.[239] verified a superior catalytic activity to that of a catalyst composed of Rh supported on Nb_2O_5. Platinum supported on alumina was tested by Richardson et al.,[240] obtaining low catalytic activity. Catalysts based on noble metals other than ruthenium used to decompose ammonia and their catalytic performances are reported in Table 3.

3.1.3. Non-noble Metals. Among the non-noble metals used as catalysts for the decomposition of ammonia, nickel is the element most studied as it shows remarkable activity. Again, the type of support has an important effect on the catalytic performance. Testing Fe and Ni catalysts supported on activated

https://doi.org/10.1021/acs.iecr.1c00843
Ind. Eng. Chem. Res. 2021, 60, 18560−18611

Table 3. Catalysts Based on Noble Metals Other than Ruthenium Used to Decompose Ammonia and Their Catalytic Performances at 1 atm

active phase	wt %	support	promoter	WHSV (mL g^{-1} h^{-1})	GHSV (h^{-1})	% NH_3 inlet flow	T (°C)	conv (%)	H_2 rate (mmol g^{-1} s^{-1})	E_a (kJ mol^{-1})	TOF (s^{-1})	ref
Ir	1	Al_2O_3				100	580				0.79	155
Ir	10	Al_2O_3		30000		100	450			82	0.7	158
Ir	10	SiO_2		30000		100	450	8	0.04	72	2.1	158
Pd					20600	100	450	13				241
Pd	0.5	Al_2O_3				100	580				0.02	155
Pd		CNTs		30000		100	500	5	0.02	100		156
Pd	1	SiO_2			20600	100	450	16				241
Pt	1	Al_2O_3				100	580				0.02	155
Pt	1.7	Al_2O_3					700	80				240
Pt	0.5	C			7500	100	570			100	0.07	242
Pt		CNTs		30000		100	500	4	0.02	88		156
Pt		MCM-41		5100		100	500		0.124			243
Pt	10	SiO_2		5100		100	500		0.084			243
Rh	0.5	Al_2O_3				100	580				2.26	155
Rh		CNTs		30000		100	500	15	0.07	81		156
Rh	5	Nb_2O_5				2.5						239
Rh	0.5	SiO_2	Nb_2O_5			2.5						239

carbon, Donald et al.[244] obtained a conversion with the Fe catalyst significantly higher with respect to the Ni catalyst. However, both catalysts showed good medium-term stability, demonstrating a progressive activation in 10 h of reaction. Comparing the catalytic activity of the transition metals Ni, Fe, and Co dispersed in an alumina matrix, Gu et al.[245] obtained a higher catalytic activity with the cobalt catalyst, followed by the Ni catalyst and finally the lowest catalytic activity was obtained with Fe/Al_2O_3. All three catalysts showed high stability for the decomposition reaction after more than 70 h. The same order of catalytic activity was obtained with the catalysts supported on MgO modified with La[246] and on CNTs.[247] Similarly, Yanran et al.[248] compared the decomposition of ammonia in the presence of Fe and Co catalysts and concluded that the latter has a higher activity (85 vs 30% conversion at 500 °C). Conversely, both catalysts showed a decrease in activity after a second reaction cycle, although the addition of lanthanum to the catalyst resulted in a better stability for both catalysts. Comparing the catalytic results of different types of low-ordered carbon with and without adding Fe or Ca, Xu et al.[249] showed that an increase in conversion can be obtained with the catalyst promoted with Fe, while adding Ca has a detrimental effect on the reaction.

3.1.3.1. Nickel. As mentioned above, the commercially available catalysts used for the industrial ammonia crackers are primarily composed of nickel supported on alumina. Catalysts based on nickel as active phase that are used to decompose ammonia and their catalytic performances are reported in Table 4. The work presented by Zhang et al.[251] reported that the best TOF with Ni/Al_2O_3 catalysts is obtained with a particle size of metallic Ni between 1.8 and 2.9 nm, and that doping alumina with lanthanum increases the catalytic activity. In terms of H_2 production, they obtained comparable results with Ru catalysts.[252] Nickel has shown to have good synergy with rare earths, in particular La and Ce, used as promoters or in the form of oxides as support. In this sense, Yan et al.[253] prepared a catalyst composed of Ni, $Ni_{0.5}Ce_{0.5}O_x$, $Ni_{0.5}Al_{0.5}O_x$, or $Ni_{0.5}Ce_{0.1}Al_{0.4}O_x$ porous microspheres, and concluded that the catalyst composed of nickel and cerium gave better results compared to $Ni_{0.5}Al_{0.5}O_x$, while $Ni_{0.5}Ce_{0.1}Al_{0.4}O_x$ allowed the stability of the catalyst to increase. Okura et al.[254] tested different rare earth (Y, La, Ce, Sm, Gd) and Al oxides as supports for Ni, obtaining the highest conversion with Y_2O_3. Similar results were obtained by Nakamura and Fujitani[255] comparing the supports Y_2O_3, CeO_2, MgO, La_2O_3, Al_2O_3, and ZrO_2. However, the highest TOF value was obtained with the ZrO_2 support. In a similar study carried out by Muroyama et al.,[256] the catalytic activity of supported Ni followed the trend: $Al_2O_3 \approx La_2O_3 > SiO_2 > MgO \approx CeO_2 > TiO_2 > ZrO_2$.

To improve the catalytic performance of Ni, rare earth promoters appear to have a positive effect. On the Ni/Al_2O_3 catalyst, Okura et al.[257] found that the promoting effect followed the trend La ≈ Pr ≈ Nd > Y > Sm > Eu ≈ Gd > Ce. They also investigated the catalytic activity of oxides or mixtures of oxides as a support for Ni, obtaining a trend of the catalytic activity that correlates well with the basicity of the materials:[258] $BaZrO_3 > SrZrO_3 > SmAlO_3 \approx GdAlO_3 > SrTiO_3 > LaAlO_3 \approx BaTiO_3 > Al_2O_3 > CaMnO_3 > CaZrO_3 > SrMnO_3 > BaMnO_3 > MnO_2 > NaNbO_3 > CaTiO_3 \approx KNbO_3 > Nb_2O_5 > TiO_2 > ZrO_2$. The catalysts supported on oxide mixtures showed superior catalytic activity compared to those prepared using simple oxides. In a similar way, Liu et al.[259] observed that the conversion of ammonia increases when Ni microfibers are modified with Al_2O_3 and CeO_2. Similar catalyst compositions were tested by Zheng et al.,[260] who doped Ni catalysts supported on alumina with ceria. The results showed that the addition of CeO_2 improves the activity and the stability of the catalyst, and it is believed that ceria increases the dispersion of Ni, improves its reducibility, and decreases metal sintering. Vacharapong et al.[261] studied the same composition, but Ce was added to the support, and Liu et al.[262] verified the promoting effect of Ce and La oxides on a Ni catalyst supported on SBA-15, obtaining an increase in conversion with CeO_2 of around 10% at 500 °C, and a limited increase using La_2O_3 (2%). In all these cases the ammonia conversion improved significantly as a result of the addition of CeO_2 to the catalyst composition. Ceria is a well-known catalyst or catalyst component, and it is used in many applications due to its redox properties and ability to disperse and prevent sintering of metal nanoparticles through robust metal-support interactions.[263−266]

https://doi.org/10.1021/acs.iecr.1c00843
Ind. Eng. Chem. Res. 2021, 60, 18560−18611

Table 4. Catalysts Based on Nickel as Active Phase Used to Decompose Ammonia and Their Catalytic Performances at 1 atm

active phase	wt %	support	promoter	WHSV (mL g^{-1} h^{-1})	GHSV (h^{-1})	% NH_3 inlet flow	T (°C)	conv (%)	H_2 rate (mmol g^{-1} s^{-1})	E_a (kJ mol^{-1})	TOF (s^{-1})	ref
Ni				30000		100	500	10	0.08			161
$Ni_{0.5}Ce_{0.1}Al_{0.4}O_x$				18000		100	500	88		118		253
$Ni_{0.5}Ce_{0.1}O_x$				18000		100	500	81		137		253
$Ni_{0.5}Al_{0.5}O_x$				18000		100	500	48		114		253
Ni					12000	100	500	1			0.27	255
Ni					10000	100	600	39		115	1.20	259
Ni					20600	100	450	12				241
Ni			Al_2O_3		10000	100	600	63		109	0.21	259
Ni			CeO_2		10000	100	600	65		113	0.51	259
Ni			CeO_2/ Al_2O_3		10000	100	600	81		105	0.30	259
Ni		@Al_2O_3		30000		100	450	9				162
Ni		@MgO		30000		100	450	10				162
Ni		@SiO_2		30000		100	500	36	0.20	63	6.5	161
Ni		@SiO_2	Ce	30000		100	500	40				161
Ni		@SiO_2	Ce			100	600	87	0.49	57		271
Ni		@SiO_2	La	30000		100	500	47	0.26			161
Ni	5	AC			6000	100	500	24			1.9	284
Ni	10	AC		30000		100	500	2				285
Ni	13	AC			45000	0.2	750	75				244
Ni		Al_2O_3		6000000		15	540			96	30	251
Ni		Al_2O_3		30000		100	450	15	0.08			252
Ni		Al_2O_3		30000		100	450	15				260
Ni		Al_2O_3		60000		100	600	29				288
Ni		Al_2O_3		60000		100	600	17				289
Ni		Al_2O_3			1800	100	650	97				290
Ni	1	Al_2O_3				100	580				4.21	155
Ni	1.7	Al_2O_3				100	500	30				282
Ni	3.6	Al_2O_3				100	550	33		100		278
Ni	8.9	Al_2O_3			9000	100	500	27		92	0.39	279
Ni	10	Al_2O_3		6000		100	450	10				254
Ni	10	Al_2O_3		6000		100	500	35				256
Ni	10	Al_2O_3		6000		100	450	10				257
Ni	10	Al_2O_3		240000	80000	50	500	93				218
Ni	10	Al_2O_3		9000		5.9	400	32				291
Ni	10	Al_2O_3		13800	3067	57	400	8			0.01	219
Ni	20	Al_2O_3		7500		100	500	28		84		261
Ni	20	Al_2O_3		2400		100	500	31	0.007			275
Ni	20	Al_2O_3		7500		100	500	27	0.03	88		276
Ni	30	Al_2O_3			12000	100	500	42			0.39	255
Ni	40	Al_2O_3		6000		100	550	66				258
Ni	71.4	Al_2O_3		30000		100	550	51			0.4	223
Ni	90	Al_2O_3		36000		100	600	93		123		245
Ni		Al_2O_3	Ce	30000		100	450	28				260
Ni	9	Al_2O_3	Ce	6000		100	450	15				257
Ni	20	Al_2O_3	Ce	7500		100	500	51		83		261
Ni	9	Al_2O_3	Eu	6000		100	450	16				257
Ni	9	Al_2O_3	Gd	6000		100	450	16				257
Ni	9	Al_2O_3	La	6000		100	450	20				257
Ni	9	Al_2O_3	Nd	6000		100	450	20				257
Ni	9	Al_2O_3	Pr	6000		100	450	20				257
Ni	9	Al_2O_3	Sm	6000		100	450	18				257
Ni	9	Al_2O_3	Y	6000		100	450	19				257
Ni	20	Al_2O_3	Zr	7500		100	500	29	0.04			276
Ni	8	Al−$Ce_{0.8}Zr_{0.2}O_2$			9000	100	500	58		67	0.48	279
Ni	38.6	attapulgite		30000		100	650	90	0.50	75		273
Ni	8.7	attapulgite@SiO_2		30000		100	650	73	0.41	80		273
Ni	40	$BaMnO_3$		6000		100	550	46				258
Ni	40	$BaTiO_3$		6000		100	550	75				258

https://doi.org/10.1021/acs.iecr.1c00843
Ind. Eng. Chem. Res. 2021, 60, 18560−18611

Table 4. continued

active phase	wt %	support	promoter	WHSV (mL g^{-1} h^{-1})	GHSV (h^{-1})	% NH_3 inlet flow	T (°C)	conv (%)	H_2 rate (mmol g^{-1} s^{-1})	E_a (kJ mol^{-1})	TOF (s^{-1})	ref
Ni	40	$BaZrO_3$		6000		100	550	94				258
Ni	5	C			13000	10	400	19				224
Ni	40	$CaMnO_3$		6000		100	550	54				258
Ni	40	$CaTiO_3$		6000		100	550	36				258
Ni	40	$CaZrO_3$		6000		100	550	51				258
Ni	10	$Ce_{0.6}Zr_{0.3}Y_{0.1}O_2$		6000		100	350	7	0.007	47	0.52	292
Ni	10.7	$Ce_{0.8}Zr_{0.2}O_2$			9000	100	500	48		74	0.34	279
Ni	13.2	$Ce_{0.8}Zr_{0.2}O_2$				100	550	96		54		278
Ni	20	Ce−Al_2O_3		7500		100	500	53		41		277
Ni		CeO_2				100	600	77	0.43	70		271
Ni	3.6	CeO_2				100	550	61		71		278
Ni	10	CeO_2		6000		100	450	3				254
Ni	10	CeO_2		6000		100	500	20				256
Ni	10	CeO_2		6000		100	450	30				292
Ni	10	CeO_2		13800	3067	57	400	13			0.03	219
Ni	30	CeO_2			12000	100	500	60			0.66	255
Ni		CNTs		30000		100	500	9	0.05	90		156
Ni	5	CNTs		6000		100	500	25		121		247
Ni	5	CNTs										233
Ni	5	fumed SiO_2		30000		100	500	7				164
Ni	5	fumed SiO_2	K	30000		100	500	8				164
Ni	10	Gd_2O_3		6000		100	450	16				254
Ni	40	$GdAlO_3$		6000		100	550	81				258
Ni	10	GNP		15000	12000	10	375	17		86		235
Ni	10	GO		30000		100	500	17		65		285
Ni	5	graphene			6000	100	500	<1				283
Ni	10	HY		30000		100	450				0.8	158
Ni	23.6	hydrocalumite		10000		100	500	55				280
Ni	10	HZSM-5		30000		100	450			84	0.1	158
Ni	40	$KNbO_3$		6000		100	550	36				258
Ni	10	La_2O_3		6000		100	450	12				254
Ni	10	La_2O_3		6000		100	500	34				256
Ni	30	La_2O_3			12000	100	500	49			0.61	255
Ni		La−Al_2O_3		6000000		15	540			98	6	251
Ni		La−Al_2O_3		30000		100	450	26	0.15			252
Ni	40	$LaAlO_3$		6000		100	550	76				258
Ni	20	La-MgO		22000		100	400	28		182	0.007[a]	246
Ni		MCF-17		6000		100	500	40				269
Ni	5	MCM-41		30000		100	500	9				164
Ni	7	MCM-41		36000		100	500	58			0.62	270
Ni	5	MCM-41	K	30000		100	500	11		49	1.7	164
Ni		MgO		3000		100	500	56			0.51	281
Ni	6	MgO			1800	100	650	88				290
Ni	10	MgO		6000		100	500	22				256
Ni	30	MgO			15000	100	450	12		144		238
Ni	30	MgO			12000	100	500	51			0.46	255
Ni	15	MgO-Al_2O_3		3000		100	500	59			0.20	281
Ni	41.8	$Mg_yAl_zO_n$		30000		100	550	79			0.7	223
Ni	40	MnO_2		6000		100	550	43				258
Ni	5	MWCNTs			6000	100	500	25				283
Ni	5	MWCNTs			6000	100	500	57			1.3	284
Ni	40	$NaNbO_3$		6000		100	550	39				258
Ni	40	Nb_2O_5		6000		100	550	34				258
Ni	10	OMC		30000		100	500	8				285
Ni	15	red mud		30000		100	500	16		70		286
Ni		SBA-15		30000		100	500	57				262
Ni	5	SBA-15		30000		100	500	7				164
Ni	23.4	SBA-15		30000		100	550	89	0.50			272

https://doi.org/10.1021/acs.iecr.1c00843
Ind. Eng. Chem. Res. 2021, 60, 18560−18611

Table 4. continued

active phase	wt %	support	promoter	WHSV (mL g^{-1} h^{-1})	GHSV (h^{-1})	% NH_3 inlet flow	T (°C)	conv (%)	H_2 rate (mmol g^{-1} s^{-1})	E_a (kJ mol^{-1})	TOF (s^{-1})	ref
Ni		SBA-15	Ce	30000		100	500	66				262
Ni	5	SBA-15	K	30000		100	500	8				164
Ni		SBA-15	La	30000		100	500	59				262
Ni	5.2	sepiolite		2000		100	550	82	0.03	105		274
Ni		SiO_2			20600	100	450	4				241
Ni	10	SiO_2		30000		100	450	4	0.02		1.0	158
Ni	10	SiO_2		6000		100	500	31				256
Ni	10	SiO_2		36000	1200	100	550	50		108		268
Ni	65	SiO_2−Al_2O_3		30000		100	450	9	0.05	92		158
Ni	66	SiO_2−Al_2O_3		7200		100	450	34			0.003	32
Ni	10	Sm_2O_3		6000		100	450	15				254
Ni	40	$SmAlO_3$		6000		100	550	81				258
Ni	20	Sr−Al_2O_3		7500		100	500	45		43		277
Ni	40	$SrMnO_3$		6000		100	550	48				258
Ni	40	$SrTiO_3$		6000		100	550	80				258
Ni	40	$SrZrO_3$		6000		100	550	90				258
Ni	5	SWCNTs			6000	100	500	<1				283
Ni	10	TiO_2		6000		100	500	16				256
Ni	40	TiO_2		6000		100	550	31				258
Ni	10	Y_2O_3		6000		100	450	18			0.9	254
Ni	10	Y_2O_3		6000		100	450	23				292
Ni	30	Y_2O_3			12000	100	500	61			0.42	255
Ni	20	Y−Al_2O_3		7500		100	500	43		43		277
Ni	1.6	zeolite				100	500	61		113		282
Ni	20	Zr−Al_2O_3		7500		100	500	49		42		277
Ni	10	ZrO_2		6000		100	500	4				256
Ni	10	ZrO_2		6000		100	450	13				292
Ni	30	ZrO_2			12000	100	500	31			0.81	255
Ni	40	ZrO_2		6000		100	550	27				258
Ni	20	ZrO_2−Al_2O_3		2400		100	500	42	0.010			275
Ni	20	ZrO_2−Al_2O_3		7500		100	500	43	0.05	86		276
Ni	5	ZSM-5		30000		100	650	98	0.55	88		293

[a]Calculated at 300 °C.

In the case of nickel catalysts, silica has also been tested as a support in various forms, such as SiO_2, mesoporous structures, or as a natural mineral. Choudhary et al.[158,267] tested various types of silica and zeolites (HY and H-ZSM-5) as a support for Ni, and also a catalyst supported on a mixture of silica and alumina, obtaining the order of catalytic activity: SiO_2−Al_2O_3 > SiO_2 ≈ HY ≫ H-ZSM-5. The relationship between the catalytic activity and porosity using a Ni/SiO_2 catalyst was investigated by Atsumi et al.[268] It was found that the catalyst with the smallest pore diameter (7.7 nm) presented the highest activity at temperatures below 650 °C, while at higher temperatures the conversion was higher with larger pores as a consequence of internal mass transfer issues. Good catalytic activities were also obtained using Ni supported on mesoporous silica MCF-17[269] and MCM-41.[270] Similarly, Yao et al.[161] showed that by encapsulating Ni in SiO_2, the catalytic activity increased more than 25% at 500 °C compared to the noncapsulated catalyst. Moreover, by adding Ce or La to the catalyst, the activity increases by 11 and 4%, respectively, compared to Ni encapsulated in SiO_2 without promoters. The same Ni nanoparticles encapsulated in Al_2O_3 or MgO presented a lower catalytic activity, 9 and 10% conversion at 450 °C, respectively, compared to a conversion of 17% for the catalyst encapsulated in SiO_2.[162] Zhang et al.[271] expanded the study of the Ni catalyst encapsulated in SiO_2 by adding ceria as a promoter, obtaining a higher activity with respect to Ni supported on ceria. By using Ni catalyst supported on SBA-15 mesoporous silica, Liu et al.[272] obtained a higher conversion of ammonia with respect to Ru catalysts supported on various types of carbon under the same reaction conditions.[183] A nickel catalyst supported on attapulgite (a type of clay composed mostly of silica and MgO) was tested and its activity was compared with the same catalyst supported on silica. At parity of Ni content, the Ni/SiO_2 catalyst showed superior activity and stability.[273] In contrast, sepiolite (an abundant Si and Mg mineral) has demonstrated good catalytic results as a Ni support for the decomposition of ammonia.[274]

Other types of compounds tested as supports for Ni are zirconium-based supports. For instance, Henpraserttae et al.[275] tested the use of ZrO_2 as dopant for an alumina support, obtaining an increase in ammonia conversion of 11% at 500 °C compared to the catalyst supported only on alumina. The catalyst supported on the oxide mixture showed superior catalytic activity compared to the catalyst with the promoter added directly to the active Ni phase.[276] The better activity of the Zr-doped sample is attributed to a greater dispersion of Ni, as well as an increase in basic sites. Doping alumina with other elements shows that the catalytic activity follows the order Ce >

https://doi.org/10.1021/acs.iecr.1c00843
Ind. Eng. Chem. Res. 2021, 60, 18560−18611

Table 5. Catalysts Based on Iron as Active Phase Used to Decompose Ammonia and Their Catalytic Performances at 1 atm

active phase	wt %	support	promoter	WHSV (mL g^{-1} h^{-1})	GHSV (h^{-1})	% NH_3 inlet flow	T (°C)	conv (%)	H_2 rate (mmol g^{-1} s^{-1})	E_a (kJ mol^{-1})	TOF (s^{-1})	ref
Fe				30000		100	500	9	0.05			160
Fe				18000		100	500	30	0.002			248
Fe							700	100				297
Fe				15000		100	550	4				298
Fe				24000		100	550	33				308
Fe (Limonite)				45000		0.2	450	88		100		309
Fe				60		100	400	28				312
Fe ($C_{32}H_{16}FeN_8$)				60000		100	600	33				289
Fe (Amomax10)				120000		0.4	500	11				122
Fe						15	550	4				318
Fe			Al, K	1500		0.6	500	66				319
Fe (Magnetite)			Al_2O_3, CaO	30000		100	500	40				296
Fe			CaO, Al_2O_3			5	400			167	0.0110	295
Fe			CaO, Al_2O_3, K_2O			5	400			146	0.0105	295
Fe			CaO, Al_2O_3, K_2O	30000		20	450	17		93		320
Fe			CaO, K_2O	2000		100	500	46		87		321
Fe			K							96		321
Fe	12.4		La	18000		100	500	11				248
Fe	58.1		TiO_2, CaO, Al_2O_3, K_2O, SiO_2, Mn				700	100				297
Fe		@Al_2O_3		30000		100	450	9				162
Fe		@CeO_2		24000		100	550	70				308
Fe		@SiO_2		30000		100	500	27	0.15			160
Fe		@SiO_2		120000		100	400	10				305
Fe		@SiO_2		30000		100	450	8	0.05	69		306
Fe		@SiO_2	Cs	30000		100	450	17	0.09	61		306
Fe		@SiO_2−Cs		30000		100	450	16	0.09	63		306
Fe		@TiO_2		24000		100	550	60				308
Fe	13	AC			45000	0.2	750	90				244
Fe		Al_2O_3		60		5	400	77				312
Fe	1	Al_2O_3				100	580				0.33	155
Fe	10	Al_2O_3		240000	80000	50	500	25				218
Fe	90	Al_2O_3		36000		100	600	86		127		245
Fe	5.1	C/SBA-15		60000		100	600	32				288
Fe	5.9	carbon			45000	0.2	750	96				249
Fe		CeO_2		60		5	400	88				312
Fe		CeO_2/ZrO_2		60		100	400	97		21		312
Fe	12.2	CMK-5		60000		100	600	74				288
Fe	3.5	CNFs		6500		100	600	51				317
Fe	3.2	CNFs/CMFs		18000		100	550	15				315
Fe	3.5	CNFs-mica		6500		100	600	99		94		317
Fe		CNTs		30000		100	500	2	0.01	149		156
Fe	2.8	CNTs			5000	100	700	75				163
Fe	5	CNTs		6000		100	500	15		142		247
Fe	5	CNTs		36000		100	550		0.07	147		322
Fe	66	CNTs										233
Fe	5.9	coal char				0.2	750	96				123
Fe	1.29	GC		6000		100	600	71				313
Fe	24	GC	K	375000		20	400			166	0.016	314
Fe	20	La-MgO		22000		100	400	3		197	0.002[a]	246
Fe	48	MgO		120000		3	450	6				311
Fe	24	MgO	Al	120000		3	450	3				311
Fe	28	MgO	Ga	120000		3	450	24		70		311
Fe	3.5	Mica		6500		100	600	85				317

https://doi.org/10.1021/acs.iecr.1c00843
Ind. Eng. Chem. Res. 2021, 60, 18560−18611

Table 5. continued

active phase	wt %	support	promoter	WHSV (mL g^{-1} h^{-1})	GHSV (h^{-1})	% NH_3 inlet flow	T (°C)	conv (%)	H_2 rate (mmol g^{-1} s^{-1})	E_a (kJ mol^{-1})	TOF (s^{-1})	ref
Fe	31	SBA-15		15000		100	550	18				298
Fe		SiO_2		60		5	400	61				312
Fe		SrO		60		5	400	61				312
Fe	10	Y_2O_3−ZrO_2		46000		100	550	6				323
Fe		ZrO_2		60		100	400	57				312
Fe	5	ZSM-5		30000		100	500	13				307

[a]Calculated at 300 °C.

Zr > Sr > Y.[277] Deng et al.[278] modified the support of a Ni/CeO_2 catalyst with ZrO_2, obtaining an increase in conversion of 30% compared to the catalyst with the unmodified support, and an increase of almost three times compared to a catalyst composed of Ni/Al_2O_3 with the same metal content. A Ni alumina catalyst modified with CeO_2−ZrO_2 was tested by Sima et al.,[279] obtaining a remarkable increase in catalytic activity. Other modifications of the alumina support were tested by Zhao et al.,[280] who prepared a catalyst composed by Ni introduced into the hydrocalumite double-layered hydroxide structure. Similarly, Su et al.[223] tested a Mg−Al double-layered hydroxide as a support for Ni and concluded that its activity was similar to that of Ru/Al_2O_3, but did not exceed the one obtained with Ru/Al_2O_3 promoted with K. The activity of the Ni/MgO catalyst was compared with that of Ni supported on different compositions of MgO and Al_2O_3 by Sato et al.[281] Using a zeolite support for Ni, Inokawa et al.[282] obtained a conversion three times higher than that of a conventional Ni/Al_2O_3 catalyst. The same authors reported that by changing the catalyst preparation method they were able to reduce the size of the Ni particles from 50 to 5 nm, obtaining significantly better catalytic results (32 vs 61% ammonia conversion at 500 °C).

Carbon-based supports have also been tested in the case of Ni, although they do not show the good synergy with the metal as observed for Ru. Carbon nanotubes (CNTs) and graphene were first tested as supports by Alhamed et al.,[283] but ammonia conversion was only obtained by using Ni supported on CNTs, which in turn presented higher conversion values compared to Ni/AC.[284] By using oxidized graphene (GO) as a support for Ni, Meng et al.[285] reported a higher catalytic activity compared to Ni supported on ordered mesoporous carbon or activated carbon (17 vs 8 and 2% at 500 °C, respectively). Finally, red mud has also been used as a low cost support for Ni.[286,287]

3.1.3.2. Iron. As already mentioned, catalysts active for the Haber-Bosch synthesis of ammonia, such as the iron catalyst promoted with K_2O, Al_2O_3, and CaO, were initially tested to decompose ammonia.[294,295] A catalyst prepared by melting magnetite with Al_2O_3 and CaO resulted in good catalytic activity.[296] A catalyst composed by a natural iron mineral with impurities of TiO_2, CaO, Al_2O_3, K_2O, SiO_2, and Mn showed good activity, but is unstable over time, with a rapid decrease in a 3 h test.[297] The same behavior was obtained with a reference catalyst composed only of Fe_2O_3.[297] Through *in situ* experiments, Tseng et al.[298] claimed that the active form of catalysts composed of Fe is Fe_3N_x, while at high temperatures (>675 °C) FeN_x is formed, which has a negative influence on ammonia conversion. A Fe_2O_3 catalyst supported on SBA-15 mesoporous silica shows better catalytic activity than the bare iron oxide (18 vs 4% at 500 °C).[298] Pelka et al.[299] observed that the catalytic decomposition reaction rate of ammonia is higher in the case of nanocrystalline iron compared to iron nitride Fe_4N. The decrease of ammonia conversion in the presence of Fe_4N has also been evidenced with a Fe catalyst promoted with Al_2O_3, CaO, and K_2O with or without SiO_2.[300−303] Temperature influences the degree of nitriding, being favored at temperatures above 400 °C.[304] Also in the case of iron, encapsulation in an oxide has been shown to improve the catalytic activity of the catalyst. Li et al.[160] compared Fe nanoparticles alone and encapsulated in silica, finding that the latter are considerably more active (conversion of 9 vs 27% at 500 °C). The encapsulation of Fe particles in SiO_2 has been demonstrated to significantly increase the stability of Fe for the reaction.[305] Adding Cs to this catalyst, Li et al. obtained around twice the conversion of ammonia at 450 °C with respect to the catalyst without promoting.[306] Also, by encapsulating Fe nanoparticles in Al_2O_3, the catalytic activity showed an increase with respect to SiO_2 under the same reaction conditions (9 vs 4% at 450 °C).[162]

By varying the proportions between the oxides of Si and Al, the acid−base characteristics of the support and the interaction between the metal and the support can be modulated, obtaining an improvement in the conversion of ammonia by increasing the basicity of the catalyst.[307] In this sense, Cui et al.[308] compared the activity of iron oxide alone or modified with cerium or titanium oxide, obtaining a higher and more stable conversion over time in the case of composite catalysts. It is worth mentioning that the modification with ceria was the most effective. Using natural limonite, a Fe mineral with small amounts of Si, Al, Ca, and Mg, Tsubouchi et al.[309] obtained good conversion values and proposed that the decomposition of ammonia catalyzed with Fe proceeds through a cyclic mechanism that involves both metallic iron and its nitride form. Similarly, a series of Fe catalysts supported on MgO and promoted with Ga were prepared and tested for the decomposition of ammonia, obtaining good activity compared to a catalyst composed only of Fe,[310] and also with respect to Fe/MgO and Fe/MgO promoted with Al.[311] Other supports that have been used for Fe are SiO_2, Al_2O_3, CeO_2, SrO, ZrO_2, and CeO_2−ZrO_2, obtaining the highest conversion with the ceria-zirconia mixture.[312] It is important to mention that 40% of the N_2 produced during the reaction was incorporated into the catalyst to form Fe_2N.

The synergy between Fe and carbon-based supports are superior to the case of nickel. Supported on ordered mesoporous carbon CMK-5, Fe showed superior catalytic activity compared to Ni/Al_2O_3 and to Fe supported on a mixture of carbon and SBA-15 (74 vs 32 and 29% at 600 °C, respectively).[288] Moreover, high activity and stability can be obtained when graphitized carbon (GC) is used as support for Fe.[313] When K is added to a Fe catalyst supported on GC, the catalytic activity in the decomposition of ammonia increases.[314] In a similar way, Ji

https://doi.org/10.1021/acs.iecr.1c00843
Ind. Eng. Chem. Res. 2021, 60, 18560−18611

Table 6. Catalysts Based on Cobalt As Active Phase Used to Decompose Ammonia and Their Catalytic Performances at 1 atm

active phase	wt %	support	promoter	WHSV (mL g^{-1} h^{-1})	GHSV (h^{-1})	% NH_3 inlet flow	T (°C)	conv (%)	H_2 rate (mmol g^{-1} s^{-1})	E_a (kJ mol^{-1})	TOF (s^{-1})	ref
Co				18000		100	500	85	0.003			248
Co				18000		100	500	21				325
Co				18000		100	500	18				327
Co				22000		100	400	28				246
Co				24000		100	500	5	0.02			337
Co						15	550	25				318
Co			Al_2O_3,CaO,K_2O	24000		100	500	40	0.14			337
Co_3O_4			CaO,Al_2O_3,K_2O	19544		100	500	85				326
Co	6.8		La	18000		100	500	63				248
Co		@SiO_2		30000		100	450	4				162
Co	5	AC			6000	100	500	34				329
Co	7.0	AC		5200	33	100	450	2				226
Co	1	Al_2O_3				100	580				1.33	155
Co	5	Al_2O_3		36000		100	500	21				338
Co	90	Al_2O_3		36000		100	600	100		123		245
Co	90	Al_2O_3		18000		100	500	44	0.9	148		325
Co	90	Al_2O_3		18000		100	500	57				327
Co	7.0	AX-21		5200	33	100	450	25		89		226
Co	7.0	AX-21	Cs	5200	33	100	450	3				226
Co	10	$Ce_{0.6}Zr_{0.3}Y_{0.1}O_2$		6000		100	350	7	0.008	50	0.54	292
Co	10	CeO_2		6000		100	450	30				292
Co	4.1	CNTs			20000	100	700	100				163
Co	5	CNTs		6000		100	500	61		93		247
Co	5	CNTs		36000		100	550		0.18	79		322
Co	5	CNTs										233
Co	7.0	CNTs		5200	33	100	450	8		94		226
Co	7.0	CNTs	Cs	5200	33	100	450	9				226
Co	20	La-MgO		22000		100	400	37		167	0.009[a]	246
Co	5	MCM-41		36000		100	500	28				339
Co	7.0	MESO-C		5200	33	100	450	10		104		226
Co	20	MgO		22000		100	400	25				246
Co	5	MgO-Al_2O_3			6000	100	550	32		192		331
Co	5	MgO-CeO_2			6000	100	550	69		81		331
Co	5	MgO-La_2O_3			6000	100	550	92		67		332
Co	7.0	MSC-30		5200	33	100	450	12		102		226
Co	7.0	MSC-30	Cs	5200	33	100	450	10				226
Co	10	MWCNTs			6000	100	500	75		69		328
Co	5	MWCNTs			6000	100	500	61				329
Co	5	RGO			6000	100	500	4				329
Co		silicate		150000		100	600	51	1.2			335
Co		silicate	KOH	150000		100	600	67	1.7			335
Co	42	SiO_2								155		334
Co		sodium silicate		150000		100	600	71	1.6			336
Co	5	SWCNTs			6000	100	500	2				329
Co	6.5	Ti-NT		6000		30	550	25		85		330
Co	14	Ti-NT	Na	6000		30	550	41		89		330
Co	10	Y_2O_3		6000		100	450	28				292
Co	10	ZrO_2		6000		100	450	19				292

[a]Calculated at 300 °C.

et al.[315,316] tested Fe catalysts supported on carbon nanofibers (CNFs), obtaining an outstanding catalytic activity. Duan et al.[317] compared the Fe/CNFs catalyst with a Fe catalyst supported on mica and a mixture of the two materials. The Fe/CNFs-mica catalyst showed superior activity and stability, which could be related to a better dispersion of the Fe particles. Ohtsuka et al.[123] used Fe and Ca catalysts supported on lignite doped with Fe and Ca ions and obtained a higher ammonia conversion with respect to a Fe catalyst supported on activated carbon. Finally, an organic compound, Fe(II) phthalocyanine ($C_{32}H_{16}FeN_8$), was used in the ammonia decomposition reaction, obtaining higher conversion of ammonia than with a commercial Ni/Al_2O_3 catalyst (33 vs 17% at 600 °C).[289] Catalysts based on iron as an active phase used to decompose ammonia and their catalytic performances are reported in Table 5.

3.1.3.3. Cobalt. Although cobalt is less active than iron in the ammonia synthesis, it is more efficient in the ammonia

https://doi.org/10.1021/acs.iecr.1c00843
Ind. Eng. Chem. Res. 2021, 60, 18560−18611

Table 7. Catalysts Based on Molybdenum as Active Phase Used to Decompose Ammonia and Their Catalytic Performances at 1 atm

active phase	wt %	support	promoter	WHSV (mL g^{-1} h^{-1})	GHSV (h^{-1})	% NH_3 inlet flow	T (°C)	conv (%)	H_2 rate (mmol g^{-1} s^{-1})	E_a (kJ mol^{-1})	TOF (s^{-1})	ref
Mo				15000		100	500	13				340
Mo	5	Al_2O_3		36000		100	500	22				338
Mo		C		15000		100	600	66		137		344
Mo	5	MCM-41		36000		100	500	28				339
Mo	10	Y_2O_3–ZrO_2		46000		100	550	10				323
Mo_2C					7500	100	570			151	18.3	242
Mo_2C				36000		100	600	77		89		236
Mo_2N				22000		100	550	94	0.4	139		342
Mo_2N					170000	100	500	10		148		345
Mo_2N				15000		100	500	100				346
Mo_2N					6000	100	500	27		131		347
Mo_2N				6000		100	550	72		131		348
Mo_2N				6000		100	550	72		131		349
Mo_2N				6000		100	550	69		97		350
Mo_2N					6000	100	500	27		131		351
MoN					7500	100	570			151	12.6	352
MoN	25.9	C		15000		100	600	89		124		344
MoN	51	SBA-15		60000		100	500	62				157
MoN	80	SiO_2		60000		100	500	50				157
MoN_x	10	Al_2O_3			1800	100	650	99				290
MoS_2	5.7	Al-laponite			19200	10	600	46	0.23		4.1	341
MoS_2	6.0	laponite			24000	10	600	35	0.16		3.6	341
MoS_2	5.9	Ti-laponite			16000	10	600	75	0.24		4.0	341
MoS_2	6.1	Zr-laponite			16000	10	600	94	0.29		4.5	341

decomposition reaction.[324] However, cobalt in its oxide form does not show good catalytic activity in the decomposition of ammonia.[325] In the work of Zhang et al. the conversion of ammonia using Co_3O_4 reaches its maximum at a reaction temperature of 500 °C, while at higher temperatures the conversion decreases.[325] Czekajło and Lendzion-Bieluń[326] were able to increase the conversion by adding the oxides of Al, Ca, and K as promoters. The addition of promoter oxides is believed to stabilize the surface area of the catalysts. Therefore, by adding a small amount of alumina (10 wt %) to cobalt oxide, the conversion of ammonia increased significantly.[325] Using a catalyst with the same composition, Gu et al.[327] obtained a similar result; the conversion increased by around 20% compared to pure cobalt oxide.

Using cobalt supported on different forms of carbon (CNTs, AX-21, MSC-30, MESO-C, and AC), Torrente-Murciano et al.[226] found that the use of Cs as a promoter causes a decrease in conversion compared to the nonpromoted form, which constitutes an opposite behavior with respect to Ru catalysts supported on carbon.[185] Co was also studied supported on carbon nanotubes, showing good catalytic activity.[328] In a comparison of different carbon supports for Co, multiwalled carbon nanotubes (MWCNTs) showed better results than activated carbon (AC), reduced graphene oxide (RGO), and single-walled carbon nanotubes (SWCNTs).[329]

Lara-García et al.[330] demonstrated the promoting effect of Na on a cobalt catalyst supported on titania nanotubes. They observed that the best catalytic results were obtained with the catalyst with Co particles of 15 nm, which is in agreement with the literature that reports the highest activity for Co nanoparticles with dimensions between 10 and 20 nm.[144] Podila et al.[331] studied cobalt catalysts supported on different mixed oxide systems of MgO with Al_2O_3, La_2O_3, and CeO_2, obtaining the following order of the catalytic activity: La_2O_3 > CeO_2 > Al_2O_3. The best catalytic activity of the Co/MgO-La_2O_3 catalyst was attributed to its higher basicity compared to other formulations, and different preparations were tested to optimize its activity.[332,333] Similarly, Hu et al.[246] verified the promoting effect of La on the activity of Co supported on MgO. The conversion of pure ammonia at 400 °C increases by 12% with respect to the nonpromoted catalyst. A Co catalyst supported on SiO_2 was also tested by Hu et al.[334] Co shows good activity when silicates are used as support. In this sense, the use of cobalt incorporated into a structured mesoporous silicate increased notably the ammonia conversion.[335] Similarly, cobalt incorporated in the structure of a sodium silicate showed high activity.[336] Catalysts based on cobalt as the active phase used to decompose ammonia and their catalytic performances are reported in Table 6.

3.1.3.4. Molybdenum. Another non-noble metal that has been studied for the decomposition of ammonia is Mo. Catalysts based on molybdenum as the active phase used to decompose ammonia and their catalytic performances are reported in Table 7. Molybdenum oxide (MoO_3) showed low catalytic activity, but it could be improved through a mechanochemical pretreatment (ball milling).[340] In successive cycles, the catalyst increased its catalytic activity due to the formation of molybdenum nitride, which is catalytically active and is formed during the reaction. Santhana Krishnan et al.[341] tested catalysts with MoS_2 as the active phase supported on laponite and laponite modified with Al, Ti, and Zr, obtaining the best results with the support modified with Zr, reaching a conversion of 94% at 600 °C. They concluded that the modification of the support with heteroatoms allows an increase in both the dispersion of MoS_2 and the basicity of the catalyst. Xu et al.[342] synthesized a Mo_2N catalyst from molybdenum oxide nanobelts, which showed an

https://doi.org/10.1021/acs.iecr.1c00843
Ind. Eng. Chem. Res. 2021, 60, 18560−18611

Table 8. Catalysts Based on Carbides and Nitrides of Metals Other than Molybdenum Used to Decompose Ammonia and Their Catalytic Performances at 1 atm

active phase	wt %	support	promoter	WHSV (mL g^{-1} h^{-1})	GHSV (h^{-1})	% NH_3 inlet flow	T (°C)	conv (%)	H_2 rate (mmol g^{-1} s^{-1})	E_a (kJ mol^{-1})	TOF (s^{-1})	ref
CrN				60000		100	500	0				233
Fe_2N				60000		100	500	4				359
Fe_2N										181		233
Fe_3C				15000		100	550	23				355
MnN				60000		5	500	15				360
MnN				60000		100	500	3				233
TaC					7500	100	570			134	9.24	354
TiN				60000		100	500	0				233
V_8C_7					7500	100	570			146	12.9	242
VN				22000		100	550	22		194		342
VN					7500	100	570			218	0.8	352
VN					7500	100	380	25				353
VN				60000		100	500	1				233
W_2N				22000		100	550	36		173		342
WC				120000		0.4	500	22		166		122
WC				66000		1.8	500	100				357
WZ				120000		0.4	500	18		209		122
ZrON				1500		0.6	500	12		187		319
ZrON/ZrO_2	49/51			750		0.41	500	30		106		358

ammonia conversion around 3 times higher compared to VN and W_2N nitrides under the same reaction conditions. Liu et al.[157] carried out a systematic study of a large number of supported transition metals on SiO_2 and concluded that MoN_x could be a promising catalyst for the decomposition of ammonia. When the catalytic activity of MoN_x supported on SiO_2 is compared with that obtained with SBA-15, a higher ammonia conversion is obtained with the second support (62 vs 50% at 500 °C). The same authors also studied the influence of the MoN_x/SBA-15 catalyst preparation method to achieve its optimization.[343]

Molybdenum carbide catalysts are also promising candidates for the decomposition of ammonia. Zheng et al.[236] prepared and tested Mo_2C. The catalyst had a tendency to form MoN when pure ammonia was used at high temperature (600 °C), which caused a significant loss of specific surface area. Anyhow, the catalyst was less active than Ru supported on graphite.[236] Similarly, Li et al.[344] tested catalysts composed by MoO_2 and Mo_2C nanoparticles dispersed in a porous carbon matrix, observing that they rapidly formed MoN under reaction, which turned out to be the active phase.

3.1.3.5. Carbides and Nitrides. Choi[242] tested various forms of vanadium carbides and compared their activity with that of Mo_2C, showing that in all cases it is lower than that of the molybdenum catalyst, while it is notably higher than that of a catalyst composed of Pt supported on carbon. In another work, Choi et al.[352] compared the activity of vanadium and molybdenum carbides with the corresponding nitrides, VN and MoN. The results showed that the carbides of the two elements are more active for the decomposition of the ammonia. However, the VN catalyst showed superior activity with respect to $Ni/Al_2O_3-SiO_2$.[353] Also, the tantalum carbide TaC showed a good activity, comparable to that obtained using the other nitrides and carbides.[354] Finally, using Fe_3C iron carbide, Kraupner et al.[355] obtained good ammonia conversion and high stability at 600 °C. Pansare et al.[122,356] studied the conversion of ammonia using tungsten carbide and zirconium tungstate as catalysts, obtaining a higher conversion in both cases compared to a conventional Fe catalyst (22, 18, and 11% at 500 °C, respectively). A modified tungsten carbide catalyst studied by Cui et al.[357] showed noticeably higher activity. Zirconium was also tested in the form of zirconium oxynitride, ZrON, and it showed good catalytic activity in decomposing ammonia when mixed with ZrO_2.[358] However, it shows limited and lower catalytic activity compared to a nonpromoted iron oxide catalyst.[319] Catalysts based on carbides and nitrides of metals other than molybdenum used to decompose ammonia and their catalytic performances are reported in Table 8.

3.1.4. Bimetallics and Multimetallics. Among the bimetallic and multimetallic catalysts tested in the ammonia decomposition reaction, combinations of the metals Co, Mo, Ni, Fe, Pt, Cu, Ir, Cr, Mn, Mg, Cu, Sn, Zn, Li, and Pd have been used, and combinations of Ru with Fe, Sr, Bi, Pb, Sn, In, Cd, Zn, Au, Ag, Cu, Pt, Pd, Ni, Ir, Rh, Co, Os, Re, Mn, W, Mo, Cr, Ta, Nb, Hf, Zr, Y, Sc, Ca, and Mg have been studied. However, the combination of cobalt and molybdenum is one of the most studied bimetallic catalysts since it exhibits significant catalytic activity. By testing an unsupported Co−Mo catalyst, Duan et al.[361] observed that the active phase of the bimetallic catalyst was, indeed, Co_3Mo_3N. The bimetallic Co_3Mo_3N catalyst showed higher conversion than the monometallic form, Mo_2N.[347,348] Also, the catalyst composed of Fe_3Mo_3N prepared by nitriding $FeMoO_4$ showed a higher catalytic activity than the monometallic nitride, Mo_2N.[349] Similarly, catalysts composed of Co−Mo in its nitride form promoted with K, Ba, La, Ce, and Zr were tested, showing that the promoter effect follows the order: La > Ba > K ≈ Ce, while Zr exhibits a promotion effect only at a temperature higher than 500 °C.[362] Following the results obtained previously, Srifa et al.[350] tested bimetallic catalysts of Mo combined with Co, Ni, and Fe, prepared by a nitriding process of the corresponding oxides using NH_3 and a temperature of 350 °C. They reported the catalytic activity order Co_3Mo_3N > Ni_3Mo_3N > Fe_3Mo_3N > Mo_2N. The same authors verified that the activity of the Co_3Mo_3N catalyst increased by adding a small amount of Cs;[363] a 22% increase in conversion was measured at 450 °C with respect to the unmodified catalyst. It should be mentioned that

https://doi.org/10.1021/acs.iecr.1c00843
Ind. Eng. Chem. Res. 2021, 60, 18560−18611

similar compositions have also been tested, such as Ni_2Mo_3N, obtaining similar results.[351,350,364]

The compositions presented above have been tested alone or supported on different materials. For example, Liang et al.[290] compared the catalytic activity of MoN_x with that of Ni and $NiMoN_x$ bimetallic catalyst supported on alumina. As a reference, they also prepared the Ni/MgO catalyst and concluded that the bimetallic catalysts had a higher catalytic activity with respect to the monometallic form and that all the prepared catalysts supported on alumina present a higher conversion than Ni/MgO. Similarly, a catalyst composed of Co−Mo was tested supported on SiO_2 and compared with its form promoted with CaP, obtaining an increase in activity until reaching a Ca content of 1 wt %.[365] Nevertheless, when Co−Mo was supported directly on CaP, the catalytic activity was minimal.[365] Lorenzut et al.[323] prepared several Fe and Mo bimetallic catalysts supported on ZrO_2 mixed with Y_2O_3, La_2O_3, and CeO_2, and supported on La_2O_3−Al_2O_3 and $Ce_{0.6}Zr_{0.4}O_2$−Al_2O_3. They verified the superior activity of the bimetallic catalyst supported on ZrO_2−Y_2O_3 that showed a 16% conversion with respect to a conversion of 6% for Fe and 10% for Mo at 550 °C. Among the supports tested, La_2O_3−Al_2O_3 is the one with the best activity. Catalysts composed of Co−Mo have generated a lot of interest in recent times, and have been tested in many types of formulations, for example in its supported form on MCM-41[339] or Al_2O_3.[338,366] In both cases, the bimetallic catalysts showed superior catalytic activity with respect to both monometallic compositions.[339,338]

The use of carbon nanofibers (CNFs) as supports was tested by Xie et al.[228] The nanofiber was combined with a Co−Mo−Fe−Ni-Cu alloy and its catalytic activity was compared with that of a Co−Mo bimetallic catalyst and Ru using the same support. They obtained a TOF 20 times higher than that obtained with Ru, and an even greater increase with respect to the conventional Co−Mo catalyst by varying the amount of Co and Mo in the composition. This multimetallic formulation showed good stability in a 50 h test at 500 °C. Different ceramic supports have also been used to test the catalytic activity of several bimetallic formulations. For instance, Huang et al.[292] compared the catalytic activity of bimetallic catalysts composed of Ni and Co on different oxide supports. The order of catalytic activity of the supports was $Ce_{0.6}Zr_{0.3}Y_{0.1}O_2$ > CeO_2 > Y_2O_3 > ZrO_2. The Ni−Co bimetallic catalyst supported on $Ce_{0.6}Zr_{0.3}Y_{0.1}O_2$ showed an increase in ammonia conversion with respect to the monometallic catalysts, a higher TOF, and a great stability in a 72 h test, demonstrating the synergy between the two metals. Lendzion-Bieluń et al.[367] modified a Fe catalyst promoted with CaO, Al_2O_3, and K_2O with cobalt, and obtained a higher conversion with respect to the monometallic catalyst. They also tested a catalyst with a Fe−Co alloy promoted with CaO, Al_2O_3, and K_2O,[368] and determined that the catalytic activity depends on the nitriding potential of Fe. In contrast, the addition of chromium or manganese leads to a decrease of the activity of the Co catalyst.[337] Wang et al.[318] also tested a Co−Fe bimetallic catalyst and obtained a higher catalytic activity with respect to the monometallic forms of Co and Fe (53 vs 25 and 4% of conversion at 550 °C, respectively). In addition, Zhang et al.[322] observed that the Co−Fe bimetallic catalyst supported on carbon nanotubes is more active than the Fe catalyst on the same support, but it does not exceed the hydrogen production obtained with the Co catalyst. Comparing the catalytic activity of Mg−Fe, Co−Fe and Mg−Co−Fe bimetallic catalysts, Podila et al.[369] obtained an activity that follows the order: Mg−Co−Fe > Mg−Fe > Co−Fe. It is interesting to note that in the bimetallic samples the formation of FeN_2 was not observed. Following their previous works, Simonsen et al.[218] synthesized different catalysts composed of Ni, Fe, and their bimetallic form Ni−Fe supported on various materials. In their tests they considered the change in gas composition throughout the reactor, comparing the catalytic performance in the absence of H_2 and introducing it into the reagent stream to simulate the conditions in the final part of the reactor. Under the conditions of the first part of the reactor, the bimetallic catalyst supported on alumina showed a much higher activity than the Fe catalyst and activity similar to the Ni catalyst supported on the same oxide. With the Ni−Fe bimetallic catalyst they obtained the same conversion as with a Ru on alumina catalyst. In the presence of hydrogen, the Ni catalyst decreases its activity with respect to the bimetallic composition. Regarding the support, they verified that the best catalytic results were obtained with Al_2O_3 and Mg−Al spinels with respect to SiO_2, ZrO_2 and TiO_2.

Bimetallic catalysts have not only been tested with the aim of replacing ruthenium or other noble metals, but also to increase their catalytic activity and to be able to reduce their content in the catalyst. In this sense, McCullough et al.[222] tested more than 100 bimetallic catalysts based on Ru−metal−K supported on Al_2O_3 through a high-throughput method for the decomposition of ammonia at low temperature. For each catalyst they tested three different metal loadings (Ru/Metal = 3:1, 2:2, and 1:3 on a weight basis). They concluded that the bimetallic catalysts that have a higher activity with respect to the K-promoted Ru catalyst follow the order of activity Ir ≈ Sc ≈ Zr ≈ Ta > Sr ≈ Y > Ca > Mg > Hf. The K-promoted Ru−Sr and Ru−Fe catalysts supported on Al_2O_3 showed higher TOF values than the K-promoted Ru/Al_2O_3 catalyst (1.8, 1.0, and 0.3 s^{-1} at 400 °C, respectively, using pure ammonia). Ruthenium bimetallic catalysts have not only been tested to increase catalytic activity, but also to increase stability. Thus, Chen et al.[231] prepared a Ru−Fe catalyst supported on CNTs obtaining a slightly lower catalytic activity than the monometallic Ru/CNTs catalyst, but a superior long-term stability (60 h).

Varisli and Rona[243] compared the H_2 production of Pt−Ni and Pt−Sn catalysts supported on SiO_2 and MCM-41.They reported a higher activity of the monometallic Pt/MCM-41 compared to the bimetallic forms, and that Pt−Ni/MCM-41 presents a very low ammonia conversion. In contrast, the bimetallic catalyst supported on SiO_2 had a slightly higher activity compared to the monometallic catalyst. Chellappa et al.[370] also estimated the apparent activation energy for a Ni−Pt bimetallic catalyst supported on alumina and found that it is very similar to that obtained for nickel, concluding that platinum behaves more like a stabilizer to prevent sintering of nickel active sites instead of increasing catalytic activity.

A catalyst composed of Ni−Pd[241] exhibited superior catalytic activity compared to monometallic catalysts. The bimetallic catalyst demonstrated the synergistic effect of Pd and Ni for the decomposition of ammonia. A bimetallic catalyst composed of Ir and Ni supported on alumina also presented good catalytic results, with a 12% higher conversion at 500 °C with respect to the monometallic Ni/Al_2O_3 catalyst under the same reaction conditions.[291] Similarly, Dasireddy and Likozar[250] prepared a bimetallic catalyst composed of Cu and Zn supported on alumina, demonstrating its superior catalytic activity with respect to the corresponding monometallic catalysts (78 vs 61 and 15% at 500 °C, respectively). The same authors also improved the activity and stability of the Cu−Zn/Al_2O_3 catalyst

https://doi.org/10.1021/acs.iecr.1c00843
Ind. Eng. Chem. Res. 2021, 60, 18560−18611

Table 9. Catalysts with Bimetallic and Multimetallic Active Phase Used to Decompose Ammonia and Their Catalytic Performances at 1 atm

active phase	wt %	support	promoter	WHSV (mL g^{-1} h^{-1})	GHSV (h^{-1})	% NH_3 inlet flow	T (°C)	conv (%)	H_2 rate (mmol g^{-1} s^{-1})	E_a (kJ mol^{-1})	TOF (s^{-1})	ref
Co_3Mo_3N					6000	100	500	39		93		347
Co_3Mo_3N				6000		100	550	97		60		348
Co_3Mo_3N				6000		100	550	94		70		350
Co_3Mo_3N				6000		100	450	26		86	0.7	363
Co_3Mo_3N			Cs	6000		100	450	48		71	1.3	363
Co−Cr			Al_2O_3,CaO,K_2O	24000		100	500	35	0.12			337
Co−Fe						15	550	53				318
Co−Fe					6000	100	550	77		63		369
Co−Fe			CaO,Al_2O_3,K_2O	24000		100	500	13				368
Co−Fe	5	CNTs		36000		100	550		0.17	110	5.4	322
Co−Mn			Al_2O_3,CaO,K_2O	24000		100	500	23	0.10			337
Co−Mo				36000		100	550	37				361
Co−Mo	5	Al_2O_3		36000		100	500	55				338
Co−Mo	5/8	Al_2O_3		30000		5	527	60		106		366
Co−Mo	2.5/2.5	CaP		6000		100	500	10				365
Co−Mo	10	CNFs		36000		100	500	5			0.06	228
Co−Mo	5	MCM-41		36000		100	500	52				339
Co−Mo	2.5/2.5	SiO_2		6000		100	500	20		82		365
Co−Mo	5	SiO_2		36000		100	500	15				339
Co−Mo	2.5/2.5	SiO_2	CaP	6000		100	500	24		76		365
Co−Mo−Fe−Ni−Cu	9.3	CNFs		36000		100	500	100		123	7.0	228
$CoMoN_x$	10/2	CNTs			11000	10	550	50				362
$CoMoN_x$	10/2	CNTs	Ba		11000	10	550	67				362
$CoMoN_x$	10/2	CNTs	Ce		11000	10	550	50				362
$CoMoN_x$	10/2	CNTs	K		11000	10	550	56				362
$CoMoN_x$	10/2	CNTs	La		11000	10	550	83				362
$CoMoN_x$	10/2	CNTs	Zr		11000	10	550	50				362
Cu−Zn	50/30	Al_2O_3		60000		9.8	500	78	0.60	56		250
Fe_3Mo_3N				6000		100	550	78		73		349
Fe_3Mo_3N				6000		100	550	75		89		350
Fe−Mo	5/5	$Ce_{0.6}Zr_{0.4}O_2$−Al_2O_3		46000		100	550	17				323
Fe−Mo	5/5	CeO_2−ZrO_2		46000		100	550	16				323
Fe−Mo	5/5	La_2O_3−Al_2O_3		46000		100	550	50				323
Fe−Mo	5/5	La_2O_3−ZrO_2		46000		100	550	16				323
Fe−Mo	5/5	Y_2O_3−ZrO_2		46000		100	550	16				323
Li_3FeN_2				60000		100	500	31				359
Mg−Co−Fe					6000	100	550	99		45		369
Mg−Fe					6000	100	550	86		59		369
Ni_2Mo_3N					6000	100	500	87		66		351
Ni_3Mo_3N				6000		100	550	83		84		350
Ni−Co	1−9	$Ce_{0.6}Zr_{0.3}Y_{0.1}O_2$		6000		100	350	10	0.012	41	0.68	292
Ni−Fe	2/8	Al_2O_3		240000	80000	50	500	98			0.037	218
Ni−Fe	2/8	Mg−Al spinel		240000	80000	50	500	98				218
Ni−Fe	2/8	SiO_2		240000	80000	50	500	35				218
Ni−Fe	2/8	TiO_2		240000	80000	50	500	9				218
Ni−Fe	2/8	ZrO_2		240000	80000	50	500	60				218
Ni−Ir	10/0.7	Al_2O_3		9500		5.9	400	44				291
$NiMoN_x$					21600	100	500	29				364
$NiMoN_x$	6/10	Al_2O_3			1800	100	650	100				290
Pd−Ni					20600	100	450	50		64		241
Pd−Ni			Ca		20600	100	450	85		59		241
Pt−Ni		Al_2O_3				100	540	97		47		370
Pt−Ni		MCM-41		5100		100	500		0.009			243
Pt−Ni		SiO_2		5100		100	500		0.086			243
Pt−Sn		MCM-41		5100		100	500		0.103			243
Pt−Sn		SiO_2		5100		100	500		0.089			243
Ru−Ag	3/1	Al_2O_3	K	30000		1	300	64				222
Ru−Au	3/1	Al_2O_3	K	30000		1	300	58				222
Ru−Bi	3/1	Al_2O_3	K	30000		1	300	23				222

https://doi.org/10.1021/acs.iecr.1c00843
Ind. Eng. Chem. Res. 2021, 60, 18560−18611

Table 9. continued

active phase	wt %	support	promoter	WHSV (mL g^{-1} h^{-1})	GHSV (h^{-1})	% NH_3 inlet flow	T (°C)	conv (%)	H_2 rate (mmol g^{-1} s^{-1})	E_a (kJ mol^{-1})	TOF (s^{-1})	ref
Ru−Ca	3/1	Al_2O_3	K	30000		1	300	91				222
Ru−Cd	2/2	Al_2O_3	K	30000		1	300	29				222
Ru−Co	3/1	Al_2O_3	K	30000		1	300	43				222
Ru−Cr	3/1	Al_2O_3	K	30000		1	300	56				222
Ru−Cu	3/1	Al_2O_3	K	30000		1	300	30				222
Ru−Fe	2/2	Al_2O_3	K	30000		1	300	39				222
Ru−Fe	3/1	Al_2O_3	K	5400		100	400	44		248	0.97	222
Ru−Fe	1.7	CNTs		6000		100	450	85				231
Ru−Hf	1/3	Al_2O_3	K	30000		1	300	82				222
Ru−In	3/1	Al_2O_3	K	30000		1	300	24				222
Ru−Ir	3/1	Al_2O_3	K	30000		1	300	100				222
Ru−Mg	3/1	Al_2O_3	K	30000		1	300	90				222
Ru−Mn	2/2	Al_2O_3	K	30000		1	300	47				222
Ru−Mo	3/1	Al_2O_3	K	30000		1	300	18				222
Ru−Nb	1/3	Al_2O_3	K	30000		1	300	17				222
Ru−Ni	3/1	Al_2O_3	K	30000		1	300	55				222
Ru−Ni	2.5/0.5	CeO_2		15000	3660	55	400	50		107	2.0	372
Ru−Os	1/3	Al_2O_3	K	30000		1	300	34				222
Ru−Pb	1/3	Al_2O_3	K	30000		1	300	12				222
Ru−Pd	3/1	Al_2O_3	K	30000		1	300	62				222
Ru−Pt	3/1	Al_2O_3	K	30000		1	300	28				222
Ru−Re	2/2	Al_2O_3	K	30000		1	300	10				222
Ru−Rh	2/2	Al_2O_3	K	30000		1	300	79				222
Ru−Sc	3/1	Al_2O_3	K	30000		1	300	100				222
Ru−Sn	3/1	Al_2O_3	K	30000		1	300	20				222
Ru−Sr	1/3	Al_2O_3	K	30000		1	300	93				222
Ru−Sr	1/3	Al_2O_3	K	5400		100	400	80		156	1.78	222
Ru−Ta	3/1	Al_2O_3	K	30000		1	300	100				222
Ru−W	3/1	Al_2O_3	K	30000		1	300	57				222
Ru−Y	2/2	Al_2O_3	K	30000		1	300	93				222
Ru−Zn	3/1	Al_2O_3	K	30000		1	300	49				222
Ru−Zr	3/1	Al_2O_3	K	30000		1	300	100				222

by varying the composition and the preparation method.[371] Finally, the superior stability of a bimetallic catalyst composed of Ni and Ru supported on ceria compared to Ru/CeO_2 and its superior activity compared to Ni/CeO_2 has recently been demonstrated.[219,372] Catalysts with bimetallic and multimetallic active phases used to decompose ammonia and their catalytic performances are reported in Table 9.

3.1.5. Metal Amides and Imides. The alkali metal amides, such as $LiNH_2$, KNH_2, and $NaNH_2$, have proven to be promising materials in the decomposition of ammonia, offering comparable or better conversion results with respect to catalysts composed of ruthenium. For instance, under the same catalytic conditions, lithium amide showed a much higher activity compared to the Ru/Al_2O_3 and $Ni/SiO_2−Al_2O_3$ catalysts (91 vs 54 and 34% at 500 °C, respectively).[32] Using the amide $NaNH_2$, a conversion equivalent to that of Ru/Al_2O_3 was obtained.[373] Moreover, $NaNH_2$ showed higher conversion than $LiNH_2$ at temperatures below ca. 420 °C, while at higher temperature the two amides presented a similar activity.[32]

It was determined that the active phase of catalysts composed of amides varies according to the reaction conditions and the alkali metal chosen. In the case of Li amides, the active phase is the imide form, −NH.[32] Makepeace et al.[374] prepared lithium imide, modified it with Ca and Mg, and compared the results with a lithium amide−imide mixture. They observed that the modified forms show a higher conversion at low temperatures with respect to the unmodified catalyst (48 and 40 vs 33% at 440 °C, respectively), and that $Li_2Ca(NH)_2$ presents a higher activity with respect to $Li_2Mg(NH)_2$. Moreover, Wood and Makepeace also analyzed the compatibility of the lithium amide−imide catalyst with various support materials: activated carbon, silicon dioxide, aluminum oxide, and magnesium oxide.[375] However, for all configurations there was no improvement in the catalytic performance compared to the unsupported lithium amide−imide. Carbon is not a suitable support despite its high surface area since it reacts with the catalyst to form the lithium carbodiimide species, Li_2NCN. Similarly, silica and alumina are also not good supports because they react with the catalyst and form lithium oxides. In contrast, MgO shows better synergy with amide−imide, allowing the formation of a ternary nitride instead of a ternary oxide, which is active for the decomposition of ammonia. However, there is no consensus in the literature about the role of ternary nitrides in the decomposition of ammonia.[376,377] Bramwell et al.[224] compared the catalytic activity of $LiNH_2$ alone or supported on carbon. In the case of the supported catalyst, no activity was recorded due to the formation of Li_2NCN. However, by adding Ni to the supported catalyst, the reaction can be retarded to 450 °C. Therefore, the $LiNH_2/Ni/C$ catalyst showed higher catalytic activity with respect to $LiNH_2$ (53 vs 13% at 400 °C). When these results are compared with those obtained using a Ru catalyst supported on alumina, the latter allows a 26% higher conversion to $LiNH_2/Ni/C$ at 400 °C under the reaction conditions analyzed.

Amides and imides have been tested alone or in combination with other compounds. For example, Chang et al.[378] prepared

https://doi.org/10.1021/acs.iecr.1c00843
Ind. Eng. Chem. Res. 2021, 60, 18560−18611

Table 10. Catalysts with Metal Amides and Imides As Active Phase Used to Decompose Ammonia and Their Catalytic Performances at 1 atm

active phase	wt %	support	promoter	WHSV (mL g^{-1} h^{-1})	GHSV (h^{-1})	% NH_3 inlet flow	T (°C)	conv (%)	H_2 rate (mmol g^{-1} s^{-1})	E_a (kJ mol^{-1})	TOF (s^{-1})	ref
$K_2[Mn(NH_2)_4]$				60000		5	500	48				360
$Li_2Ca(NH)_2$				7200		100	440	48		120		374
$Li_2Mg(NH)_2$				7200		100	440	40		112		374
Li_2NH				60000		5	400	0		150		232
Li_2NH				60000		100	500	26				233
Li_2NH-Co												233
Li_2NH-CrN												233
Li_2NH-Cu												233
Li_2NH-Fe_2N										50		233
Li_2NH-MnN												233
Li_2NH-Ni												233
Li_2NH-TiN												233
Li_2NH-VN												233
$Li_{2-x}NH_{1+x}$				7200		100	440	33		120		374
$LiNH_2$				7200		100	450	91			0.002	32
$LiNH_2$					13000	10	400	13				224
$LiNH_2$	50	activated charcoal		1800		100	475	23				375
$LiNH_2$	50	Al_2O_3		1800		100	475	60				375
$LiNH_2$	27	C			13000	10	400	0				224
$LiNH_2$	50	MgO		1800		100	475	98				375
$LiNH_2$	50	SiO_2		1800		100	475	88				375
Mn_6N_5−CaNH				36000		100	450	20		86		380
MnN-KNH_2	39.1			13500		100	465	21		88	1.2	378
MnN−Li_2NH				20000		100	550	90		75		379
MnN-$LiNH_2$	49.9			13500		100	465	58		80	2.0	378
MnN-$NaNH_2$	46.7			13500		100	465	20		89	0.9	378
$NaNH_2$				7200		100	450	55			0.002	32
$NaNH_2$				60000		100	500	20				233
Ni-KNH_2	8/20	GNP		15000	12000	10	375	44		63		235
Ni-$LiNH_2$	27	C			13000	10	400	53				224
Ni-$NaNH_2$	8/20	GNP		15000	12000	10	375	33		62		235
$Rb_2[Mn(NH_2)_4]$				60000		5	500	68				360
Ru−$Ba(NH_2)_2$	4.4			60000		100	400	20	0.13	73	1.29	237
Ru−$Ca(NH_2)_2$	4.6			60000		100	400	8	0.08	77	0.42	237
Ru-KNH_2	0.8/20	GNP		15000	12000	10	375	96		53		235
Ru-$LiNH_2$	5	MgO		60000		5	400	100		53		232
Ru−$Mg(NH_2)_2$	5.0			60000		100	400	3	0.02	101	0.14	237
Ru-$NaNH_2$	0.8/20	GNP		15000	12000	10	375	97		53		235

catalysts composed of MnN and amides of the metals Li, Na and K through mechanochemical methods, obtaining significantly higher catalytic activity with MnN−$LiNH_2$. The three alkali metals used have shown an ability to promote the decomposition of ammonia (Li > K > Na), which is reversed with respect to when they were used as promoters in other formulations. Therefore, in the case of being linked with $-NH_2$, these metals participate in the reaction as cocatalyst, instead of having only an electronic influence.[378] In this context, Guo et al.[379] analyzed the catalytic activity of MnN combined with the imide Li_2NH and compared the results with a Ru/CNTs catalyst, obtaining a higher activity with the MnN-Li_2NH catalyst under the same reaction conditions. The nitride Mn_6N_5, which is almost inactive in the decomposition of ammonia, showed relatively high catalytic activity when mixed with the imide CaNH.[380]

Other types of catalysts have been prepared by adding amides to ruthenium, typically using mechanochemical methods, such as the alkaline earth metal amides of Ba, Ca, and Mg.[237] Catalytic tests indicated that the best catalytic activity is reached with Ru−$Ba(NH_2)_2$ and Ru−$Ca(NH_2)_2$ with respect to Ru−$Mg(NH_2)_2$ and to the reference catalyst Ru/MgO. Similarly, Guo et al. used MgO as a support for Ru-$LiNH_2$ and compared the catalytic results with Ru/CNTs and Ru/MgO; the latter was also promoted with K.[232] The highest catalytic activity was reached with Ru-$LiNH_2$/MgO, followed by the Ru catalyst supported on carbon nanotubes, the catalyst supported on MgO promoted with K, and finally, the nonpromoted Ru/MgO. Furthermore, with the catalyst composed of lithium imide and ruthenium, complete ammonia conversion was achieved at 400 °C with an ammonia concentration of 5 vol %. In addition, Chang et al.[235] tested Ru and Ni catalysts with Na and K amides supported on graphite nanoplatelets (GNP), obtaining very high ammonia conversion with respect to the same samples prepared through ball milling. Additionally, they were able to compare the effect of doping the $NaNH_2$ and KNH_2 amides with Na and K used as promoters of the Ru/GNP catalyst, obtaining a conversion 53% higher in the case of Ru-$NaNH_2$ and 34% in the case of Ru-

https://doi.org/10.1021/acs.iecr.1c00843
Ind. Eng. Chem. Res. 2021, 60, 18560−18611

KNH_2 at temperatures as low as 375 °C with respect to Ru/GNP promoted with Na and K. The use of the Na and K promoters had already allowed an increase in the ammonia conversion of 9 and 27%, respectively, with respect to the nonpromoted catalyst. It is worth mentioning that doping Ni/GNP with Na amide allowed a higher conversion with respect to KNH_2 (44 vs 33% at 375 °C), although the catalyst undergoes deactivation at lower temperatures.

An exhaustive study on the catalytic activity of catalysts composed of lithium imides and transition metal nitrides (TMN) was carried out by preparing a series of catalysts from the respective chlorides of the transition metals and $LiNH_2$, and a successive nitriding process with NH_3.[233] The Li_2NH-Fe_2N catalyst exhibits a higher ammonia decomposition rate with respect to Fe_2N, Li_2NH, and Fe supported on CNTs. The relative order of the catalytic activity of the transition metals in Li_2NH-TMN at 500 °C is Mn > Co ≈ Fe ≈ Cr > Ni > V > Ti ≈ Cu. In their mixed forms with lithium imide, the nitrides of the transition metals showed a significantly higher activity compared to the form without Li_2NH. In the case of Co, Ni, and Cu, the catalysts were compared with their supported form on CNTs. Using the catalyst Li_2NH-MnN, a higher activity was reported with respect to Ru/CNTs. Wang et al.[359] prepared a catalyst composed of Li_3FeN_2 with which they obtained a 27% higher conversion than with a Fe_2N catalyst. Cao et al.[360] tested catalysts containing ternary amides of the alkali metals K, Rb, and Mn prepared with mechanochemical methods. The results showed that $Rb_2[Mn(NH_2)_4]$ has a catalytic activity higher than $K_2[Mn(NH_2)_4]$ and also higher than a Ru/MgO reference catalyst. Catalysts with metal amides and imides as active phase used to decompose ammonia and their catalytic performances are reported in Table 10.

3.2. Kinetics and Reaction Mechanism. In recent years, a large number of studies have been carried out on the kinetics of ammonia decomposition using different catalysts to determine the expression of the reaction rate and to understand the decomposition mechanism. The first kinetic expressions proposed considered that the decomposition of ammonia followed a first order kinetics,[381,382] which in some cases is still used today.[131,184,250,317,321,341] However, other authors proposed that the reaction rate is a combination of zero order and first order as a function of temperature,[383,384] while more recent studies have shown that the reaction is inhibited by the presence of H_2.[238,385] The inhibition is manifested particularly at low temperatures, and it has been proposed that it is due to the hydrogen that accumulates on the surface of the catalyst.[143] Different methods have been used to determine the expression of the reaction rate; on the one hand, the Langmuir−Hinshelwood−Hougen−Watson (LHHW) approach, which considers coverage-independent parameters.[166,295,386−389] On the other hand, the Temkin−Pyzhev model considers that the associative desorption of nitrogen is the rate-limiting step, and that if the influence of the inverse reaction can be neglected the reaction rate is expressed as a power law.[97,390−392] Finally, the Tamaru model considers that a different model is applied depending on the pressure and temperature conditions.[370,393,394] The model proposed by Tamaru et al. was verified for a W catalyst[395−397] and confirmed to be valid for other types of catalysts as well, such as Pt,[398] VN,[384] Mo_2N,[345] and TiN_xO_y.[394] To determine the parameters of the rate expression, a parameter estimation problem can be applied. This is done by testing different kinetic expressions obtained by alternatively considering each elementary step of the reaction as the rate limiting step to find the one that best fits the experimental results, considering all the other steps in equilibrium (quasi-equilibrium approach).[399]

As proposed by Temkin,[400] the mechanism considered for the decomposition of ammonia occurs following the opposite steps of ammonia synthesis and starts with the adsorption of ammonia on the catalyst surface, followed by subsequent dehydrogenation steps, and finally nitrogen and hydrogen atoms desorb as N_2 and H_2 (eq 1−6):

$$NH_{3(g)} + s \leftrightarrows NH_{3(a)} \quad (1)$$

$$NH_{3(a)} + s \leftrightarrows NH_{2(a)} + H_{(a)} \quad (2)$$

$$NH_{2(a)} + s \leftrightarrows NH_{(a)} + H_{(a)} \quad (3)$$

$$NH_{(a)} + s \leftrightarrows N_{(a)} + H_{(a)} \quad (4)$$

$$2N_{(a)} \leftrightarrows N_{2(g)} + 2s \quad (5)$$

$$2H_{(a)} \leftrightarrows H_{2(g)} + 2s \quad (6)$$

where s represents an empty site on the catalyst surface and the subscript (a) refers to a species adsorbed on the surface.

The first analyses of the reaction kinetics were based on the concept that in the synthesis of ammonia the limiting step of the mechanism is the cleavage of the N−N bond of the nitrogen molecule. Therefore, recombinative desorption of N_2 was proposed as the limiting step of the ammonia decomposition reaction. Logan and Kemball in 1959 analyzed the reaction rates of several catalysts and their dependence on the pressure of ammonia and hydrogen, concluding that, for all the catalysts tested (Ni, Co, Rh, Pt, Ru, Re, Fe, VN, and W) the step that determines the reaction rate is the desorption of nitrogen from the catalyst surface.[401] Actually, the limiting step of the reaction can vary depending on different properties of the catalyst, such as its composition or the architecture of the active sites. For noble metals such as Ru, Rh, Ir, Pt, Pd, or Cu, the cleavage of N−H bonds was proposed as a limiting step,[166] while for metals such as Fe, Co, Ni, or Cr it seems to be the desorption of nitrogen.[155] However, Takahashi and Fujitani[238] obtained a different result analyzing the kinetics of two catalysts composed of Ni or Ru supported on MgO. They concluded that for Ru, nitrogen desorption is the limiting step, as it requires a higher energy, while for Ni the limiting step is the total dehydrogenation of ammonia. This suggests that the catalyst support also has a strong influence on the reaction mechanism. In the case of Ni, it was proposed that the dehydrogenation of NH_3 is the determining step of the reaction rate in the case of supported catalysts with low Ni−N binding energy, and the desorption of nitrogen in the case of high Ni−N binding energy.[255] A similar result was obtained by Hansgen et al.;[402] they concluded that the determining step of the reaction rate is the elimination of the second hydrogen atom (eq 3) for surfaces with a M−N bond energy lower than 125 kcal mol^{-1}, while, for surfaces with higher M−N bond energies, the removal of the first and second hydrogen atoms (eqs 2−3) and the desorption of nitrogen (eq 5) are kinetically significant. These authors developed a method to predict the composition of a bimetallic catalyst with high catalytic activity through the analysis of nitrogen binding energy values. They tested a large number of Pt compositions bound with Ti, V, Cr, Mn, Fe, Co, and Ni, obtaining the energy closest to the optimum (the energy of Ru) with catalysts Pt−Ni−Pt(111), Fe−Pt−Pt(111), and Co−Pt−Pt(111).[403] Duan et al.[404] determined a linear relationship between the apparent

https://doi.org/10.1021/acs.iecr.1c00843
Ind. Eng. Chem. Res. 2021, 60, 18560−18611

activation energy of the nitrogen recombination reaction and the adsorption energy of N on the surfaces of Fe, Co, Ni, and Cu, known as the Brønsted−Evans−Polanyi relationship. The calculated apparent activation energy followed the order: Fe > Co ≈ Ni > Cu. However, by applying this method to Ni−Ru, Ni−Pt, and Ni-WC bimetallic catalysts, which have a similar nitrogen binding energy, Hansgen et al.[405] concluded that this cannot be considered as the only determining factor to evaluate the catalytic activity, since the three compositions have different activity. In this sense, by comparing the binding energy of monometallic Ni and Pt catalysts with their bimetallic forms, Zhong et al.[406] obtained a reduction in the activation energy for the bimetallic Pt−Ni−Pt(111) catalyst. Also, Zheng et al.[236] considered the binding energy of N comparing the nitride and carbide forms of molybdenum, and concluded that although the binding energy of N is stronger on MoN than on Mo_2C, the former is more active due to a greater number of active sites.

One of the first experimental studies of the kinetics of the ammonia decomposition reaction was carried out in 1941 and it focused on a Fe catalyst promoted with Al_2O_3 and K_2O, comparing its behavior with a catalyst promoted only with Al_2O_3, and with an nonpromoted Fe catalyst.[407] The reaction rate of $Fe(K_2O)/Al_2O_3$ showed a linear behavior with respect to temperature. It was proposed that the reaction rate depended on the pressure of ammonia and hydrogen, and that the limiting step in the entire temperature range was the desorption of nitrogen (eq 5). On the contrary, for the other two catalysts, the reaction rate showed a dependence on temperature, and depending on the reaction conditions the limiting step also varied, from the desorption of nitrogen to one of the last two dehydrogenations (eqs 3 and 4). Using a Fe catalyst promoted with Al_2O_3, K_2O, and SiO_2, Takezawa and Toyoshima[408,409] determined a change in the limiting step of the reaction with increasing reaction temperature, from nitrogen desorption to dehydrogenation of NH_2 on the catalyst surface.

By carrying out experiments with other catalysts at low pressures down to ultrahigh vacuum, the same behavior was observed; that is, the limiting step of the reaction can vary, not only according to the type of catalyst and active phase, but also changing the reaction temperature.[70,71] Furthermore, the activation energy can vary in the different ranges of reaction temperature, as in the case of the metals Pt, Ni, Rh, Ta, and W.[70,71] For example, with a Fe catalyst, a variation of the apparent activation energy was determined from a value of 188 kJ mol^{-1} at temperatures up to approximately 370 °C, to 21 kJ mol^{-1} above 440 °C, while at around 580 °C the reaction rate becomes practically independent from temperature.[410] Kunsman in 1928 was already able to determine the change in apparent activation energy according to the reaction temperature for Ni, Mo, W, and Fe catalysts.[411,412] Using an expression similar to Temkin−Pyzhev, Lamb et al.[225] determined for a Ru catalyst supported on alumina and promoted with LiOH an apparent activation energy of 83 kJ mol^{-1} up to 475 °C and of 77 kJ mol^{-1} for higher temperatures. Also, the exponents of NH_3 and H_2 concentrations vary in the two temperature ranges, which are most likely due to a combination of factors, among which there is the inhibition effect of H_2, which can also vary according to the temperature. Tsai and Weinberg[382] reported a change in the limiting step of the reaction and the apparent activation energy for a Ru(001) surface, and McCabe[383] reported a change in the limiting step of the reaction from the desorption of nitrogen to the adsorption of NH_3 on the surface at high temperatures (greater than 727 °C) with a Ni catalyst. Likewise, Rasim et al.[413] observed that, with the use of a Pt catalyst and a Pt−Au bimetallic catalyst at low temperature and high ammonia pressure, the decomposition rate of ammonia has a zero-order dependence on the ammonia pressure, while at high temperature the decomposition rate becomes almost independent of temperature. It is important to mention that the bimetallic catalyst showed superior potential to decompose ammonia. Similarly, Richardson et al.[240] studied a Pt catalyst supported on alumina and confirmed that the mechanism previously proposed by Vajo et al.,[414] who stated that for high temperatures and/or low pressures, the determining step is the dissociation of the first N−H bond, while, at low temperatures and high pressures, the nitrogen desorption is the limiting step and the reaction rate does not depend on the ammonia concentration. In contrast, Egawa et al.[415] observed the opposite behavior with Ru; at low temperatures the reaction rate follows the Temkin−Pyzhev mechanism and the cleavage of the N−H bond is the determining step of the reaction, while at high temperature the reaction rate is proportional to the concentration of ammonia and independent of the concentrations of the products, the limiting step being the desorption of nitrogen. However, Choudhary et al.,[72] focusing on an Ir(100) surface in a pressure range from ultrahigh vacuum to 1.5 Torr, found a constant activation energy and that the limiting step of the reaction is the desorption of nitrogen for all the temperatures used. But a different result was obtained by Huang et al.[416] using the same catalyst; the cleavage of the first two N−H bonds (eqs 2 and 3) needs a similar energy, and those bonds are the determining steps of the reaction, while the desorption of nitrogen has a lower energy barrier than the dehydrogenation steps.

Analyzing the kinetics of the reaction on Ru/CNTs catalysts with different sizes of Ru particles, Zhou et al.[417] observed that although in all cases the recombination of nitrogen is the determining step of the reaction, the apparent activation energy changed with the particle size. In a similar manner, but using a Ru catalyst supported on Al_2O_3, Zheng et al.[217] found a linear relationship between the apparent activation energy and the mean size of Ru particles, with a higher apparent activation energy with small particle sizes.

Considering that the dehydrogenation of NH_3 and the desorption of N_2 are both the determining steps of the ammonia decomposition mechanism, Henpraserttae et al.[277] proposed that by increasing the number of active sites of a Ni/Al_2O_3 catalyst and its basicity, the dehydrogenation of NH_3 would be promoted. At the same time, a high dispersion of Ni would allow a higher number of active sites to be close, increasing the possibility that the adsorbed nitrogen will recombine and desorb to form N_2 gas. Chellappa et al.[370] determined for a Pt−Ni catalyst supported on alumina that at high temperatures (>520 °C) the reaction rate could be expressed using a first order equation, and that under these conditions there is no inhibition by hydrogen. On a Ni/Al_2O_3 catalyst, the inhibition effect of hydrogen on the reaction rate changes according to the temperature range.[418] Similarly, using a Pt catalyst, Tsai et al.[419] reported that hydrogen inhibition depends on temperature, and also on pressure. Comparing the reaction kinetics of Fe and Pt catalysts, Löffler and Schmidt concluded that hydrogen inhibition was strong for Pt,[420] while for Fe the inhibition was observed only at low temperatures and high pressures.[421] For a Ru-ceria catalyst supported on Y_2O_3−ZrO_2 the decomposition rate is first order in ammonia, and hydrogen

https://doi.org/10.1021/acs.iecr.1c00843
Ind. Eng. Chem. Res. 2021, 60, 18560−18611

Table 11. Catalysts Used to Study the Kinetics of Ammonia Decomposition, The Limiting Step of the Reaction Mechanism, and Apparent Activation Energy. The Limiting Step of the Reaction Refers to the Steps Described in eq 1 to 6

active phase	support	promoter	rate limiting step	activation energy (kJ mol^{-1})	ref
Pt			2, 2−4, 3, 4, 5	69−247	70,166,398,401−403,406,413,414,419,421,426,428−430,435
Ta				59	71
Rh			2, 2−4, 4, 5	88−238	71,166,401,426,436
Ni			2, 5	70−286	71,255,270,383,401,402,404,406,412,427−429,432,437−444
W			4, 5	87−300	71,396,401,412,445,446
Ir			2, 3, 2−4, 5	64−131	72,166,416,447,448
Ru	CaO			96	73
Ru	CaO	K		75	73
Ru	Al_2O_3		2, 3, 2−4, 4, 5	92−130	74,155,217,220,221,393,424,449
Co	$MgAl_2O_4$		5		153
Cu	$MgAl_2O_4$		5		153
Fe	$MgAl_2O_4$		5		153
Ni	$MgAl_2O_4$		5		153
Ru	$MgAl_2O_4$		5		153
Co_3Mo_3N			5	70	153,350
Cr	Al_2O_3		5		155
Cu	Al_2O_3		4		155
Ir	Al_2O_3		4		155
Pb	Al_2O_3				155
Se	Al_2O_3				155
Te	Al_2O_3				155
Pt	Al_2O_3		2, 4, 5		155,240
Ni	Al_2O_3		2−4, 5	88−96	155,251,254,255,257,276,393,418
Co	Al_2O_3		2−4, 5		155,393
Fe	Al_2O_3		5	212	155,407
Pd	Al_2O_3		4	132	155,449
Rh	Al_2O_3		4	126	155,449
Pd			2, 2−4, 4	37−130	166,426,427,431,447
Ni	La−Al_2O_3		5	98	251
Ni	Gd_2O_3				254
Ni	Sm_2O_3				254
Ni	CeO_2				254,255
Ni	La_2O_3				254,255
Ni	Y_2O_3				254,255
Ni	ZrO_2				255
Ni	MgO		2−4, 3	144	238,255
Ni	Al_2O_3	Ce			257
Ni	Al_2O_3	Eu			257
Ni	Al_2O_3	Gd			257
Ni	Al_2O_3	La			257
Ni	Al_2O_3	Nd			257
Ni	Al_2O_3	Pr			257
Ni	Al_2O_3	Sm			257
Ni	Al_2O_3	Y			257
Ni	ZrO_2−Al_2O_3		2, 5	86	276
Mo_2C			5	89	236
Mo_2N			5	97−251	236,349,350,450
ZnON			5	187	319
Fe		Al, Ca	5	167	295
Fe		Al, Ca, K	5	93−146	295,302−304,320
Fe_4N				143	299
Fe			1, 2, 3 or 4, 5	68−275	299,324,400,401,403,404,407,410,421,430,437,451
Fe		Al, Ca, K, Si	5		301
Co			4, 5	111−180	324,400,401,403,404
Fe_3Mo_3N			5	73−89	349,350
Ni_3Mo_3N				84	350
Co−Mo	Al_2O_3		5	106	366
Ni−Pt	Al_2O_3		5	47	370
Li_2NH−$Fe_{2-4}N$					376

https://doi.org/10.1021/acs.iecr.1c00843
Ind. Eng. Chem. Res. 2021, 60, 18560−18611

Table 11. continued

active phase	support	promoter	rate limiting step	activation energy (kJ mol^{-1})	ref
$Li_2NH-MnN$			6	75	376,379
Mn					377
Ru			5	91−209	382,401,415,425,430,452,453
Fe		Ca, K			321
Fe		K			321
VN			5	135−209	384,401,454
Ru	MgO		5	124	238
Fe−Cr	Al_2O_3		2−4		393
TiN_xO_y			5	215	394
Co−Fe			5		400
Re			5	137−259	401,430,455
Cr−Pt					402
Mn−Pt					402
Pt−Mn					402
Pt−Ti					402
Pt−V					402
Ti−Pt					402
V−Pt					402
Co−Pt					402,403,429
Fe−Pt					402,403,429
Ni−Pt			2, 5	42	402,405,406,428,429
Cu−Pt					403
Cu			2, 4	87−317	403,431,456,457
Ni−Ru					405
Ni-WC					405
Fe		Al	3 or 4, 5		407
Fe		Al, K	5	183−191	407,411,458
Fe		Al, K, Si	3, 5		409
Fe		Al, Sn			411
Mo					412
Ru	Al_2O_3	LiOH		77−83	225
Pt−Au			2	93	413
Ru	CNTs		5	82	417
Ru	CeO_2−YZ		5	67	422
Ru	C			88	424
Cu−Pd			4	96−275	431
Ni	SiO_2			81	432
Ni−Pd				59	432
Pd	SiO_2			92	432
Mo_3N_2			3	172	433
$NaNH_2$			4, 6		434
GaN					459
Ir	AC				460
Ru	AC				460

has a negligible inhibitory effect on the decomposition rate below 320 °C.[422]

Wang et al.[400] examined the behaviors of Fe, Co, and the Fe−Co bimetallic catalysts, determining that these three metals differ intrinsically. For Fe, the adsorption of ammonia was shown to be the limiting step of the reaction, while for Co both the cleavage of the N−H bond and the desorption of N_2 are slow. For Co−Fe, nitrogen desorption from the catalyst surface was determined as the limiting step. Prasad et al.[220] analyzed the kinetics of the reaction on Ru/Al_2O_3 using different models. They concluded that there is no single limiting step, but that both N_2 desorption and NH_x dehydrogenation reactions are kinetically significant.[221,423] Moreover, for a Ru/C catalyst a dependence on NH_3 concentration close to the first order and a strong H_2 inhibition were observed.[424] The model that best fit the reaction kinetics involved both the cleavage of the NH_2-H bond and the desorption of nitrogen. Observing the kinetics of the reaction on Ru, Mortensen et al.[425] proposed that the mechanism had to consider the diffusion of the adsorbed NH_3 and the diffusion of the reaction products from the active sites, for which the latter step determines the reaction rate.

The analysis of the kinetics of the reaction and the estimation of the apparent activation energy would also make it possible to foresee the formulation of the catalyst that would lead to a higher performance in the conversion of ammonia. For example, by analyzing the kinetics of the decomposition reaction on different exposed faces of Rh, Pt, and Pd, Novell-Leruth et al.[426] determined that the first dehydrogenation (eq 2) is the determining step for Pt(100) and Pd(100), while on Rh(100) the dehydrogenation of NH_3 is relatively fast and the

https://doi.org/10.1021/acs.iecr.1c00843
Ind. Eng. Chem. Res. 2021, 60, 18560−18611

Table 12. Structured Catalysts Used to Decompose Ammonia and Their Catalytic Performances

structured catalyst	catalyst	P (bar)	reactor vol (mL)	total flow (mL min^{-1})	% NH_3 inlet flow	T (°C)	conv (%)	mol H_2 mol_{met}^{-1} s^{-1}	E_a (kJ mol^{-1})	ref
SiN_X reactor	Ir/Al_2O_3	1	0.12	6	100	600	12			103
cordierite monolith covered with Al_2O_3	5 wt % Ru	1		100	100	500	45		104	385
SiCN monolith	Ru	1		2	100	600	80			462
CeO_2 monolith	0.7 wt %Ni	1	1	25	57	500	82			463
cordierite monolith	5 wt %Ni/CeO_2	1	1	25	57	500	53			463
microcanales covered with Al_2O_3	3.5 wt % Ru-0.8 wt % K	1	0.35	145	100	525	88			464
microchannels covered with Al_2O_3	3.5 wt % Ru	1	0.35	145	100	525	75			464
microreactor with posts covered with Al_2O_3	3.5 wt % Ru	1	0.25	145	100	525	51			464
SiC monolith covered with Al_2O_3	5.8 wt % Ru	1	0.55	5	100	500	99			465
stainless steel microchannels	4.7 wt %Ni-0.1 wt % Pt/Al_2O_3	0.9	0.36	50	100	700	99		205	466,381
stainless steel microchannels	8.5 wt % Ru−Cs/Al_2O_3	0.9	0.36	100	100	500	99		117	467,468
silica plate covered with Al_2O_3	0.4 wt % Co	1	0.002		50	575		11.4		469
silica plate covered with Al_2O_3	0.9 wt % Pd	1	0.002		50	575		6.4		469
silica plate covered with Al_2O_3	1.0 wt % Fe	1	0.002		50	575		2.1		469
silica plate covered with Al_2O_3	1.3 wt % Ru	1	0.002		50	575		2.5		469
silica plate covered with Al_2O_3	7.9 wt % Ru−Ba	1	0.002							469
silica plate covered with graphite	10 wt % Ru	1	0.004							470
silica plate covered with graphite	7.2 wt % Ru-28.3 wt % Cs	1	0.004							470
silica plate covered with graphite	8.8 wt % Ru-12 wt % Ba	1	0.004							470
Cordierite monolith covered with Al_2O_3	15 wt % Ni	1		100	100	500	20		153	471
cordierite monolith covered with Al_2O_3	0.18 wt % Ru									472
cordierite monolith covered with Al_2O_3	0.26 wt % Ru/CNFs									472
cordierite monolith covered with Al_2O_3	0.30 wt % Ru/N-CNFs									472
TiO_2 monolith covered with Ca-montmorillonite	8 wt % Fe_2O_3-15 wt % MnO_2	1			1	860	97			473
TiO_2 monolith covered with Na-montmorillonite	5 wt % MnO_2	1			1	750	88			473
stainless steel microfibers	10 wt % Ni/Al_2O_3	1	0.5	15	100	500	56			474
Ni microfibers	10 wt % Ni/Al_2O_3	1	0.5	145	100	600	83			475
Ni microfibers	10 wt % Ni-10 wt % Ce/Al_2O_3	1	0.5	145	100	600	99			475
Ni microfibers	10 wt % Ni-10 wt % La/Al_2O_3	1	0.5	145	100	600	93			475

dehydrogenation of NH (eq 4) limits the reaction rate. From the analysis of the apparent activation energy, it was proposed that Rh was the most efficient catalyst among the three elements considered because it had the lowest apparent activation energy. Stolbov and Rahman[427] analyzed the kinetics of the decomposition reaction on the Ni(111) and Pd(111) surfaces, concluding that ammonia dissociation is the limiting step for Pd. In a similar manner, Guo and Vlachos[428] compared the kinetics of the reaction on Ni, Pt, and bimetallic Ni−Pt catalysts, obtaining that Ni−Pt should be a more active catalyst than Pt and Ni surfaces due to a lower ammonia dissociation energy barrier. Through the analysis of reaction kinetics of various Ni and Pt monometallic catalysts and Ni−Pt and Fe−Pt bimetallic catalysts, Wu et al.[429] concluded that the bimetallic catalysts should be more active. By analyzing Pt, Ru, Fe, and Re catalysts, Shustorovich and Bell[430] determined that the recombinative desorption of nitrogen is the limiting step of the ammonia decomposition reaction, and that Pt is the most efficient catalyst, followed by Ru, Fe, and finally Re. Although the apparent activation energy value calculated for Cu is very high, 317 kJ mol^{-1}, it shows high activity when combined with Pd.[431] Mianowski et al.[432] compared Ni, Pd, and Pd−Ni catalysts supported on SiO_2, obtaining the lowest activation energy with the bimetallic catalyst.

Srifa et al.[350] determined that with the use of bimetallic catalysts made up of Mo combined with Co, Ni, and Fe in their nitride forms, the expression of the reaction rate does not depend on the concentration of N_2, but it depends on that of H_2. Moreover, the inhibition effect by hydrogen decreases compared to that of the catalyst composed only of molybdenum, which explains its higher catalytic activity. A kinetic study of the decomposition using a Mo_3N_2 catalyst concluded that the determining step of the reaction in this case is the second dehydrogenation (eq 3), and that the catalyst has a higher

https://doi.org/10.1021/acs.iecr.1c00843
Ind. Eng. Chem. Res. 2021, 60, 18560−18611

apparent activation energy compared to Ru or V catalysts, confirming its lower catalytic activity.[433]

Okura et al.[254] determined that, for Ni catalysts supported on rare earth (Y, La, Ce, Sm, Gd) and Al oxides, the catalytic activity is governed by the inhibition of hydrogen, the inhibition being particularly severe for Ni/CeO_2 and Ni/Al_2O_3. A similar result was obtained by the same group,[257] who compared the influence of the partial pressure of hydrogen on the reaction rate, obtaining that the catalyst that presents the best results among those of Ni/Al_2O_3 promoted with rare earths (Y, La, Ce, Pr, Nd, Sm, Eu and Gd) is the one modified with La, which is the one that is least inhibited by the presence of H_2. Similarly, Zhang et al.[251] compared Ni/Al_2O_3 with $Ni/La{-}Al_2O_3$ and suggested that the best catalytic activity obtained by adding La to the support is due to its ability to destabilize the reaction intermediates on the active sites, and consequently facilitating their evolution. Sayas et al.[73] observed that K allows a decrease in the H_2 inhibition effect of a Ru/CaO catalyst promoted with K with respect to the nonpromoted catalyst.

The ammonia decomposition using transition metal amides or imides follow a different reaction mechanism, where the functional group ($-NH_2$ or $-NH$) participates.[434] For example, with a MnN-Li_2NH catalyst, the desorption of N_2, which was determined as the most commonly limiting step for nitrides or transition metals, appears to be fast, while the desorption of H_2 is kinetically slow.[379]

Table 11 shows the catalysts used to study the kinetics of ammonia decomposition, the limiting step of the reaction, and the apparent activation energy ranges. A single limiting step has not been determined for most catalysts, which shows that the reaction mechanism does not depend only on the composition of the catalyst, but on many other factors, such as the synthesis method, the metal content, or the reaction conditions. Estimated apparent activation energy values for bimetallic catalysts are generally lower compared to monometallic ones. The lowest values of apparent activation energy are obtained in the case of Ni−Pt and Ni−Pd, while the highest values of apparent activation energy are obtained for Fe, Cu, and Mo_2N catalysts that in turn have low catalytic activity.

3.3. Structured Systems. Since fixed-bed reactors with powder catalysts are not suitable for practical application,[391,461] different structured catalytic reactors have been developed for the decomposition of ammonia. In particular, structured reactors with straight channels (honeycombs) and microreactors are the most common structured reactors developed up to date.[46,148] Table 12 shows the types of structured systems described in the literature used to obtain hydrogen from the catalytic decomposition of ammonia along with the catalysts used, the reaction conditions, and the ammonia conversion or hydrogen production obtained. The apparent activation energy is also included when it was reported.

3.3.1. Types of Structured Systems. In some microreactors, the ammonia decomposition reaction was coupled with exothermic reactions, as discussed in section 2.1, in order to generate the heat necessary for the process and to achieve an autothermal regime, or close to it. Arana et al.[103] designed a reactor composed of four microtubes of SiN_x with a wall thickness of 2 μm coated with an Ir/Al_2O_3 catalyst. In addition, the decomposition reaction of ammonia was coupled with the combustion of butane. Using a power of 1 W they were able to reach a temperature of ~600 °C and an ammonia conversion of 12% at atmospheric pressure. Chen and Yan[98] modeled a parallel plate microreactor with conductive walls with a thickness of 0.3 mm and channels 0.3 mm wide coated with a ruthenium catalyst, where the decomposition of ammonia was coupled with the combustion of methane. Similarly, Kaisare et al.[104] created a model for an analogous catalytic reactor, with parallel plates with catalytic combustion of propane and ammonia decomposition channels that used a Ru/Al_2O_3 catalyst. In a separate work they analyzed a perpendicular configuration of channels.[105] Deshmukh and Vlachos[106] considered propane combustion as an exothermic reaction in channels parallel to the decomposition of ammonia in a microreactor with channels 150 μm wide and a wall thickness of 300 μm using a Ru catalyst. They also created a model to study the best strategy for the thermal coupling of the two reactions.[476] Engelbrecht et al.[99] and Chiuta et al.[100] coupled decomposition with ammonia oxidation in an autothermal parallel plate steel microreactor, using a Ru/Al_2O_3 catalyst.

Another type of microreactor investigated for the decomposition of ammonia is the one containing geometrically distributed posts coated with a catalyst. A 3D-printed SiCN ceramic support with 139 pillars (Figure 6) was impregnated with Ru and tested for the reaction, obtaining an ammonia conversion of 80% at 600 °C.[462] The microreactor maintained its integrity and functionality after prolonged exposure to ammonia at temperatures up to 1000 °C for 48 h. Ganley et al.[464,477] developed a similar post microreactor with Ru/Al_2O_3 and compared its activity with various types of parallel microchannel microreactors with different geometries. The best conversion results were obtained with 140 μm wide microchannels. It is important to mention that the promoting effect of K on Ru/Al_2O_3 was also verified. In a similar manner and by preparing a ceramic microreactor composed of porous silicon carbide with microchannels impregnated with Ru, Christian et al.[465] obtained the best catalytic results with pores having a diameter of 0.75 μm and a complete conversion at 500 °C. Using the 3D printing technique, a microchannel structure

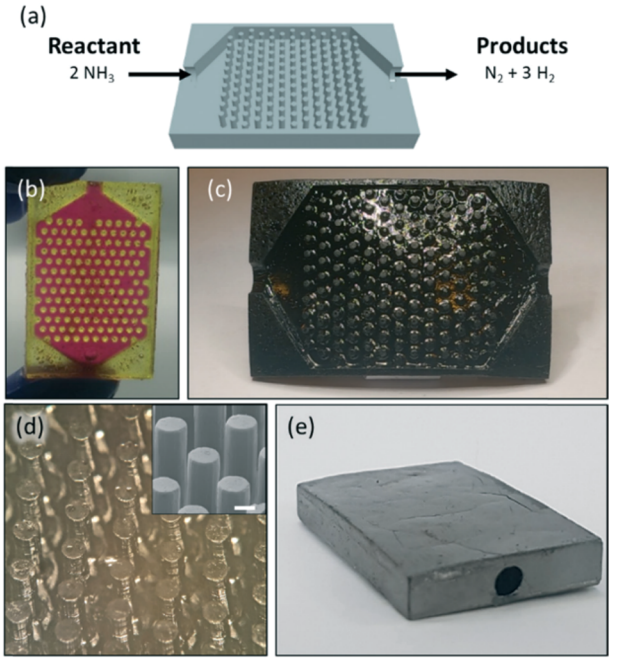

Figure 6. Catalytic microreactor designed for the ammonia decomposition reaction by Gyak et al.[462] Reprinted with permission from ref 462. Copyright 2019 Royal Society of Chemistry.

https://doi.org/10.1021/acs.iecr.1c00843
Ind. Eng. Chem. Res. 2021, 60, 18560−18611

made entirely of cerium dioxide was prepared and subsequently impregnated with nickel. The catalyst thus prepared showed a higher catalytic activity in the decomposition of ammonia than a conventional cordierite monolith washcoated with a catalyst with a similar composition (Ni/CeO_2).[463] Another type of stainless steel microchannel reactor loaded with a $Ni-Pt/Al_2O_3$ bimetallic catalyst deposited on 450 μm wide channels was designed by Chiuta et al.[466] The reactor showed good activity and stability in a 150 h test. Using the same microreactor but with a Ru/Al_2O_3 catalyst promoted with Cs, they obtained total ammonia conversion at 200 °C less than using $Ni-Pt/Al_2O_3$ and a good stability over time.[467]

Dillon et al.[478] demonstrated by infrared spectroscopy that a silicon plate without catalyst is active in the decomposition of ammonia. Taking advantage of the Dillon results, Sørensen et al.[469] deposited alumina on a silicon plate and impregnated it with different metals, obtaining the following order of catalytic activity in the decomposition of ammonia: Co > Pd > Ru > Fe at 575 °C. An increase in H_2 production was obtained by adding Ba as a promoter of Ru. Following this work, Sørensen et al.[470] used a Ru catalyst without promoter or promoted with Ba and Cs in a graphite microreactor and obtained a higher catalytic activity in the case of Ru promoted with Ba with respect to the catalyst promoted with Cs or without promoters.

Regarding honeycomb structures, Plana et al.[471] deposited a Ni/Al_2O_3 catalyst on the walls of a cordierite monolith. By using a honeycomb configuration a higher ammonia conversion was obtained compared to a catalyst with the same composition but in a fixed bed reactor, although it is important to mention that the Ni content of the powdered catalyst used in the fixed bed reactor was around 4.5 times less by weight than the structured catalyst. They also tested the catalytic honeycomb after crushing it, and they observed a higher activity for the structured reactor, probably due to a more uniform reagent flow distribution.[479] In a similar manner, Armenise et al.[385] coated a cordierite honeycomb with Al_2O_3 and subsequently Ru. A comparison of the conversion of ammonia with that obtained in the work described previously[471] with the monolith prepared using the same method but with Ni showed that a higher conversion was obtained with Ru with respect to Ni. Subsequently, Armenise et al.[472] prepared and tested a cordierite honeycomb functionalized with nitrogen-doped carbon nanofibers, which served as support for Ru, obtaining higher catalytic activity. Another type of honeycomb catalytic structures were prepared by Ismagilov et al.,[473] who deposited MnO_2 on the walls of TiO_2 honeycombs with Ca- or Na-montmorillonite as binder.

Liu et al.[474] prepared stainless steel microfibers with alumina in their pores and impregnated with nickel, obtaining complete ammonia conversion at 650 °C with a high contact velocity. By using the same technique, Ni/Al_2O_3 catalysts promoted with Ce or La supported on nickel microfibers were also prepared.[475] The microfibers with the catalyst promoted with Ce had the highest catalytic activity, and the two promoted catalysts had a higher activity compared to the microfibers with the non-promoted catalyst. Similarly, Wang et al.[480] developed a 50 cm^3 reactor with nickel microfibers and Ni/Al_2O_3 promoted with CeO_2, obtaining a complete ammonia conversion at 550 °C and high stability in a test of 300 h. Finally, Zou et al.[481] proposed a cylindrical structured reactor composed of MgO, to which small amounts of $CaCO_3$, $MgCO_3$, TiO_2, activated carbon, and graphite were added, and subsequently impregnated with Ni.

3.3.2. Modeling. A chemical reactor model is a suitable tool to understand the relationship between the catalytic properties and the geometry of a structure, and also to predict its catalytic behavior under different conditions.[482] A model can also be classified as washcoat (it only provides information within the catalytic layer), channel (where one channel represents the entire reactor), or a scale model of the reactor.[483] The choice of the scale of the model depends on the purpose of the application and the complexity of the model. In the literature, several mathematical models have been developed for the decomposition of ammonia using catalytic monoliths or microchannel structures, from 1D to 3D models at different scales.

Deshmukh et al.[388] modeled the microreactor proposed by Ganley et al.[477] using a 2D model. They studied the kinetics of the reaction and tested different types of models. Chen et al.[484] created a model for a reactor loaded with $Ni-Pt/Al_2O_3$ and used it to optimize the reactor and the reaction conditions. Molaeimanesh and Davarani[485] designed a 2D model to analyze the behavior of various types of microreactors equipped either with microfibers or posts and concluded that the best activity was achieved with microfiber microreactors. Armenise et al.[386] used the Langmuir−Hinshelwood approach to analyze the kinetics of the cordierite honeycomb washcoated with Ni/Al_2O_3 described previously[471] for modeling purposes. In a similar manner, Chiuta et al.[381] created a model for the microchannels loaded with $Ni-Pt/Al_2O_3$ presented previously.[466] They considered a single microchannel as representative of the entire structure and optimized the design conditions taking into account the NH_3 flow rate, the thickness of the catalyst layer, and the hydraulic diameter of the channel. They created a similar model with Ru/Al_2O_3 promoted with Cs using the microchannels of the same stainless steel structure[468] based on their previous experimental results.[467] Using a 2D model of a single channel, Waghode et al.[486] simulated the behavior of a microreactor loaded with a Ni catalyst for the generation of H_2 from ammonia to feed a fuel cell and compared the results with those obtained with a fuel cell that directly uses ammonia. Similarly, Zade et al.[487] used one channel as representative of the entire structure, and they designed a model for a 15 μm wide microchannel loaded with a Ru catalyst, analyzing the effect of gas velocity, temperature, and reaction kinetics along the channel.

Models have also been developed to describe fixed bed reactors, considering mass and energy transfer issues. The models are useful to optimize the reaction conditions and the characteristics of the catalytic bed itself. For example, Badescu[488] designed a model of a fixed-bed reactor with a Ni/Al_2O_3 catalyst in order to minimize the presence of ammonia at the outlet and the energy required to control the temperature in the reactor, controlling not only the reaction conditions, but also the geometry of the reactor. Moreover, Chein et al.[489] designed a model for a $Ni-Pt/Al_2O_3$ catalyst to analyze the relationship between the decomposition of ammonia with the porosity and the size of the catalyst particles, as well as the effect of temperature, pressure, and ammonia flow rate, obtaining that a 1D plug flow model was a good approximation of the experimental results. Finally, Alagharu et al.[490] simulated the behavior of a fixed bed reactor loaded with a Ni−Pt catalyst with the objective of generating 100 W of net power in a PEM-type fuel cell with the hydrogen produced.

3.4. Membrane Reactors. To obtain high purity hydrogen outflows, metallic membranes composed of palladium or its alloys and proton-conducting ceramic membranes are currently the most suitable materials due to their high hydrogen selectivity. These types of membranes can work in a wide

https://doi.org/10.1021/acs.iecr.1c00843
Ind. Eng. Chem. Res. 2021, 60, 18560−18611

Table 13. Studies Related to Membrane Reactors Used for Ammonia Decomposition

membrane comp	catalyst	P (bar)	WHSV (mL g^{-1} h^{-1})	NH_3 flow (mL min^{-1})	% NH_3 inlet flow	T (°C)	conv (%)	conv (no membrane) (%)	E_a (kJ mol^{-1})	ref
Ru/YSZ + Pd		5			100	400	93	31	160	391
Ru−Cs/YSZ + Pd		5		61	100	400	98		160	391
Pd + stainless steel support + MnO_x	Ru/MgO	3	1950	47	100	400	100	91		499
Pd−Ag + stainless steel support + MnO_x	Ru/MgO									499
Pd + Al_2O_3 support + MnO_x	Ru/MgO									499
Pd + Al_2O_3 support	Ru/MgO									499
Ru/γ-Al_2O_3/α-Al_2O_3 + silica		1		10	100	450	95	45		500−502
$Nd_{5.5}Mo_{0.5}W_{0.5}O_{11.25-\delta}$/ $Nd_{5.5}Mo_{0.5}W_{0.5}O_{11.25-\delta}$-Ni		1	27273	50	20	600	42	24		503
Pd + ceramic support	Ni/La−Al_2O_3	3	2000		100	475	100	91		504
Pd + stainless steel support	Ru−Na/AC	1	20000	100	10	367	100	76		505
Pd	Ru/SiO_2	1		10	100	450	87	73		389
Pd + Al_2O_3 ceramic support	Ni/Al_2O_3	16	20060	410	0.33	550	79	17	230	506
Pd+ metallic support	Ru/Al_2O_3	6		400	100	450	99			507
Pd + Al_2O_3 support + Ru		1		10	100	375	99			508
Pd−Ag		1		10	100	375	51			508
Pd/γ-Al_2O_3/α-Al_2O_3	Ni/Al_2O_3	3	100		100	500	98	94	80	509
Pd/α-Al_2O_3	Ni/Al_2O_3	3	100		100	500	97	94		509
Pd−Ag	Ru/Al_2O_3	1		25	100	500	96	57		510
Pd−Ag+ Al_2O_3 support + Al_2O_3−YSZ	Ru/Al_2O_3	4		500	100	425	98	86		512

range of temperatures, between 300 and 700 °C for metals and from 600 to 900 °C for ceramics.[491] In the case of the metallic membranes, to lower the cost, increase the permeability of hydrogen, and increase the robustness of the reactor, a stainless steel porous support for the membrane is frequently used.[492] Hydrogen permeation through the membrane is generally a process assisted by an inert sweep gas on the permeate side of the membrane, such as Ar or N_2. The sweep gas can be used cocurrent or counter-current with respect to the permeated hydrogen flow, and the two configurations can give different results.[493,494] However, if an inert sweep gas is used the hydrogen stream is diluted, which is contrary to the objective pursued. The membranes can have a separation function, or catalytic properties for the reaction.[495] When the membrane is surrounded by the catalyst, it is defined as a catalytic membrane reactor (CMR), while if the membrane is placed downstream of the catalytic reaction, it is referred to as a staged membrane reactor (SMR), where the separation occurs after the catalytic reaction.[496] An important advantage of CMRs is that they shift the equilibrium toward hydrogen; this is the so-called "shift effect" and allows the process to proceed at lower temperature and with more compact reactors.

In the case of ammonia decomposition, various types of membrane reactors have been used, mainly CMRs-based. One of the main applications is the generation of pure hydrogen to feed low temperature PEM fuel cells without corrosion problems caused by the presence of ammonia.[390] In a study developed by Lundin et al.,[497] the feasibility of using Pd membranes in the decomposition of ammonia was determined in terms of the effect of N_2 and NH_3 on the membrane. No inhibition of the hydrogen permeation was observed by exposure to pure N_2 or NH_3 or H_2/N_2 and H_2/NH_3 mixtures for pressures up to 10 bar and temperatures in the range of 325 to 500 °C. A similar analysis was carried out by Sakamoto et al.[498] using various types of Pd alloy membranes. The experimental studies performed with membrane reactors for ammonia decomposition are compiled in Table 13, where the reaction conditions, the conversion obtained in comparison with the configuration without a membrane, and the apparent activation energy in the cases where it has been determined, are presented. There are two types of techniques used to create the necessary pressure difference between the two sides of the membrane (retentate and permeate sides): elevated pressure on the retentate side and atmospheric in the permeate, or low pressure on the retentate side and vacuum in the permeate. For obvious reasons, the first configuration is preferred in practical applications, especially considering that fuel cells operate at pressures slightly above atmospheric.

Most of the studies have used Pd or Pd−M (M = Ag, Cu) membranes supported on a metal (usually porous stainless steel) or a ceramic support (especially Al_2O_3). Nevertheless, novel membrane compositions have also been studied, such as that reported by Zhang et al.,[391] who prepared a tube of yttria stabilized zirconia impregnated with Ru where a layer of Pd was deposited as a membrane. They also analyzed the consequences on the catalytic activity of the addition of a Cs promoter, which led to complete ammonia conversion at temperatures as low as 400 °C, exceeding equilibrium restrictions without using sweep gas.

The modification of the two types of support, steel and ceramic, with other compounds, such as MnO_x, has also been investigated. For instance, Liu et al.[499] prepared various types of membrane reactors, using Pd or Pd−Ag supported on stainless steel or Al_2O_3. Both supports were modified with MnO_x, to create an intermediate layer between the support and the membrane. Using a Ru/MgO catalyst they obtained good results for the ammonia decomposition, especially with the Pd membrane supported on porous stainless steel modified with MnO_x, with which they obtained good stability after a 200 h run at 400 °C. Cechetto et al.[512] recently performed the reaction in a Pd−Ag membrane with an Al_2O_3 support, adding to the selective layer a protective layer of porous Al_2O_3 with yttria-

https://doi.org/10.1021/acs.iecr.1c00843
Ind. Eng. Chem. Res. 2021, 60, 18560−18611

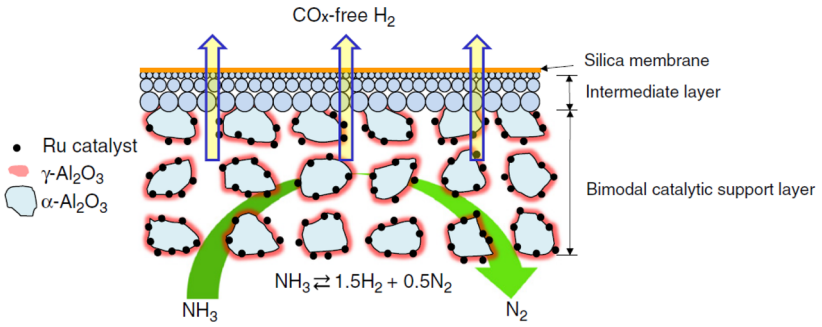

Figure 7. Scheme of the catalytic membrane used by Li et al.[501] Reprinted with permission from ref 501. Copyright 2011 Elsevier.

stabilized zirconia to improve the membrane stability. They used a Ru-based catalyst supported on Al_2O_3 pellets, and they compared ammonia conversion and membrane recovery efficiency with 1 bar of pressure on the permeate side, or by applying vacuum. A higher H_2 recovery and, consequently, faster kinetics and conversion, was obtained when vacuum was applied.

Other types of membranes used are silica[500] or materials composed of Nd, Mo, and W.[503] Li et al.[501] tested a catalytic membrane reactor loaded with Ru/γ-Al_2O_3/α-Al_2O_3 and a hydrogen-selective silica membrane (Figure 7). The conversion of NH_3 in the presence of the membrane increases significantly, from 45% to 95% at 450 °C, as a consequence of the shift effect due to the extraction of H_2.[502]

Using a different approach, Cheng et al.[503] used a double layered membrane $Nd_{5.5}Mo_{0.5}W_{0.5}O_{11.25-\delta}$/$Nd_{5.5}Mo_{0.5}W_{0.5}O_{11.25-\delta}$-Ni that maintained a very high NH_3 conversion and H_2 permeation flux, stable during a continuous test of 75 h at 750 °C.

Regarding the catalysts, most of the studies have used conventional Ru or Ni supported on alumina, while in other works alternative catalysts have been tested, for example promoted with La,[504] or supported on carbon,[505] SiO_2[389] or MgO.[499] In this sense, Zhang et al.[504] used a Ni/La–Al_2O_3 catalyst with a membrane of Pd and ceramic material (Al_2O_3) supported on stainless steel. They were able to determine an optimal catalytic activity and stability of the reactor during a 500 h test. Residual ammonia slightly inhibited the permeability of the membrane, but through a treatment with air followed by H_2 the permeability could be recovered. With a Pd membrane supported on porous stainless steel and a Ru/C catalyst promoted with Na, complete ammonia conversion was achieved at 367 °C, exceeding the corresponding thermodynamic equilibrium conversion by approximately 2%.[505] Collins et al.[506] analyzed the conversion of a small amount of ammonia (0.33 mol %) on Ni/Al_2O_3 for gas cleaning, obtaining a conversion of 79% at 450 °C using a Pd membrane on an Al_2O_3 ceramic support. This conversion is 62% higher than with the same catalyst in a conventional reactor.

Itoh et al.[389] used a Ru/SiO_2 catalyst with a 200 μm thick palladium membrane and obtained a 15% increase in conversion compared to the conventional reactor, and 60% of hydrogen recovery at 450 °C. Similarly, a ruthenium catalyst supported on alumina was tested in pellet form by Rizzuto et al. in a CMR equipped with a Pd membrane,[507] obtaining a complete conversion with a space velocity of 653 h^{-1} at 450 °C and 6 bar. Also, Itoh et al.[508] investigated a reactor with a 2 μm thick Pd membrane deposited on an Al_2O_3 tube and impregnated with Ru, and compared the catalytic results with an Ag–Pd membrane, obtaining a significantly higher NH_3 conversion with the first configuration, reaching complete conversion at 375 °C with a reduced flow of pure ammonia.

Some studies have used the experimental results to build a model, and use it to simulate different reaction conditions to optimize the CMR reactor. For example, using a Ni/Al_2O_3 catalyst and a 4 μm Pd membrane supported and encapsulated over two Al_2O_3 phases, Israni et al.[509] created a model to describe the behavior of the membrane reactor and compare it with that of a Pd membrane reactor and a conventional 13 μm Al_2O_3 support. Using the same approach, Prasad et al.[510] designed a model for a CMR reactor with a Pd–Ag membrane and a Ru/Al_2O_3 catalyst and experimentally confirmed the results, obtaining complete conversion at lower temperatures compared to the reactor without a membrane.

Without confirming the results experimentally, Abashar[387,392] simulated the behavior of a Pd–Ag membrane reactor coupled with a pellet catalyst through a model, and concluded that using more than one reactor, that is, a multistage configuration, would have significant advantages in terms of ammonia decomposition. By using a single stage they predicted an ammonia conversion of around 29% at 40 bar, while with seven stages the conversion becomes complete. Di Carlo et al.[511] designed a reactor with more than one Pd membrane inside it and a Ni/Al_2O_3 catalyst, and optimized the reaction conditions through a model using seven membranes, a temperature of 550 °C and a pressure of 10 bar. Another work which focused on analyzing the performance of a reactor with 19 vanadium-based alloy membrane tubes was carried out by Hla and Dolan,[513] who obtained a very high hydrogen yield at a low ammonia inlet flow and a reaction pressure of 7.8 bar.

4. SUMMARY AND CONCLUSIONS

Ammonia decomposition is a well-known reaction that was first used essentially for fundamental studies. With the imminent arrival of the energy transition, hydrogen technologies are gaining relevance, and the generation of hydrogen from the decomposition reaction of ammonia represents an interesting route to produce carbon-free hydrogen on-site and on-demand. Ammonia can be considered as a hydrogen storage system, as it is liquid at low pressure at ambient temperature, which means a high hydrogen density both in volume and weight. For this reason, numerous efforts have been devoted to the development of highly active and robust catalysts, aimed at the decomposition of ammonia at the lowest possible temperature. The most studied catalysts contain a metallic function (frequently Ni or Ru) supported on an inorganic oxide and modified by different types of promoters, usually alkaline. It is well established that ruthenium is the most active metal for the decomposition of

https://doi.org/10.1021/acs.iecr.1c00843
Ind. Eng. Chem. Res. 2021, 60, 18560–18611

ammonia, as it allows to obtain the highest conversion at the lowest temperature, of the order of 400 °C, while Ni-based catalysts yield similar results, but at temperatures between 500 and 600 °C. It should be noted, however, that a higher Ni content can be used due to its lower cost. Because of the high price of ruthenium, alternative systems based on easily obtainable non-noble metals are being investigated, generally composed of elements such as iron, cobalt, or molybdenum, even if they currently do not reach the activity of ruthenium-based catalysts. However, it should be noted that many of these inexpensive catalytic systems have not yet been studied as extensively as ruthenium or nickel and therefore it may be a lot of room for improvement. Nitrides and carbides of transition metals also show catalytic activity for the decomposition of ammonia; however, at present the catalytic activities that have been obtained are far from being considered an alternative to noble metals. Using theoretical models it has been predicted that bimetallic catalysts, such as Co−Mo, are suitable cost-effective candidates, but bimetallic systems are complex and an extensive characterization is needed to fully understand the nature of the active sites involved under reaction conditions to predict a proper combination of metals.[514] The combinations tested so far confirm that bimetallic catalysts are more promising than monometallic ones. The investigation of novel compounds based on amide and imide of transition metals has recently started, and these materials already show remarkable potential as future catalysts for low temperature ammonia decomposition, especially when coupled with other active metals and nitrides, or used in a supported form.

The active phase, the support, and the promoters all play a determinant role in the reaction. It is generally accepted that for NH_3 decomposition a catalyst support should present a high basicity, along with high conductivity, low concentration of electron-withdrawing groups, high thermal stability, and high surface area. In particular, many studies have related the activity of catalyst to basicity, and this has been reported for different active phases such as Ru, Ni, Fe, Co, and Mo. Basicity has been related to an increase in the dispersion of the active metal, but also to an enhancement for ammonia dehydrogenation and for the recombinative desorption of surface N atoms, which are the most likely rate-limiting steps of the reaction. Generally, the basicity of the catalyst is modulated by adding a promoter, which also allows to increase the electrodonating properties of the catalyst, since the promoters can have an indirect interaction with the support to induce stronger basicity. Although, in general, the relationship between the electrodonating properties of the promoter and the activity of the catalyst has been determined, the effect can be different depending on the active phase used due to direct electronic interaction with the active metal. For example, in the case of ruthenium, the alkali metals have proven to be good promoters, while in the case of cobalt or amides/imides the activity decreases. In the case of nickel, rare earths such as Ce and La have shown to be better promoters than alkali metals. In summary, the combination of properties such as basicity and a high electrodonation capacity of the support and promoters seems to be fundamental for the development of efficient catalysts for NH_3 decomposition.

The development of these catalysts has been accompanied by the design of compact and efficient reactors in order to keep the reactor volume low for small and medium applications. In addition, structured reactors are superior to fixed-bed reactors due to their portability, superior heat and mass transfer capacity, and uniform flow distribution. In particular, microchannel reactors are most likely the structure with the highest potential for ammonia decomposition compared to conventional honeycomb structures and other types of structured reactors.

Kinetic studies and reactor modeling are useful and necessary tools for a better understanding of the reaction mechanism and for a rational design of catalytic devices. Many studies have focused on determining the limiting step of the decomposition reaction using different types of catalysts. Although initially it was proposed that the limiting step was the desorption of nitrogen from the surface of the catalyst and that, therefore, the binding energy with nitrogen could determine the activity of the catalyst, it was later seen that for various types of catalysts the limiting step was different. It has been proposed that for noble metals the limiting step is the cleavage of N−H bonds, while that for non-noble metals it is the desorption of nitrogen. However, this issue is more complex since the limiting step for a given catalyst can vary with reaction conditions. Another important element that kinetic studies have focused on is the inhibition of hydrogen generated on the catalyst; in fact, it has been proposed that it is the inhibitory effect of hydrogen that governs catalytic activity. The extent of inhibition has been determined to vary with temperature and is greater at low temperatures due to hydrogen accumulation on the catalyst surface. For catalysts composed of Ni, Pt, or Mo, it is found that the inhibition is stronger than that of other metals such as Ru or Fe, and some promoters decrease the H_2 inhibitory effect, such as K for Ru catalysts. Bimetallic formulations also decrease hydrogen inhibition.

Another method that makes it possible to reduce the inhibitory effect of hydrogen on the catalyst is the use of a selective membrane to remove it while it is being generated. Furthermore, the use of a catalytic membrane reactor implies a change in the reaction equilibrium (shift effect) and, therefore, an increase in the hydrogen yield. Also, when hydrogen is intended to power low-temperature fuel cells to produce electricity, as in PEM-type fuel cells, catalytic membrane reactors appear as the ideal solution to obtain a stream of pure hydrogen from ammonia decomposition. The only drawback is the current high price of Pd-based dense metallic membranes. A proper balance between catalyst characteristics and membrane properties is necessary for optimized performance.

While it is true that studies related to catalysts are at a very advanced stage, the development of practical catalytic systems for use in specific applications still requires great efforts. The optimization of the ammonia decomposition reaction for its application in a real hydrogen production system must be comprehensive and consider not only the type of catalyst, but also the type of reactor to allow the realization of a totally carbon-free energy technology.

AUTHOR INFORMATION

Corresponding Author

Jordi Llorca − *Institute of Energy Technologies, Department of Chemical Engineering and Barcelona Research Center in Multiscale Science and Engineering, Universitat Politècnica de Catalunya, Barcelona 08019, Spain;* orcid.org/0000-0002-7447-9582; Phone: +34 934011708; Email: jordi.llorca@upc.edu

Authors

Ilaria Lucentini − *Institute of Energy Technologies, Department of Chemical Engineering and Barcelona Research Center in*

https://doi.org/10.1021/acs.iecr.1c00843
Ind. Eng. Chem. Res. 2021, 60, 18560−18611

Multiscale Science and Engineering, Universitat Politècnica de Catalunya, Barcelona 08019, Spain

Xènia Garcia − *Institute of Energy Technologies, Department of Chemical Engineering and Barcelona Research Center in Multiscale Science and Engineering, Universitat Politècnica de Catalunya, Barcelona 08019, Spain*

Xavier Vendrell − *Institute of Energy Technologies, Department of Chemical Engineering and Barcelona Research Center in Multiscale Science and Engineering, Universitat Politècnica de Catalunya, Barcelona 08019, Spain*

Complete contact information is available at: https://pubs.acs.org/10.1021/acs.iecr.1c00843

Notes

The authors declare no competing financial interest.

■ ACKNOWLEDGMENTS

This work was supported by projects MICINN/FEDER RTI2018-093996-B-C31 and GC 2017 SGR 128. I.L. is grateful to MINECO for Ph.D. Grant BES-2016-076507. X.G. is grateful for a FI-DGR 2016 grant. X.V. is grateful to MICIU-Juan de la Cierva-Incorporación program for the individual fellowship grant agreement IJCI-2017-31449. J.L. is a Serra Húnter Fellow and is grateful to the ICREA Academia program.

■ ACRONYMS AND ABBREVIATIONS

AC	activated carbon
AFC	alkaline fuel cell
BHA	barium hexaaluminate
CMFs	carbon microfibers
CMR	catalytic membrane reactor
CNFs	carbon nanofibers
CNTs	carbon nanotubes
conv	conversion (in tables)
comp	composition (in tables)
DBD	dielectric barrier discharges
DMFC	direct methanol fuel cell
E_a	apparent activation energy
GC	graphitized carbon
GHSV	gas hourly space velocity
GNP	graphene nanoplatelet
GO	graphene oxide
GWP	global warming power
HNTs	halloysite nanotubes
LHHW	Langmuir−Hinshelwood-Hougen-Watson
MCFC	molten carbonate fuel cell
MOFs	metal−organic frameworks
MSC	microporous superactivated carbon
MW	multiwalled
NT	nanotube
OMC	ordered mesoporous carbon
P	pressure
PAFC	phosphoric acid fuel cell
PEMFC	proton exchange membrane fuel cell
RGO	reduced graphene oxide
SMR	staged membrane reactor
SOFC	solid oxide fuel cell
SW	single-walled
T	temperature
TMN	transition metal nitrides
TOF	turn over frequency
WHSV	weight hourly space velocity
wt	weight
YSZ	yttria-stabilized zirconia
$\Delta H°$	standard enthalpy of reaction

■ REFERENCES

(1) York, R.; Bell, S. E. Energy Transitions or Additions? Why a Transition from Fossil Fuels Requires More than the Growth of Renewable Energy. *Energy Res. Soc. Sci.* **2019**, *51*, 40−43.

(2) Braff, W. A.; Mueller, J. M.; Trancik, J. E. Value of Storage Technologies for Wind and Solar Energy. *Nat. Clim. Change* **2016**, *6* (10), 964−969.

(3) Markard, J. The next Phase of the Energy Transition and Its Implications for Research and Policy. *Nat. Energy* **2018**, *3* (8), 628−633.

(4) Bockris, J. O. M. The Hydrogen Economy: Its History. *Int. J. Hydrogen Energy* **2013**, *38* (6), 2579−2588.

(5) Staffell, I.; Scamman, D.; Velazquez Abad, A.; Balcombe, P.; Dodds, P. E.; Ekins, P.; Shah, N.; Ward, K. R. The Role of Hydrogen and Fuel Cells in the Global Energy System. *Energy Environ. Sci.* **2019**, *12* (2), 463−491.

(6) Pandev, M.; Lucchese, P.; Mansilla, C.; Le Duigou, A.; Abrashev, B.; Vladikova, D. Hydrogen Economy: The Future for a Sustainable and Green Society. *Bulg. Chem. Commun.* **2017**, *49* (C), 84−92.

(7) Navarro, R. M.; Peña, M. A.; Fierro, J. L. G. Hydrogen Production Reactions from Carbon Feedstocks: Fossil Fuels and Biomass. *Chem. Rev.* **2007**, *107* (10), 3952−3991.

(8) Kalamaras, C. M.; Efstathiou, A. M. Hydrogen Production Technologies: Current State and Future Developments. *Conf. Pap. Energy* **2013**, *2013*, 1−9.

(9) Crabtree, G. W.; Dresselhaus, M. S.; Buchanan, M. V. The Hydrogen Economy. *Phys. Today* **2004**, *57* (12), 39−45.

(10) Ursúa, A.; Gandía, L. M.; Sanchis, P. Hydrogen Production from Water Electrolysis: Current Status and Future Trends. *Proc. IEEE* **2012**, *100* (2), 410−426.

(11) International Renewable Energy Agency (IRENA). *Hydrogen: A Renewable Energy Perspective*; IRENA, 2019.

(12) International Energy Agency (IEA). *Future of Hydrogen*; IEA, 2019.

(13) Yacobucci, B. D.; Curtright, A. E. *A Hydrogen Economy and Fuel Cells: An Overview*; Congressional Resource Service, 2004.

(14) White, C. M.; Steeper, R. R.; Lutz, A. E. The Hydrogen-Fueled Internal Combustion Engine: A Technical Review. *Int. J. Hydrogen Energy* **2006**, *31* (10), 1292−1305.

(15) van den Berg, A. W. C.; Otero Areán, C. Materials for Hydrogen Storage: Current Research Trends and Perspectives. *Chem. Commun.* **2008**, *6*, 668−681.

(16) Robertson, I. M.; Sofronis, P.; Nagao, A.; Martin, M. L.; Wang, S.; Gross, D. W.; Nygren, K. E. Hydrogen Embrittlement Understood. *Metall. Mater. Trans. A* **2015**, *46* (6), 1085−1103.

(17) Zheng, J.; Liu, X.; Xu, P.; Liu, P.; Zhao, Y.; Yang, J. Development of High Pressure Gaseous Hydrogen Storage Technologies. *Int. J. Hydrogen Energy* **2012**, *37* (1), 1048−1057.

(18) Züttel, A. Hydrogen Storage Methods. *Naturwissenschaften* **2004**, *91* (4), 157−172.

(19) Ahluwalia, R. K.; Hua, T. Q.; Peng, J.-K.; Lasher, S.; McKenney, K.; Sinha, J.; Gardiner, M. Technical Assessment of Cryo-Compressed Hydrogen Storage Tank Systems for Automotive Applications. *Int. J. Hydrogen Energy* **2010**, *35* (9), 4171−4184.

(20) Hwang, H. T.; Varma, A. Hydrogen Storage for Fuel Cell Vehicles. *Curr. Opin. Chem. Eng.* **2014**, *5*, 42−48.

(21) Subrahmanyam, K. S.; Kumar, P.; Maitra, U.; Govindaraj, A.; Hembram, K. P. S. S.; Waghmare, U. V.; Rao, C. N. R. Chemical Storage of Hydrogen in Few-Layer Graphene. *Proc. Natl. Acad. Sci. U. S. A.* **2011**, *108* (7), 2674−2677.

(22) Nijkamp, M. G.; Raaymakers, J. E. M. J.; van Dillen, A. J.; de Jong, K. P. Hydrogen Storage Using Physisorption−Materials Demands. *Appl. Phys. A: Mater. Sci. Process.* **2001**, *72*, 619−623.

(23) Sakintuna, B.; Lamari-Darkrim, F.; Hirscher, M. Metal Hydride Materials for Solid Hydrogen Storage: A Review. *Int. J. Hydrogen Energy* **2007**, *32* (9), 1121−1140.
(24) Suh, M. P.; Park, H. J.; Prasad, T. K.; Lim, D.-W. Hydrogen Storage in Metal-Organic Frameworks. *Chem. Rev.* **2012**, *112*, 782−835.
(25) Rowsell, J. L. C.; Yaghi, O. M. Strategies for Hydrogen Storage in Metal-Organic Frameworks. *Angew. Chem., Int. Ed.* **2005**, *44* (30), 4670−4679.
(26) Murray, L. J.; Dincă, M.; Long, J. R. Hydrogen Storage in Metal−Organic Frameworks. *Chem. Soc. Rev.* **2009**, *38* (5), 1294.
(27) Jensen, J. O.; Li, Q.; Bjerrum, N. J.; Palm, J. The Energy Efficiency of Onboard Hydrogen Storage Techniques. *Energy Efficiency* **2010**, 143−156, DOI: 10.1016/j.jallcom.2007.04.051.
(28) Bossel, U.; Eliasson, B. Energy and the Hydrogen Economy. *Eur. Fuel Cell Forum, Lucerne* **2002**, 1−36.
(29) Kojima, Y.; Suzuki, K.-I.; Fukumoto, K.; Sasaki, M.; Yamamoto, T.; Kawai, Y.; Hayashi, H. Hydrogen Generation Using Sodium Borohydride Solution and Metal Catalyst Coated on Metal Oxide. *Int. J. Hydrogen Energy* **2002**, *27* (10), 1029−1034.
(30) Biniwale, R. B.; Rayalu, S.; Devotta, S.; Ichikawa, M. Chemical Hydrides: A Solution to High Capacity Hydrogen Storage and Supply. *Int. J. Hydrogen Energy* **2008**, *33* (1), 360−365.
(31) Eberle, U.; Felderhoff, M.; Schüth, F. Chemical and Physical Solutions for Hydrogen Storage. *Angew. Chem., Int. Ed.* **2009**, *48* (36), 6608−6630.
(32) Makepeace, J. W.; Wood, T. J.; Hunter, H. M. A.; Jones, M. O.; David, W. I. F. Ammonia Decomposition Catalysis Using Non-Stoichiometric Lithium Imide. *Chem. Sci.* **2015**, *6* (7), 3805−3815.
(33) Lan, R.; Irvine, J. T. S.; Tao, S. Ammonia and Related Chemicals as Potential Indirect Hydrogen Storage Materials. *Int. J. Hydrogen Energy* **2012**, *37* (2), 1482−1494.
(34) Klerke, A.; Christensen, C. H.; Nørskov, J. K.; Vegge, T. Ammonia for Hydrogen Storage: Challenges and Opportunities. *J. Mater. Chem.* **2008**, *18* (20), 2304−2310.
(35) Zamfirescu, C.; Dincer, I. Using Ammonia as a Sustainable Fuel. *J. Power Sources* **2008**, *185* (1), 459−465.
(36) Giddey, S.; Badwal, S. P. S.; Munnings, C.; Dolan, M. Ammonia as a Renewable Energy Transportation Media. *ACS Sustainable Chem. Eng.* **2017**, *5* (11), 10231−10239.
(37) Lipman, T.; Shah, N. *Ammonia as an Alternative Energy Storage Medium for Hydrogen Fuel Cells: Scientific and Technical Review for Near-Term Stationary Power Demonstration Projects*; Transportation Sustainability Research Center, 2007.
(38) Venkat, P.; Richardson, J. Introduction to Ammonia Production. *CEP Mag.* **2016**, No. 2, 69−75.
(39) Appl, M. Ammonia, 2. Production Processes. *Ullmann's Encyclopedia of industrial chemistry* **2011**, *3*, 1−88.
(40) Barona, A.; Etxebarria, B.; Aleksanyan, A.; Gallastegui, G.; Rojo, N.; Diaz-Tena, E. A Unique Historical Case to Understand the Present Sustainable Development. *Sci. Eng. Ethics* **2018**, *24* (1), 261−274.
(41) The Royal Society. *Ammonia: Zero-Carbon Fertiliser, Fuel and Energy Store. Policy Briefing*; The Royal Society, 2020.
(42) Maruti Co. *Ammonia Cracker*; 2013, https://www.exportersindia.com/maruti-corporation-company5789622/ammonia-cracker-4133077.htm (accessed 2021).
(43) Rouwenhorst, K. H. R.; Van der Ham, A. G. J.; Mul, G.; Kersten, S. R. A. Islanded Ammonia Power Systems: Technology Review & Conceptual Process Design. *Renewable Sustainable Energy Rev.* **2019**, *114*, 109339.
(44) Lamb, K. E.; Dolan, M. D.; Kennedy, D. F. Ammonia for Hydrogen Storage; A Review of Catalytic Ammonia Decomposition and Hydrogen Separation and Purification. *Int. J. Hydrogen Energy* **2019**, *44* (7), 3580−3593.
(45) Hejze, T.; Besenhard, J. O.; Kordesch, K.; Cifrain, M.; Aronsson, R. R. Current Status of Combined Systems Using Alkaline Fuel Cells and Ammonia as a Hydrogen Carrier. *J. Power Sources* **2008**, *176* (2), 490−493.
(46) Chiuta, S.; Everson, R. C.; Neomagus, H. W. J. P.; Van Der Gryp, P.; Bessarabov, D. G. Reactor Technology Options for Distributed Hydrogen Generation via Ammonia Decomposition: A Review. *Int. J. Hydrogen Energy* **2013**, *38* (35), 14968−14991.
(47) Valera-Medina, A.; Xiao, H.; Owen-Jones, M.; David, W. I. F.; Bowen, P. J. Ammonia for Power. *Prog. Energy Combust. Sci.* **2018**, *69*, 63−102.
(48) Zamfirescu, C.; Dincer, I. Ammonia as a Green Fuel and Hydrogen Source for Vehicular Applications. *Fuel Process. Technol.* **2009**, *90* (5), 729−737.
(49) Ibrahim, O. M.; Klein, S. A. Absorption Power Cycles. *Energy* **1996**, *21* (1), 21−27.
(50) Arias, J. *Hydrogen and Fuel Cells in Japan*; EU-Japan Centre for Industrial Cooperation, 2019.
(51) Kroch, E. Ammonia-A Fuel for Motor Buses. *J. Inst. Pet.* **1945**, *31*, 213−223.
(52) Siemer, D. *Nuclear Power: Policies, Practices, and the Future*; Wiley, 2019.
(53) Comotti, M.; Frigo, S. Hydrogen Generation System for Ammonia-Hydrogen Fuelled Internal Combustion Engines. *Int. J. Hydrogen Energy* **2015**, *40* (33), 10673−10686.
(54) Hacker, V.; Kordesch, K. Ammonia Crackers. *Handbook of Fuel Cells − Fundamentals, Technology and Applications* **2003**, *3*, 121−127.
(55) Intelligent Energy. Fuel-Flexible Hestia Hydrogen-Generating System Demonstrated. *Fuel Cells Bull.* **2006**, *2006* (8), 6 DOI: 10.1016/S1464-2859(06)71153-1.
(56) *Compact Microchannel Ammonia Crackers*. https://pocharitechnologies.com/2019/09/20/micro-ammonia-cracker-for-on-demand-mobile-hydrogen/ (accessed 2020-06-25).
(57) Tower Power Ltd. About Us http://towerpowerlimited.com/about.php (accessed 2020-06-25).
(58) GenCell Ltd. GenCell Ltd. The Off-grid Challenge. https://www.gencellenergy.com/our-products/gencell-a5/ (accessed 2020-06-25).
(59) AFCEnergy. AFC Wraps Ammonia-to-Power Fuel Cell Generator Trials, Plans Commercial System. *Fuel Cells Bull.* **2019**, *2019* (6), 11−12.
(60) STFC UK Researchers. Change Game for Hydrogen from Ammonia for Cars. *Fuel Cells Bull.* **2014**, *2014* (7), 11.
(61) Fothergill, K.; Greenwood, S.; Makepeace, J.; Wilkinson, I. *Ammonia to Green Hydrogen Project - Feasibility Study*; Science and Technology Facilities Council, 2015; *Vol. 33*.
(62) Brown, Trevor. Engie, Siemens, STFC, and Ecuity awarded funding for green ammonia-to-hydrogen in UK. https://www.ammoniaenergy.org/articles/engie-siemens-stfc-and-ecuity-awarded-funding-for-green-ammonia-to-hydrogen-in-uk/ (accessed 2020-06-25).
(63) Powell, M. R.; Chellappa, A. S.; Vencill, T. R. Compact Fuel Cell Power Supplies with Safe Fuel Storage. *Army Science Conference (24th)* **2004**, 1−10.
(64) T-Raissi, A. Hydrogen from Ammonia and Ammonia-Borane Complex for Fuel Cell Applications. *2002 U.S. DOE Hydrogen Review* **2002**, 581−597.
(65) Rencat. Fuel Cell Grade H_2 from ammonia without using Palladium membrane. https://www.rencat.net/Technology/ (accessed 2020-06-25).
(66) Badwal, S.; Giddey, S. S.; Kulkarni, F. T. C. A.; Hughes, A. E.; Kennedy, D. F. US Patent US 9,895,652 B2, 2018.
(67) ARPA-E. Funding for New Projects to Power Cleaner Transportation. *Fuel Cells Bull.* **2017**, *2017* (1), 12−13.
(68) Perman, E. P.; Atkinson, G. A. S. The Decomposition of Ammonia by Heat. *Proc. R. Soc. London* **1905**, *74*, 110−117.
(69) Tyler, C. Ammonia as a Source of Hydrogen for Hardening Oils. *J. Am. Oil Chem. Soc.* **1934**, *11*, 231.
(70) Robertson, A. J. B.; Willhoft, E. M. A. Kinetics of the Decomposition of Ammonia on Platinum at Low Pressures. *Trans. Faraday Soc.* **1967**, *63*, 476−487.
(71) Willhoft, E. M. A. Kinetics of Decomposition of Ammonia at Low Pressures on Metal Surfaces. *Trans. Faraday Soc.* **1968**, *64*, 1925−1933.

(72) Choudhary, T. V.; Santra, A. K.; Sivadinarayana, C.; Min, B. K.; Yi, C. W.; Davis, K.; Goodman, D. W. Ammonia Decomposition on Ir(100): From Ultrahigh Vacuum to Elevated Pressures. *Catal. Lett.* **2001**, *77* (1−3), 1−5.
(73) Sayas, S.; Morlanés, N.; Katikaneni, S. P.; Harale, A.; Solami, B.; Gascon, J. High Pressure Ammonia Decomposition on Ru-K/CaO Catalysts. *Catal. Sci. Technol.* **2020**, *10* (15), 5027−5035.
(74) Carlo, A.; Di; Vecchione, L.; Del Prete, Z. Ammonia Decomposition over Commercial Ru/Al_2O_3 Catalyst: An Experimental Evaluation at Different Operative Pressures and Temperatures. *Int. J. Hydrogen Energy* **2014**, *39* (2), 808−814.
(75) Pitselis, G. E.; Petrolekas, P. D.; Vayenas, C. G. Electrochemical Promotion of Ammonia Decomposition over Fe Catalyst Films Interfaced with K^+- & H^+- Conductors. *Ionics* **1997**, *3* (1−2), 110−116.
(76) Marnellos, G.; Zisekas, S.; Stoukides, M. Synthesis of Ammonia at Atmospheric Pressure with the Use of Solid State Proton Conductors. *J. Catal.* **2000**, *193* (1), 80−87.
(77) Zisekas, S.; Karagiannakis, G.; Marnellos, G.; Stoukides, M. Study of Ammonia Decomposition in a Proton Conducting Solid Electrolyte Cell. *Ionics* **2002**, *8* (1−2), 118−122.
(78) Smith, C.; Essex, H. Effect of Electric Fields on the Decomposition of Ammonia by AlphaRays. *J. Chem. Phys.* **1938**, *6* (4), 188−196.
(79) Zhao, Y.; Wang, L.; Zhang, J.; Gong, W.; Guo, H. Decomposition of Ammonia by Atmospheric Pressure AC Discharge: Catalytic Effect of the Electrodes. *Catal. Today* **2013**, *211*, 72−77.
(80) McLennan, J. C.; Greenwood, G. On the Decomposition of Ammonia by High-Speed Electrons. *R. Soc.* **1928**, *120* (785), 283−295.
(81) Seabury, C. W.; Rhodin, T. N.; Purtell, R. J.; Merrill, R. P. Chemisorption and Reaction of NH_3 on Ni(111). *Surf. Sci.* **1980**, *93* (1), 117−126.
(82) Dawson, P. T.; Peng, Y. K. Ammonia Decomposition on Tungsten Surfaces. *J. Chem. Phys.* **1970**, *52* (2), 1014−1015.
(83) Son, Y.-S.; Kim, K.-H.; Kim, K.-J.; Kim, J.-C. Ammonia Decomposition Using Electron Beam. *Plasma Chem. Plasma Process.* **2013**, *33* (3), 617−629.
(84) Hirabayashi, S.; Ichihashi, M. Adsorption and Dehydrogenation of Ammonia on Vanadium and Niobium Nitride Cluster Cations. *Int. J. Mass Spectrom.* **2016**, *407*, 86−91.
(85) Guler, M.; Dogu, T.; Varışlı, D. Hydrogen Production over Molybdenum Loaded Mesoporous Carbon Catalysts in Microwave Heated Reactor System. *Appl. Catal., B* **2017**, *219*, 173−182.
(86) Varışlı, D.; Korkusuz, C.; Dogu, T. Microwave-Assisted Ammonia Decomposition Reaction over Iron Incorporated Mesoporous Carbon Catalysts. *Appl. Catal., B* **2017**, *201*, 370−380.
(87) Barker, R. Decomposition of Ammonia in a Microwave Discharge. *J. Chem. Soc., Faraday Trans. 1* **1972**, *68*, 315−322.
(88) Carbaugh, D. C.; Munno, F. J.; Marchello, J. M. Ammonia Decomposition in Glow Discharge. *J. Chem. Phys.* **1967**, *47* (12), 5211−5214.
(89) Wang, L.; Zhao, Y.; Liu, C.; Gong, W.; Guo, H. Plasma Driven Ammonia Decomposition on a Fe-Catalyst: Eliminating Surface Nitrogen Poisoning. *Chem. Commun.* **2013**, *49* (36), 3787−3789.
(90) Yi, Y.; Wang, L.; Guo, Y.; Sun, S.; Guo, H. Plasma-Assisted Ammonia Decomposition over Fe−Ni Alloy Catalysts for CO_x-Free Hydrogen. *AIChE J.* **2018**, *65* (2), 691−701.
(91) Hayakawa, Y.; Miura, T.; Shizuya, K.; Wakazono, S.; Tokunaga, K.; Kambara, S. Hydrogen Production System Combined with a Catalytic Reactor and a Plasma Membrane Reactor from Ammonia. *Int. J. Hydrogen Energy* **2019**, *44* (20), 9987−9993.
(92) Inoue, Y.; Hayakawa, Y.; Takeyama, A.; Miura, T.; Kambara, S. Hydrogen Production by Ammonia Decomposition Using Pulsed Plasma. *International Symposium on Electrohydrodynamics (ISEHD)* **2014**, 2−5.
(93) Goto, Y.; Hayakawa, Y.; Kambara, S. Reaction Mechanism of Ammonia Decomposition by Atmospheric Plasma. *Ninth JSME-KSME Thermal and Fluids Engineering Conference* **2017**, 1−4.
(94) Akiyama, M.; Aihara, K.; Sawaguchi, T.; Matsukata, M.; Iwamoto, M. Ammonia Decomposition to Clean Hydrogen Using Non-Thermal Atmospheric-Pressure Plasma. *Int. J. Hydrogen Energy* **2018**, *43* (31), 14493−14497.
(95) Wang, L.; Yi, Y.; Zhao, Y.; Zhang, R.; Zhang, J.; Guo, H. NH_3 Decomposition for H_2 Generation: Effects of Cheap Metals and Supports on Plasma-Catalyst Synergy. *ACS Catal.* **2015**, *5* (7), 4167−4174.
(96) Hu, T.; Wang, Y. Effect of Operating and Geometrical Parameters on Ammonia Decomposition in a Tubular Reactor Driven by Concentrating Solar Power. *J. Energy Eng.* **2020**, *146* (4), 040200181−040200188.
(97) Wang, B.; Kong, H.; Wang, H.; Wang, Y.; Hu, X. Kinetic and Thermodynamic Analyses of Mid/Low-Temperature Ammonia Decomposition in Solar-Driven Hydrogen Permeation Membrane Reactor. *Int. J. Hydrogen Energy* **2019**, *44* (49), 26874−26887.
(98) Chen, J.; Yan, L. Ammonia Decomposition Coupled with Methane Combustion in Catalytic Microreactors for Hydrogen Production. *Chem. Biomol. Eng.* **2017**, *2* (1), 19−26.
(99) Engelbrecht, N.; Chiuta, S.; Bessarabov, D. G. A Highly Efficient Autothermal Microchannel Reactor for Ammonia Decomposition: Analysis of Hydrogen Production in Transient and Steady-State Regimes. *J. Power Sources* **2018**, *386*, 47−55.
(100) Chiuta, S.; Bessarabov, D. G. Design and Operation of an Ammonia-Fueled Microchannel Reactor for Autothermal Hydrogen Production. *Catal. Today* **2018**, *310* (1), 187−194.
(101) Kim, J. H.; Um, D. H.; Kwon, O. C. Hydrogen Production from Burning and Reforming of Ammonia in a Microreforming System. *Energy Convers. Manage.* **2012**, *56*, 184−191.
(102) Kim, J. H.; Kwon, O. C. A Micro Reforming System Integrated with a Heat-Recirculating Micro-Combustor to Produce Hydrogen from Ammonia. *Int. J. Hydrogen Energy* **2011**, *36* (3), 1974−1983.
(103) Arana, L. R.; Schaevitz, S. B.; Franz, A. J.; Schmidt, M. A.; Jensen, K. F. A Microfabricated Suspended-Tube Chemical Reactor for Thermally Efficient Fuel Processing. *J. Microelectromech. Syst.* **2003**, *12* (5), 600−612.
(104) Kaisare, N. S.; Stefanidis, G. D.; Vlachos, D. G. Millisecond Production of Hydrogen from Alternative, High Hydrogen Density Fuels in a Cocurrent Multifunctional Microreactor. *Ind. Eng. Chem. Res.* **2009**, *48* (4), 1749−1760.
(105) Regatte, V. R.; Kaisare, N. S. Hydrogen Generation in Spatially Coupled Cross-Flow Microreactors. *Chem. Eng. J.* **2013**, *215−216*, 876−885.
(106) Deshmukh, S. R.; Vlachos, D. G. Effect of Flow Configuration on the Operation of Coupled Combustor/Reformer Microdevices for Hydrogen Production. *Chem. Eng. Sci.* **2005**, *60* (21), 5718−5728.
(107) Hanada, N.; Hino, S.; Ichikawa, T.; Suzuki, H.; Takai, K.; Kojima, Y. Hydrogen Generation by Electrolysis of Liquid Ammonia. *Chem. Commun.* **2010**, *46* (41), 7775−7777.
(108) Modisha, P.; Bessarabov, D. Electrocatalytic Process for Ammonia Electrolysis: A Remediation Technique with Hydrogen Co-Generation. *Int. J. Electrochem. Sci.* **2016**, *11* (8), 6627−6635.
(109) Reli, M.; Ambrožová, N.; Šihor, M.; Matějová, L.; Čapek, L.; Obalová, L.; Matěj, Z.; Kotarba, A.; Kočí, K. Novel Cerium Doped Titania Catalysts for Photocatalytic Decomposition of Ammonia. *Appl. Catal., B* **2015**, *178*, 108−116.
(110) Iwase, A.; Ii, K.; Kudo, A. Decomposition of an Aqueous Ammonia Solution as a Photon Energy Conversion Reaction Using a Ru-Loaded ZnS Photocatalyst. *Chem. Commun.* **2018**, *54* (48), 6117−6119.
(111) Wiig, E. O.; Kistiakowsky, G. B. The Photochemical Decomposition of Ammonia. *J. Am. Chem. Soc.* **1932**, *54* (5), 1806−1820.
(112) Li, Q.-s.; Domen, K.; Naito, S.; Onishi, T.; Tamaru, K. Photocatalytic Synthesis and Photodecomposition of Ammonia over $SrTiO_3$ and $BaTiO_3$ Based Catalysts. *Chem. Lett.* **1983**, *12*, 321−324.
(113) Yuzawa, H.; Mori, T.; Itoh, H.; Yoshida, H. Reaction Mechanism of Ammonia Decomposition to Nitrogen and Hydrogen over Metal Loaded Titanium Oxide Photocatalyst. *J. Phys. Chem. C* **2012**, *116* (6), 4126−4136.

(114) Paik, B.; Tsubota, M.; Ichikawa, T.; Kojima, Y. Catalytic Effect of $ATiO_3$ (A = Sr, Ba) on Ammonia Decomposition during Mechanical Milling. *Chem. Commun.* **2010**, *46* (22), 3982−3984.
(115) Li, L.; Hurley, J. A. Ammonia-Based Hydrogen Source for Fuel Cell Applications. *Int. J. Hydrogen Energy* **2007**, *32* (1), 6−10.
(116) White, A. H.; Melville, W. The Decomposition of Ammonia at High Temperatures. *J. Am. Chem. Soc.* **1905**, *27* (4), 373−386.
(117) Chambers, A.; Yoshii, Y.; Inada, T.; Miyamoto, T. Ammonia Decomposition in Coal Gasification Atmospheres. *Can. J. Chem. Eng.* **1996**, *74* (6), 929−934.
(118) Wang, W.; Padban, N.; Ye, Z.; Andersson, A.; Bjerle, I. Kinetics of Ammonia Decomposition in Hot Gas Cleaning. *Ind. Eng. Chem. Res.* **1999**, *38* (11), 4175−4182.
(119) Mojtahedi, W.; Abbasian, J. Catalytic Decomposition of Ammonia in a Fuel Gas at High Temperature and Pressure. *Fuel* **1995**, *74* (11), 1698−1703.
(120) Simell, P. A.; Hepola, J. O.; Krause, A. O. I. Effects of Gasification Gas Components on Tar and Ammonia Decomposition over Hot Gas Cleanup Catalysts. *Fuel* **1997**, *76* (12), 1117−1127.
(121) Platonov, O. I.; Stepanov, E. N. Monitoring Catalyst Activity in Removing Ammonia from Coke-Oven Gas. *Coke Chem.* **2008**, *51* (4), 153−154.
(122) Pansare, S. S.; Goodwin, J. G., Jr. Ammonia Decomposition on Tungsten-Based Catalysts in the Absence and Presence of Syngas. *Ind. Eng. Chem. Res.* **2008**, *47* (12), 4063−4070.
(123) Ohtsuka, Y.; Xu, C.; Kong, D.; Tsubouchi, N. Decomposition of Ammonia with Iron and Calcium Catalysts Supported on Coal Chars. *Fuel* **2004**, *83* (6), 685−692.
(124) Collins, J. P.; Way, J. D.; Kraisuwansarn, N. A Mathematical Model of a Catalytic Membrane Reactor for the Decomposition of NH_3. *J. Membr. Sci.* **1993**, *77* (2−3), 265−282.
(125) Gobina, E. N.; Oklany, J. S.; Hughes, R. Elimination of Ammonia from Coal Gasification Streams by Using a Catalytic Membrane Reactor. *Ind. Eng. Chem. Res.* **1995**, *34* (11), 3777−3783.
(126) Abashar, M. E. E. Integrated Catalytic Membrane Reactors for Decomposition of Ammonia. *Chem. Eng. Process.* **2002**, *41* (5), 403−412.
(127) Abashar, M. E. E.; Al-Sughair, Y. S.; Al-Mutaz, I. S. Investigation of Low Temperature Decomposition of Ammonia Using Spatially Patterned Catalytic Membrane Reactors. *Appl. Catal., A* **2002**, *236* (1−2), 35−53.
(128) Tsubouchi, N.; Hashimoto, H.; Ohtsuka, Y. Sulfur Tolerance of an Inexpensive Limonite Catalyst for High Temperature Decomposition of Ammonia. *Powder Technol.* **2008**, *180* (1−2), 184−189.
(129) Uemiya, S.; Uchida, M.; Moritomi, H.; Yoshiie, R.; Nishimura, M. Ammonia Decomposition Catalyst with Resistance to Coexisting Sulfur Compounds. *Mater. Trans.* **2005**, *46* (12), 2709−2712.
(130) Wang, W.; Padban, N.; Ye, Z.; Olofsson, G.; Andersson, A.; Bjerle, I. Catalytic Hot Gas Cleaning of Fuel Gas from an Air-Blown Pressurized Fluidized-Bed Gasifier. *Ind. Eng. Chem. Res.* **2000**, *39* (11), 4075−4081.
(131) Arabczyk, W.; Narkiewicz, U. A New Method for in Situ Determination of Number of Active Sites in Iron Catalysts for Ammonia Synthesis and Decomposition. *Appl. Surf. Sci.* **2002**, *196* (1−4), 423−428.
(132) He, C.; Wang, H.; Huai, L.; Liu, J. Mechanism of Ammonia Decomposition and Oxidation on Ir(100): A First-Principles Study. *J. Phys. Chem. C* **2012**, *116* (45), 24035−24045.
(133) Hung, C.-M. Catalytic Decomposition of Ammonia over Bimetallic CuO/CeO_2 Nanoparticle Catalyst. *Aerosol Air Qual. Res.* **2008**, *8* (4), 447−458.
(134) Lee, J. Y.; Lim, Y. H.; Park, B. H.; Adelodun, A. A.; Jo, Y. M. Preparation of Ag-Cu/Al_2O_3 Composite Catalyst for Ammonia Decomposition. *Bull. Korean Chem. Soc.* **2015**, *36* (1), 162−167.
(135) Bera, P.; Hegde, M. S. Oxidation and Decomposition of NH_3 over Combustion Synthesized Al_2O_3 and CeO_2 Supported Pt, Pd and Ag Catalysts. *Indian J. Chem. - Sect. A Inorganic, Phys. Theor. Anal. Chem.* **2002**, *41* (8), 1554−1561.
(136) Nagaoka, K.; Eboshi, T.; Takeishi, Y.; Tasaki, R.; Honda, K.; Imamura, K.; Sato, K. Carbon-Free H_2 Production from Ammonia Triggered at Room Temperature with an Acidic RuO_2/γ-Al_2O_3 Catalyst. *Sci. Adv.* **2017**, *3* (4), 1−8.
(137) Goto, M.; Shiramizu, D.; Kodama, A.; Hirose, T. Kinetic Analysis for Ammonia Decomposition in Supercritical Water Oxidation of Sewage Sludge. *Ind. Eng. Chem. Res.* **1999**, *38* (11), 4500−4503.
(138) Friedlander, A. G.; Courty, P. R.; Montarnal, R. E. Ammonia Decomposition in the Presence of Water Vapor. II. Kinetics of the Reaction on Nickel Catalyst. *J. Catal.* **1977**, *48* (1−3), 322−332.
(139) Atsumi, R.; Noda, R.; Takagi, H.; Vecchione, L.; Di Carlo, A.; Del Prete, Z.; Kuramoto, K. Effects of Steam on Ni/Al_2O_3 Catalysts for Ammonia Decomposition. *Ind. Eng. Chem. Res.* **2014**, *53* (45), 17849−17853.
(140) Hung, C.-M. Decomposition Kinetics of Ammonia in Gaseous Stream by a Nanoscale Copper-Cerium Bimetallic Catalyst. *J. Hazard. Mater.* **2008**, *150* (1), 53−61.
(141) Makepeace, J. W.; He, T.; Weidenthaler, C.; Jensen, T. R.; Chang, F.; Vegge, T.; Ngene, P.; Kojima, Y.; de Jongh, P. E.; Chen, P.; David, W. I. F. Reversible Ammonia-Based and Liquid Organic Hydrogen Carriers for High-Density Hydrogen Storage: Recent Progress. *Int. J. Hydrogen Energy* **2019**, *44* (15), 7746−7767.
(142) Dixon, J. K. The Kinetics of the Decomposition of Ammonia on Copper. *J. Am. Chem. Soc.* **1931**, *53* (5), 1763−1773.
(143) Mukherjee, S.; Devaguptapu, S. V.; Sviripa, A.; Lund, C. R. F.; Wu, G. Low-Temperature Ammonia Decomposition Catalysts for Hydrogen Generation. *Appl. Catal., B* **2018**, *226*, 162−181.
(144) Bell, T. E.; Torrente-Murciano, L. H_2 Production via Ammonia Decomposition Using Non-Noble Metal Catalysts: A Review. *Top. Catal.* **2016**, *59* (15−16), 1438−1457.
(145) Schüth, F.; Palkovits, R.; Schlögl, R.; Su, D. S. Ammonia as a Possible Element in an Energy Infrastructure: Catalysts for Ammonia Decomposition. *Energy Environ. Sci.* **2012**, *5* (4), 6278−6289.
(146) Chemical elements by market price. 13 Nov. 2020, http://www.leonland.de/elements_by_price/en/list (accessed 2020-11-13).
(147) Nuss, P.; Eckelman, M. J. Life Cycle Assessment of Metals: A Scientific Synthesis. *PLoS One* **2014**, *9* (7), e101298.
(148) García-Bordejé, E.; Armenise, S.; Roldán, L. Toward Practical Application of H_2 Generation from Ammonia Decomposition Guided by Rational Catalyst Design. *Catal. Rev.: Sci. Eng.* **2014**, *56* (2), 220−237.
(149) Cheddie, D. Ammonia as a Hydrogen Source for Fuel Cells: A Review. *Hydrogen Energy - Challenges and Perspectives* **2012**, 333−362.
(150) Abd Ali, Z. D.; Allami, S.; Jwad, B. H. Ammonia as Hydrogen Storage Media, Sustainable Method to Hydrogen Evolution. *J. Phys.: Conf. Ser.* **2018**, *1032* (1), 1−10.
(151) Yin, S. F.; Xu, B. Q.; Zhou, X. P.; Au, C. T. A Mini-Review on Ammonia Decomposition Catalysts for on-Site Generation of Hydrogen for Fuel Cell Applications. *Appl. Catal., A* **2004**, *277* (1−2), 1−9.
(152) Duan, X.; Zhou, X.; Chen, D. Structural Manipulation of the Catalysts for Ammonia Decomposition. *Catalysis* **2013**, *25*, 118−140.
(153) Boisen, A.; Dahl, S.; Nørskov, J. K.; Christensen, C. H. Why the Optimal Ammonia Synthesis Catalyst Is Not the Optimal Ammonia Decomposition Catalyst. *J. Catal.* **2005**, *230* (2), 309−312.
(154) Jacobsen, C. J. H.; Dahl, S.; Boisen, A.; Clausen, B. S.; Topsøe, H.; Logadottir, A.; Nørskov, J. K. Optimal Catalyst Curves: Connecting Density Functional Theory Calculations with Industrial Reactor Design and Catalyst Selection. *J. Catal.* **2002**, *205* (2), 382−387.
(155) Ganley, J. C.; Thomas, F. S.; Seebauer, E. G.; Masel, R. I. A *Priori* Catalytic Activity Correlations: The Difficult Case of Hydrogen Production from Ammonia. *Catal. Lett.* **2004**, *96* (3−4), 117−122.
(156) Yin, S.-F.; Zhang, Q.-H.; Xu, B.-Q.; Zhu, W.-X.; Ng, C.-F.; Au, C.-T. Investigation on the Catalysis of CO_x-Free Hydrogen Generation from Ammonia. *J. Catal.* **2004**, *224* (2), 384−396.
(157) Liu, H.; Wang, H.; Shen, J.; Ying, S.; Liu, Z. Preparation and Evaluation of Ammonia Decomposition Catalysts by High-Throughput Technique. *React. Kinet. Catal. Lett.* **2008**, *93* (1), 11−17.

https://doi.org/10.1021/acs.iecr.1c00843
Ind. Eng. Chem. Res. 2021, 60, 18560−18611

(158) Choudhary, T. V.; Sivadinarayana, C.; Goodman, D. W. Catalytic Ammonia Decomposition : CO_x-Free Hydrogen Production for Fuel Cell Applications. *Catal. Lett.* **2001**, *72* (3−4), 197−201.
(159) Choudhary, T. V.; Goodman, D. W. CO-Free Fuel Processing for Fuel Cell Applications. *Catal. Today* **2002**, *77*, 65−78.
(160) Li, Y.; Liu, S.; Yao, L.; Ji, W.; Au, C.-T. Core-Shell Structured Iron Nanoparticles for the Generation of CO_x-Free Hydrogen via Ammonia Decomposition. *Catal. Commun.* **2010**, *11* (5), 368−372.
(161) Yao, L.; Shi, T.; Li, Y.; Zhao, J.; Ji, W.; Au, C.-T. Core−Shell Structured Nickel and Ruthenium Nanoparticles: Very Active and Stable Catalysts for the Generation of CO_x-Free Hydrogen via Ammonia Decomposition. *Catal. Today* **2011**, *164* (1), 112−118.
(162) Yao, L. H.; Li, Y. X.; Zhao, J.; Ji, W. J.; Au, C. T. Core-Shell Structured Nanoparticles ($M@SiO_2$, Al_2O_3, MgO; M = Fe, Co, Ni, Ru) and Their Application in CO_x-Free H_2 Production via NH_3 Decomposition. *Catal. Today* **2010**, *158* (3−4), 401−408.
(163) Zhang, J.; Comotti, M.; Schüth, F.; Schlögl, R.; Su, D. S. Commercial Fe- or Co-Containing Carbon Nanotubes as Catalysts for NH_3 Decomposition. *Chem. Commun.* **2007**, *19*, 1916−1918.
(164) Li, X.-K.; Ji, W.-J.; Zhao, J.; Wang, S.-J.; Au, C.-T. Ammonia Decomposition over Ru and Ni Catalysts Supported on Fumed SiO_2, MCM-41, and SBA-15. *J. Catal.* **2005**, *236* (2), 181−189.
(165) Seehra, M. S.; Bristow, A. D. Introductory Chapter: Overview of the Properties and Applications of Noble and Precious Metals. *Noble and Precious Metals - Properties, Nanoscale Effects and Applications* **2018**, 3−11.
(166) Papapolymerou, G.; Bontozoglou, V. Decomposition of NH_3, on Pd and Ir Comparison with Pt and Rh. *J. Mol. Catal. A: Chem.* **1997**, *120*, 165−171.
(167) Hill, A. K.; Torrente-Murciano, L. In-Situ H_2 Production via Low Temperature Decomposition of Ammonia: Insights into the Role of Cesium as a Promoter. *Int. J. Hydrogen Energy* **2014**, *39* (15), 7646−7654.
(168) Hill, A. K.; Torrente-Murciano, L. Low Temperature H_2 Production from Ammonia Using Ruthenium-Based Catalysts: Synergetic Effect of Promoter and Support. *Appl. Catal., B* **2015**, *172*−*173*, 129−135.
(169) Wang, S. J.; Yin, S. F.; Li, L.; Xu, B. Q.; Ng, C. F.; Au, C. T. Investigation on Modification of Ru/CNTs Catalyst for the Generation of CO_x-Free Hydrogen from Ammonia. *Appl. Catal., B* **2004**, *52* (4), 287−299.
(170) Raróg-Pilecka, W.; Kowalczyk, Z.; Sentek, J.; Składanowski, D.; Szmigiel, D.; Zieliński, J. Decomposition of Ammonia over Potassium Promoted Ruthenium Catalyst Supported on Carbon. *Appl. Catal., A* **2001**, *208* (1−2), 213−216.
(171) Ren, S.; Huang, F.; Zheng, J.; Chen, S.; Zhang, H. Ruthenium Supported on Nitrogen-Doped Ordered Mesoporous Carbon as Highly Active Catalyst for NH_3 Decomposition to H_2. *Int. J. Hydrogen Energy* **2017**, *42* (8), 5105−5113.
(172) Bell, T. E.; Zhan, G.; Wu, K.; Zeng, H. C.; Torrente-Murciano, L. Modification of Ammonia Decomposition Activity of Ruthenium Nanoparticles by N-Doping of CNT Supports. *Top. Catal.* **2017**, *60* (15−16), 1251−1259.
(173) García-García, F. R.; Álvarez-Rodríguez, J.; Rodríguez-Ramos, I.; Guerrero-Ruiz, A. The Use of Carbon Nanotubes with and without Nitrogen Doping as Support for Ruthenium Catalysts in the Ammonia Decomposition Reaction. *Carbon* **2010**, *48* (1), 267−276.
(174) Chen, J.; Zhu, Z. H.; Wang, S.; Ma, Q.; Rudolph, V.; Lu, G. Q. Effects of Nitrogen Doping on the Structure of Carbon Nanotubes (CNTs) and Activity of Ru/CNTs in Ammonia Decomposition. *Chem. Eng. J.* **2010**, *156* (2), 404−410.
(175) Marco, Y.; Roldán, L.; Armenise, S.; García-Bordejé, E. Support-Induced Oxidation State of Catalytic Ru Nanoparticles on Carbon Nanofibers That Were Doped with Heteroatoms (O, N) for the Decomposition of NH_3. *ChemCatChem* **2013**, *5* (12), 3829−3834.
(176) Duan, X.; Zhou, J.; Qian, G.; Li, P.; Zhou, X.; Chen, D. Carbon Nanofiber-Supported Ru Catalysts for Hydrogen Evolution by Ammonia Decomposition. *Chin. J. Catal.* **2010**, *31* (8), 979−986.
(177) García-García, F. R.; Guerrero-Ruiz, A.; Rodríguez-Ramos, I. Role of B5-Type Sites in Ru Catalysts Used for the NH_3 Decomposition Reaction. *Top. Catal.* **2009**, *52* (6−7), 758−764.
(178) García-García, F. R.; Gallegos-Suarez, E.; Fernández-García, M.; Guerrero-Ruiz, A.; Rodríguez-Ramos, I. Understanding the Role of Oxygen Surface Groups: The Key for a Smart Ruthenium-Based Carbon-Supported Heterogeneous Catalyst Design and Synthesis. *Appl. Catal., A* **2017**, *544*, 66−76.
(179) Yin, S.-F.; Xu, B.-Q.; Ng, C.-F.; Au, C.-T. Nano Ru/CNTs: A Highly Active and Stable Catalyst for the Generation of CO_x-Free Hydrogen in Ammonia Decomposition. *Appl. Catal., B* **2004**, *48* (4), 237−241.
(180) Yin, S. F.; Xu, B. Q.; Zhu, W. X.; Ng, C. F.; Zhou, X. P.; Au, C. T. Carbon Nanotubes-Supported Ru Catalyst for the Generation of CO_x-Free Hydrogen from Ammonia. *Catal. Today* **2004**, *93*−*95*, 27−38.
(181) Petrunin, D. A.; Borisov, V. A.; Iost, K. N.; Temerev, V. L.; Trenikhin, M. V.; Gulyaeva, T. I.; Shlyapin, D. A.; Tsyrulnikov, P. G. Comparison of the Activity of Ru-K/Sibunit Catalysts in Ammonia Synthesis and Decomposition. *AIP Conf. Proc.* **2018**, *2141*, 0200241−0200247.
(182) Li, G.; Kanezashi, M.; Tsuru, T. Catalytic Ammonia Decomposition over High-Performance Ru/Graphene Nanocomposites for Efficient CO_x-Free Hydrogen Production. *Catalysts* **2017**, *7* (23), 1−12.
(183) Li, L.; Zhu, Z. H.; Yan, Z. F.; Lu, G. Q.; Rintoul, L. Catalytic Ammonia Decomposition over Ru/Carbon Catalysts: The Importance of the Structure of Carbon Support. *Appl. Catal., A* **2007**, *320*, 166−172.
(184) Li, L.; Zhu, Z. H.; Wang, S. B.; Yao, X. D.; Yan, Z. F. Chromium Oxide Catalysts for CO_x-Free Hydrogen Generation via Catalytic Ammonia Decomposition. *J. Mol. Catal. A: Chem.* **2009**, *304* (1−2), 71−76.
(185) Raróg-Pilecka, W.; Szmigiel, D.; Kowalczyk, Z.; Jodzis, S.; Zieliński, J. Ammonia Decomposition over the Carbon-Based Ruthenium Catalyst Promoted with Barium or Cesium. *J. Catal.* **2003**, *218* (2), 465−469.
(186) Huang, D.-C.; Jiang, C.-H.; Liu, F.-J.; Cheng, Y.-C.; Chen, Y.-C.; Hsueh, K.-L. Preparation of Ru−Cs Catalyst and Its Application on Hydrogen Production by Ammonia Decomposition. *Int. J. Hydrogen Energy* **2013**, *38* (8), 3233−3240.
(187) Li, L.; Zhu, Z. H.; Lu, G. Q.; Yan, Z. F.; Qiao, S. Z. Catalytic Ammonia Decomposition over CMK-3 Supported Ru Catalysts: Effects of Surface Treatments of Supports. *Carbon* **2007**, *45* (1), 11−20.
(188) Yin, S. F.; Xu, B. Q.; Wang, S. J.; Ng, C. F.; Au, C. T. Magnesia-Carbon Nanotubes (MgO-CNTs) Nanocomposite: Novel Support of Ru Catalyst for the Generation of CO_x-Free Hydrogen from Ammonia. *Catal. Lett.* **2004**, *96* (3−4), 113−116.
(189) Bajus, S.; Agel, F.; Kusche, M.; Ní Bhriain, N.; Wasserscheid, P. Alkali Hydroxide-Modified Ru/γ-Al_2O_3 Catalysts for Ammonia Decomposition. *Appl. Catal., A* **2016**, *510*, 189−195.
(190) Pyrz, W.; Vijay, R.; Binz, J.; Lauterbach, J.; Buttrey, D. J. Characterization of K-Promoted Ru Catalysts for Ammonia Decomposition Discovered Using High-Throughput Experimentation. *Top. Catal.* **2008**, *50* (1−4), 180−191.
(191) Klerke, A.; Klitgaard, S. K.; Fehrmann, R. Catalytic Ammonia Decomposition Over Ruthenium Nanoparticles Supported on Nano-Titanates. *Catal. Lett.* **2009**, *130* (3−4), 541−546.
(192) Chung, D. B.; Kim, H. Y.; Jeon, M.; Lee, D. H.; Park, H. S.; Choi, S. H.; Nam, S. W.; Jang, S. C.; Park, J.-H.; Lee, K.-Y.; Yoon, C. W. Enhanced Ammonia Dehydrogenation over Ru/La(x)-Al_2O_3(X = 0−50 Mol%): Structural and Electronic Effects of La Doping. *Int. J. Hydrogen Energy* **2017**, *42* (3), 1639−1647.
(193) Huang, C.; Yu, Y.; Yang, J.; Yan, Y.; Wang, D.; Hu, F.; Wang, X.; Zhang, R.; Feng, G. Ru/La_2O_3 Catalyst for Ammonia Decomposition to Hydrogen. *Appl. Surf. Sci.* **2019**, *476*, 928−936.
(194) Szmigiel, D.; Raróg-Pilecka, W.; Miśkiewicz, E.; Kaszkur, Z.; Kowalczyk, Z. Ammonia Decomposition over the Ruthenium Catalysts

https://doi.org/10.1021/acs.iecr.1c00843
Ind. Eng. Chem. Res. 2021, 60, 18560−18611

Deposited on Magnesium-Aluminum Spinel. *Appl. Catal., A* **2004**, *264* (1), 59−63.
(195) Su, Q.; Gu, L. L.; Zhong, A. H.; Yao, Y.; Ji, W. J.; Ding, W. P.; Au, C.-T. Layered Double Hydroxide Derived Mg_2Al-LDO Supported and K-Modified Ru Catalyst for Hydrogen Production via Ammonia Decomposition. *Catal. Lett.* **2018**, *149* (9), 1−10.
(196) Tan, H.; Li, K.; Sioud, S.; Cha, D.; Amad, M. H.; Hedhili, M. N.; Al-Talla, Z. A. Synthesis of Ru Nanoparticles Confined in Magnesium Oxide-Modified Mesoporous Alumina and Their Enhanced Catalytic Performance during Ammonia Decomposition. *Catal. Commun.* **2012**, *26*, 248−252.
(197) Wang, Z.; Qu, Y.; Shen, X.; Cai, Z. Ruthenium Catalyst Supported on Ba Modified ZrO_2 for Ammonia Decomposition to CO_x-Free Hydrogen. *Int. J. Hydrogen Energy* **2019**, *44* (14), 7300−7307.
(198) Lorenzut, B.; Montini, T.; Pavel, C. C.; Comotti, M.; Vizza, F.; Bianchini, C.; Fornasiero, P. Embedded Ru@ZrO_2 Catalysts for H_2 Production by Ammonia Decomposition. *ChemCatChem* **2010**, *2* (9), 1096−1106.
(199) Miyamoto, M.; Hamajima, A.; Oumi, Y.; Uemiya, S. Effect of Basicity of Metal Doped ZrO_2 Supports on Hydrogen Production Reactions. *Int. J. Hydrogen Energy* **2018**, *43* (2), 730−738.
(200) Yin, S.-F.; Xu, B.-Q.; Wang, S.-J.; Au, C.-T. Nanosized Ru on High-Surface-Area Superbasic ZrO_2-KOH for Efficient Generation of Hydrogen via Ammonia Decomposition. *Appl. Catal., A* **2006**, *301* (2), 202−210.
(201) Zhang, J.; Xu, H.; Ge, Q.; Li, W. Highly Efficient Ru/MgO Catalysts for NH_3 Decomposition: Synthesis, Characterization and Promoter Effect. *Catal. Commun.* **2006**, *7* (3), 148−152.
(202) Ju, X.; Liu, L.; Yu, P.; Guo, J.; Zhang, X.; He, T.; Wu, G.; Chen, P. Mesoporous Ru/MgO Prepared by a Deposition-Precipitation Method as Highly Active Catalyst for Producing CO_x-Free Hydrogen from Ammonia Decomposition. *Appl. Catal., B* **2017**, *211*, 167−175.
(203) Li, J.; Wang, W.; Chen, W.; Gong, Q.; Luo, J.; Lin, R.; Xin, H.; Zhang, H.; Wang, D.; Peng, Q.; Zhu, W.; Chen, C.; Li, Y. Sub-Nm Ruthenium Cluster as an Efficient and Robust Catalyst for Decomposition and Synthesis of Ammonia: Break the "Size Shackles. *Nano Res.* **2018**, *11* (9), 4774−4785.
(204) Kurtoğlu, S. F.; Soyer-Uzun, S.; Uzun, A. Utilizing Red Mud Modified by Simple Treatments as a Support to Disperse Ruthenium Provides a High and Stable Performance for CO_x-Free Hydrogen Production from Ammonia. *Catal. Today* **2020**, *357*, 1−11.
(205) Ng, P. F.; Li, L.; Wang, S.; Zhu, Z.; Lu, G.; Yan, Z. Catalytic Ammonia Decomposition over Industrial-Waste-Supported Ru Catalysts. *Environ. Sci. Technol.* **2007**, *41* (10), 3758−3762.
(206) Li, L.; Wang, S.; Zhu, Z.; Yao, X.; Yan, Z. Catalytic Decomposition of Ammonia over Fly Ash Supported Ru Catalysts. *Fuel Process. Technol.* **2008**, *89* (11), 1106−1112.
(207) Varışlı, D.; Elverisli, E. E. Synthesizing Hydrogen from Ammonia over Ru Incorporated SiO_2 Type Nanocomposite Catalysts. *Int. J. Hydrogen Energy* **2014**, *39* (20), 10399−10408.
(208) Li, Y.; Yao, L.; Song, Y.; Liu, S.; Zhao, J.; Ji, W.; Au, C.-T. Core-Shell Structured Microcapsular-like Ru@SiO_2 Reactor for Efficient Generation of CO_x-Free Hydrogen through Ammonia Decomposition. *Chem. Commun.* **2010**, *46* (29), 5298−5300.
(209) Wang, L.; Chen, J.; Ge, L.; Zhu, Z.; Rudolph, V. Halloysite-Nanotube-Supported Ru Nanoparticles for Ammonia Catalytic Decomposition to Produce CO_x-Free Hydrogen. *Energy Fuels* **2011**, *25* (8), 3408−3416.
(210) Hu, X.-C.; Fu, X.-P.; Wang, W.-W.; Wang, X.; Wu, K.; Si, R.; Ma, C.; Jia, C.-J.; Yan, C.-H. Ceria-Supported Ruthenium Clusters Transforming from Isolated Single Atoms for Hydrogen Production via Decomposition of Ammonia. *Appl. Catal., B* **2020**, *268*, 118424.
(211) Hu, Z.; Mahin, J.; Datta, S.; Bell, T. E.; Torrente-Murciano, L. Ru-Based Catalysts for H_2 Production from Ammonia: Effect of 1D Support. *Top. Catal.* **2019**, *62* (17−20), 1169−1177.
(212) Zhao, J.; Xu, S.; Wu, H.; You, Z.; Deng, L.; Qiu, X. Metal-Support Interactions on Ru/$CaAlO_X$ Catalysts Derived from Structural Reconstruction of Ca-Al Layered Double Hydroxides for Ammonia Decomposition. *Chem. Commun.* **2019**, *55* (96), 14410−14413.
(213) Hayashi, F.; Toda, Y.; Kanie, Y.; Kitano, M.; Inoue, Y.; Yokoyama, T.; Hara, M.; Hosono, H. Ammonia Decomposition by Ruthenium Nanoparticles Loaded on Inorganic Electride C12A7:E^-. *Chem. Sci.* **2013**, *4* (8), 3124−3130.
(214) Wang, Z.; Cai, Z.; Wei, Z. Highly Active Ruthenium Catalyst Supported on Barium Hexaaluminate for Ammonia Decomposition to CO_x-Free Hydrogen. *ACS Sustainable Chem. Eng.* **2019**, *7* (9), 8226−8235.
(215) Nagaoka, K.; Eboshi, T.; Abe, N.; Miyahara, S. I.; Honda, K.; Sato, K. Influence of Basic Dopants on the Activity of Ru/Pr_6O_{11} for Hydrogen Production by Ammonia Decomposition. *Int. J. Hydrogen Energy* **2014**, *39* (35), 20731−20735.
(216) Nagaoka, K.; Honda, K.; Ibuki, M.; Sato, K.; Takita, Y. Highly Active Cs_2O/Ru/Pr_6O_{11} as a Catalyst for Ammonia Decomposition. *Chem. Lett.* **2010**, *39* (9), 918−919.
(217) Zheng, W.; Zhang, J.; Xu, H.; Li, W. NH_3 Decomposition Kinetics on Supported Ru Clusters: Morphology and Particle Size Effect. *Catal. Lett.* **2007**, *119* (3−4), 311−318.
(218) Simonsen, S. B.; Chakraborty, D.; Chorkendorff, I.; Dahl, S. Alloyed Ni-Fe Nanoparticles as Catalysts for NH_3 Decomposition. *Appl. Catal., A* **2012**, *447−448*, 22−31.
(219) Lucentini, I.; Casanovas, A.; Llorca, J. Catalytic Ammonia Decomposition for Hydrogen Production on Ni, Ru and Ni−Ru Supported on CeO_2. *Int. J. Hydrogen Energy* **2019**, *44*, 12693−12707.
(220) Prasad, V.; Karim, A. M.; Arya, A.; Vlachos, D. G. Assessment of Overall Rate Expressions and Multiscale, Microkinetic Model Uniqueness via Experimental Data Injection: Ammonia Decomposition on Ru/γ-Al_2O_3 for Hydrogen Production. *Ind. Eng. Chem. Res.* **2009**, *48* (11), 5255−5265.
(221) Karim, A. M.; Prasad, V.; Mpourmpakis, G.; Lonergan, W. W.; Frenkel, A. I.; Chen, J. G.; Vlachos, D. G. Correlating Particle Size and Shape of Supported Ru/γ-Al_2O_3 Catalysts with NH_3 Decomposition Activity. *J. Am. Chem. Soc.* **2009**, *131* (34), 12230−12239.
(222) McCullough, K.; Chiang, P.-H.; Jimenez, J. D.; Lauterbach, J. A. Material Discovery and High Throughput Exploration of Ru Based Catalysts for Low Temperature Ammonia Decomposition. *Materials* **2020**, *13* (8), 1−19.
(223) Su, Q.; Gu, L.; Yao, Y.; Zhao, J.; Ji, W.; Ding, W.; Au, C.-T. Layered Double Hydroxides Derived $Ni_x(Mg_yAl_zO_n)$ Catalysts: Enhanced Ammonia Decomposition by Hydrogen Spillover Effect. *Appl. Catal., B* **2017**, *201*, 451−460.
(224) Bramwell, P. L.; Lentink, S.; Ngene, P.; De Jongh, P. E. Effect of Pore Confinement of $LiNH_2$ on Ammonia Decomposition Catalysis and the Storage of Hydrogen and Ammonia. *J. Phys. Chem. C* **2016**, *120* (48), 27212−27220.
(225) Lamb, K.; Hla, S. S.; Dolan, M. Ammonia Decomposition Kinetics over LiOH-Promoted, α-Al_2O_3 -Supported Ru Catalyst. *Int. J. Hydrogen Energy* **2019**, *44* (7), 3726−3736.
(226) Torrente-Murciano, L.; Hill, A. K.; Bell, T. E. Ammonia Decomposition over Cobalt/Carbon Catalysts—Effect of Carbon Support and Electron Donating Promoter on Activity. *Catal. Today* **2017**, *286*, 131−140.
(227) Raróg-Pilecka, W.; Szmigiel, D.; Komornicki, A.; Zieliński, J.; Kowalczyk, Z. Catalytic Properties of Small Ruthenium Particles Deposited on Carbon: Ammonia Decomposition Studies. *Carbon* **2003**, *41* (3), 589−591.
(228) Xie, P.; Yao, Y.; Huang, Z.; Liu, Z.; Zhang, J.; Li, T.; Wang, G.; Shahbazian-Yassar, R.; Hu, L.; Wang, C. Highly Efficient Decomposition of Ammonia Using High-Entropy Alloy Catalysts. *Nat. Commun.* **2019**, *10* (4011), 1−12.
(229) Wang, L.; Chen, J.; Ge, L.; Rudolph, V.; Zhu, Z. Difference in the Cooperative Interaction between Carbon Nanotubes and Ru Particles Loaded on Their Internal/External Surface. *RSC Adv.* **2013**, *3* (31), 12641−12647.
(230) Zheng, W.; Zhang, J.; Zhu, B.; Blume, R.; Zhang, Y.; Schlichte, K.; Schlögl, R.; Schüth, F.; Su, D. S. Structure-Function Correlations for Ru/CNT in the Catalytic Decomposition of Ammonia. *ChemSusChem* **2010**, *3* (2), 226−230.

https://doi.org/10.1021/acs.iecr.1c00843
Ind. Eng. Chem. Res. 2021, 60, 18560−18611

(231) Chen, C.; Chen, Y.; Ali, A. M.; Luo, W.; Wen, J.; Zhang, L.; Zhang, H. Bimetallic Ru-Fe Nanoparticles Supported on Carbon Nanotubes for Ammonia Decomposition and Synthesis. *Chem. Eng. Technol.* **2020**, *43* (4), 719−730.
(232) Guo, J.; Chen, Z.; Wu, A.; Chang, F.; Wang, P.; Hu, D.; Wu, G.; Xiong, Z.; Yu, P.; Chen, P. Electronic Promoter or Reacting Species? The Role of $LiNH_2$ on Ru in Catalyzing NH_3 Decomposition. *Chem. Commun.* **2015**, *51* (82), 15161−15164.
(233) Guo, J.; Wang, P.; Wu, G.; Wu, A.; Hu, D.; Xiong, Z.; Wang, J.; Yu, P.; Chang, F.; Chen, Z.; Chen, P. Lithium Imide Synergy with 3d Transition-Metal Nitrides Leading to Unprecedented Catalytic Activities for Ammonia Decomposition. *Angew. Chem.* **2015**, *127* (10), 2993−2997.
(234) Li, L.; Wang, Y.; Xu, Z. P.; Zhu, Z. Catalytic Ammonia Decomposition for CO-Free Hydrogen Generation over Ru/Cr_2O_3 Catalysts. *Appl. Catal., A* **2013**, *467*, 246−252.
(235) Chang, F.; Wu, H.; Van der Pluijm, R.; Guo, J.; Ngene, P.; De Jongh, P. E. Effect of Pore Confinement of $NaNH_2$ and KNH_2 on Hydrogen Generation from Ammonia. *J. Phys. Chem. C* **2019**, *123* (35), 21487−21496.
(236) Zheng, W.; Cotter, T. P.; Kaghazchi, P.; Jacob, T.; Frank, B.; Schlichte, K.; Zhang, W.; Su, D. S.; Schüth, F.; Schlögl, R. Experimental and Theoretical Investigation of Molybdenum Carbide and Nitride as Catalysts for Ammonia Decomposition. *J. Am. Chem. Soc.* **2013**, *135* (9), 3458−3464.
(237) Yu, P.; Guo, J.; Liu, L.; Wang, P.; Chang, F.; Wang, H.; Ju, X.; Chen, P. Effects of Alkaline Earth Metal Amides on Ru in Catalytic Ammonia Decomposition. *J. Phys. Chem. C* **2016**, *120* (5), 2822−2828.
(238) Takahashi, A.; Fujitani, T. Kinetic Analysis of Decomposition of Ammonia over Nickel and Ruthenium Catalysts. *J. Chem. Eng. Jpn.* **2016**, *49* (1), 22−28.
(239) Maeda, A.; Hu, Z.; Kunimori, K.; Uchijima, T. Effect of High-Temperature Reduction on Ammonia Decomposition over Niobia-Supported and Nioba-Promoted Rhodium Catalysts. *Catal. Lett.* **1988**, *1*, 155−157.
(240) Richardson, D. J.; Hellgardt, K.; Russell, P. A.; Mason, G.; Buffman, B. A. Flux Response Analysis: A Study of Ammonia Decomposition over Pt/Alumina. *Chem. Eng. Res. Des.* **2004**, *82* (10), 1397−1403.
(241) Polański, J.; Bartczak, P.; Ambrozkiewicz, W.; Sitko, R.; Siudyga, T.; Mianowski, A.; Szade, J.; Balin, K.; Lelątko, J. Ni-Supported Pd Nanoparticles with Ca Promoter: A New Catalyst for Low-Temperature Ammonia Cracking. *PLoS One* **2015**, *10* (8), e0136805.
(242) Choi, J.-G. Ammonia Decomposition over Vanadium Carbide Catalysts. *J. Catal.* **1999**, *182* (1), 104−116.
(243) Varışlı, D.; Rona, T. CO_x Free Hydrogen Production from Ammonia Decomposition over Platinum Based Siliceous Materials. *Int. J. Chem. React. Eng.* **2012**, *10* (1), 1−30.
(244) Donald, J.; Xu, C.; Hashimoto, H.; Byambajav, E.; Ohtsuka, Y. Novel Carbon-Based Ni/Fe Catalysts Derived from Peat for Hot Gas Ammonia Decomposition in an Inert Helium Atmosphere. *Appl. Catal., A* **2010**, *375* (1), 124−133.
(245) Gu, Y.-Q.; Jin, Z.; Zhang, H.; Xu, R.-J.; Zheng, M.-J.; Guo, Y.-M.; Song, Q.-S.; Jia, C.-J. Transition Metal Nanoparticles Dispersed in an Alumina Matrix as Active and Stable Catalysts for CO_x-Free Hydrogen Production from Ammonia. *J. Mater. Chem. A* **2015**, *3* (33), 17172−17180.
(246) Hu, X.-C.; Wang, W.-W.; Jin, Z.; Wang, X.; Si, R.; Jia, C.-J. Transition Metal Nanoparticles Supported La-Promoted MgO as Catalysts for Hydrogen Production via Catalytic Decomposition of Ammonia. *J. Energy Chem.* **2019**, *38*, 41−49.
(247) Zhang, H.; Alhamed, Y. A.; Kojima, Y.; Al-Zahrani, A. A.; Petrov, L. A. Cobalt Supported on Carbon Nanotubes. An Efficient Catalyst for Ammonia Decomposition. *C. R. Acad. Bulg. Sci.* **2013**, *66* (4), 519−524.
(248) Xun, Y.; He, X.; Yan, H.; Gao, Z.; Jin, Z.; Jia, C. Fe- and Co-Doped Lanthanum Oxides Catalysts for Ammonia Decomposition: Structure and Catalytic Performances. *J. Rare Earths* **2017**, *35* (1), 15−23.
(249) Xu, C.; Tsubouchi, N.; Hashimoto, H.; Ohtsuka, Y. Catalytic Decomposition of Ammonia Gas with Metal Cations Present Naturally in Low Rank Coals. *Fuel* **2005**, *84* (14−15), 1957−1967.
(250) Dasireddy, V. D. B. C.; Likozar, B. CO_x-Free Hydrogen Generation *via* Decomposition of Ammonia over Copper and Zinc-Based Catalysts. *Fuel* **2017**, *196*, 325−335.
(251) Zhang, J.; Xu, H.; Li, W. Kinetic Study of NH_3 Decomposition over Ni Nanoparticles: The Role of La Promoter, Structure Sensitivity and Compensation Effect. *Appl. Catal., A* **2005**, *296* (12), 257−267.
(252) Zhang, J.; Xu, H.; Jin, X.; Ge, Q.; Li, W. Characterizations and Activities of the Nano-Sized Ni/Al_2O_3 and $Ni/La\text{-}Al_2O_3$ Catalysts for NH_3 Decomposition. *Appl. Catal., A* **2005**, *290* (1−2), 87−96.
(253) Yan, H.; Xu, Y.-J.; Gu, Y.-Q.; Li, H.; Wang, X.; Jin, Z.; Shi, S.; Si, R.; Jia, C.-J.; Yan, C.-H. Promoted Multimetal Oxide Catalysts for the Generation of Hydrogen via Ammonia Decomposition. *J. Phys. Chem. C* **2016**, *120* (14), 7685−7696.
(254) Okura, K.; Okanishi, T.; Muroyama, H.; Matsui, T.; Eguchi, K. Ammonia Decomposition over Nickel Catalysts Supported on Rare-Earth Oxides for the On-Site Generation of Hydrogen. *ChemCatChem* **2016**, *8*, 2988−2995.
(255) Nakamura, I.; Fujitani, T. Role of Metal Oxide Supports in NH_3 Decomposition over Ni. *Appl. Catal., A* **2016**, *524*, 45−49.
(256) Muroyama, H.; Saburi, C.; Matsui, T.; Eguchi, K. Ammonia Decomposition over Ni/La_2O_3 Catalyst for on-Site Generation of Hydrogen. *Appl. Catal., A* **2012**, *443*−*444*, 119−124.
(257) Okura, K.; Okanishi, T.; Muroyama, H.; Matsui, T.; Eguchi, K. Promotion Effect of Rare-Earth Elements on the Catalytic Decomposition of Ammonia over Ni/Al_2O_3 Catalyst. *Appl. Catal., A* **2015**, *505*, 77−85.
(258) Okura, K.; Miyazaki, K.; Muroyama, H.; Matsui, T.; Eguchi, K. Ammonia Decomposition over Ni Catalysts Supported on Perovskite-Type Oxides for the on-Site Generation of Hydrogen. *RSC Adv.* **2018**, *8* (56), 32102−32110.
(259) Liu, Y.; Wang, H.; Li, J.; Lu, Y.; Wu, H.; Xue, Q.; Chen, L. Monolithic Microfibrous Nickel Catalyst Co-Modified with Ceria and Alumina for Miniature Hydrogen Production via Ammonia Decomposition. *Appl. Catal., A* **2007**, *328* (1), 77−82.
(260) Zheng, W.; Zhang, J.; Ge, Q.; Xu, H.; Li, W. Effects of CeO_2 Addition on Ni/Al_2O_3 Catalysts for the Reaction of Ammonia Decomposition to Hydrogen. *Appl. Catal., B* **2008**, *80* (1−2), 98−105.
(261) Vacharapong, P.; Arayawate, S.; Henpraserttae, S.; Katanyutanon, S.; Charojrochkul, S.; Lawtrakul, L.; Toochinda, P. Effect of Magnetic Inducement in Preparation of Ni/Ce-Doped Al_2O_3 for Ammonia Decomposition. *ChemistrySelect* **2019**, *4* (40), 11913−11919.
(262) Liu, H.; Wang, H.; Shen, J.; Sun, Y.; Liu, Z. Promotion Effect of Cerium and Lanthanum Oxides on Ni/SBA-15 Catalyst for Ammonia Decomposition. *Catal. Today* **2008**, *131* (1−4), 444−449.
(263) Trovarelli, A.; Llorca, J. Ceria Catalysts at Nanoscale: How Do Crystal Shapes Shape Catalysis? *ACS Catal.* **2017**, *7* (7), 4716−4735.
(264) Trovarelli, A. Catalytic Properties of Ceria and CeO_2-Containing Materials. *Catal. Rev.: Sci. Eng.* **1996**, *38* (4), 439−520.
(265) Campbell, C. T.; Peden, C. H. F. Oxygen Vacancies and Catalysis on Ceria Surfaces. *Science (Washington, DC, U. S.)* **2005**, *309* (5735), 713−714.
(266) Melchionna, M.; Fornasiero, P. The Role of Ceria-Based Nanostructured Materials in Energy Applications. *Mater. Today* **2014**, *17* (7), 349−357.
(267) Choudhary, T. V.; Sivadinarayana, C.; Goodman, D. W. Production of CO_x-Free Hydrogen for Fuel Cells via Step-Wise Hydrocarbon Reforming and Catalytic Dehydrogenation of Ammonia. *Chem. Eng. J.* **2003**, *93* (1), 69−80.
(268) Atsumi, R.; Noda, R.; Takagi, H.; Vecchione, L.; Di Carlo, A.; Del Prete, Z.; Kuramoto, K. Ammonia Decomposition Activity over Ni/SiO_2 Catalysts with Different Pore Diameters. *Int. J. Hydrogen Energy* **2014**, *39* (26), 13954−13961.
(269) Li, Y.; Wen, J.; Ali, A. M.; Duan, M.; Zhu, W.; Zhang, H.; Chen, C.; Li, Y. Size Structure − Catalytic Performance Correlation of

https://doi.org/10.1021/acs.iecr.1c00843
Ind. Eng. Chem. Res. 2021, 60, 18560−18611

Supported Ni/MCF-17 Catalysts for CO_x-Free Hydrogen Production. *Chem. Commun.* **2018**, *54*, 6364−6367.
(270) Duan, X.; Qian, G.; Liu, Y.; Ji, J.; Zhou, X.; Chen, D.; Yuan, W. Structure Sensitivity of Ammonia Decomposition over Ni Catalysts: A Computational and Experimental Study. *Fuel Process. Technol.* **2013**, *108*, 112−117.
(271) Zhang, L.-F.; Li, M.; Ren, T.-Z.; Liu, X.; Yuan, Z.-Y. Ce-Modified Ni Nanoparticles Encapsulated in SiO_2 for CO_x-Free Hydrogen Production via Ammonia Decomposition. *Int. J. Hydrogen Energy* **2015**, *40* (6), 2648−2656.
(272) Liu, H.; Wang, H.; Shen, J.; Sun, Y.; Liu, Z. Preparation, Characterization and Activities of the Nano-Sized Ni/SBA-15 Catalyst for Producing CO_x-Free Hydrogen from Ammonia. *Appl. Catal., A* **2008**, *337* (2), 138−147.
(273) Li, L.; Chen, F.; Shao, J.; Dai, Y.; Ding, J.; Tang, Z. Attapulgite Clay Supported Ni Nanoparticles Encapsulated by Porous Silica: Thermally Stable Catalysts for Ammonia Decomposition to CO_x Free Hydrogen. *Int. J. Hydrogen Energy* **2016**, *41* (46), 21157−21165.
(274) Kurtoğlu, S. F.; Sarp, S.; Yılmaz Akkaya, C.; Yağcı, B.; Motallebzadeh, A.; Soyer-Uzun, S.; Uzun, A. CO_x-Free Hydrogen Production from Ammonia Decomposition over Sepiolite-Supported Nickel Catalysts. *Int. J. Hydrogen Energy* **2018**, *43* (21), 9954−9968.
(275) Henpraserttae, S.; Leong, H. W.; Ratprasatpon, P.; Moolgate, J.; Toochinda, P. Effect of Acidic Sites of Support to Nickle Catalysts for Ammonia Decomposition. *2016 2nd Asian Conference on Defence Technology (ACDT)* **2016**, 167−169.
(276) Henpraserttae, S.; Charojrochkul, S.; Klysubun, W.; Lawtrakul, L.; Toochinda, P. Reduced Temperature Ammonia Decomposition Using Ni/Zr-Doped Al_2O_3 Catalyst. *Catal. Lett.* **2018**, *148* (6), 1775−1783.
(277) Henpraserttae, S.; Charojrochkul, S.; Lawtrakul, L.; Toochinda, P. Ni-Based Catalysts for Hydrogen Production from Ammonia Decomposition: Effect of Dopants and Urine Application. *ChemistrySelect* **2018**, *3* (42), 11842−11850.
(278) Deng, Q.-F.; Zhang, H.; Hou, X.-X.; Ren, T.-Z.; Yuan, Z.-Y. High-Surface-Area $Ce_{0.8}Zr_{0.2}O_2$ Solid Solutions Supported Ni Catalysts for Ammonia Decomposition to Hydrogen. *Int. J. Hydrogen Energy* **2012**, *37* (21), 15901−15907.
(279) Sima, D.; Wu, H.; Tian, K.; Xie, S.; Foo, J. J.; Li, S.; Wang, D.; Ye, Y.; Zheng, Z.; Liu, Y. Q. Enhanced Low Temperature Catalytic Activity of Ni/Al−$Ce_{0.8}Zr_{0.2}O_2$ for Hydrogen Production from Ammonia Decomposition. *Int. J. Hydrogen Energy* **2020**, *45* (16), 9342−9352.
(280) Zhao, J.; Deng, L.; Zheng, W.; Xu, S.; Yu, Q.; Qiu, X. Nickel-Induced Structure Transformation in Hydrocalumite for Enhanced Ammonia Decomposition. *Int. J. Hydrogen Energy* **2020**, *45* (22), 12244−12255.
(281) Sato, K.; Abe, N.; Kawagoe, T.; Miyahara, S.; Honda, K.; Nagaoka, K. Supported Ni Catalysts Prepared from Hydrotalcite-like Compounds for the Production of Hydrogen by Ammonia Decomposition. *Int. J. Hydrogen Energy* **2017**, *42* (10), 6610−6617.
(282) Inokawa, H.; Ichikawa, T.; Miyaoka, H. Catalysis of Nickel Nanoparticles with High Thermal Stability for Ammonia Decomposition. *Appl. Catal., A* **2015**, *491*, 184−188.
(283) Alhamed, Y. A.; Zhang, H.; Kojima, Y.; Al-Zahrani, A. A.; Hafedh, D.; Petrov, L. A. Effect of Surface Functional Groups Attached to Carbon Nanotubes Used as Support of Nickel Catalysts on Their Structure and Catalytic Performance for Ammonia Decomposition. *Comptes Rendus L'Academie Bulg. des Sci.* **2014**, *67* (4), 519−526.
(284) Zhang, H.; Alhamed, Y. A.; Kojima, Y.; Al-Zahrani, A. A.; Miyaoka, H.; Petrov, L. A. Structure and Catalytic Properties of Ni/MWCNTs and Ni/AC Catalysts for Hydrogen Production via Ammonia Decomposition. *Int. J. Hydrogen Energy* **2014**, *39* (1), 277−287.
(285) Meng, T.; Xu, Q.-Q.; Li, Y.-T.; Chang, J.-L.; Ren, T.-Z.; Yuan, Z.-Y. Nickle Nanoparticles Highly Dispersed on Reduced Graphene Oxide for Ammonia Decomposition to Hydrogen. *J. Ind. Eng. Chem.* **2015**, *32*, 373−379.
(286) Cao, J. L.; Yan, Z.-L.; Deng, Q.-F.; Yuan, Z.-Y.; Wang, Y.; Sun, G.; Wang, X.-D.; Hari, B.; Zhang, Z.-Y. Homogeneous Precipitation Method Preparation of Modified Red Mud Supported Ni Mesoporous Catalysts for Ammonia Decomposition. *Catal. Sci. Technol.* **2014**, *4* (2), 361−368.
(287) Cao, J.-L.; Yan, Z.-L.; Deng, Q.-F.; Wang, Y.; Yuan, Z.-Y.; Sun, G.; Jia, T.-K.; Wang, X.-D.; Bala, H.; Zhang, Z.-Y. Mesoporous Modified-Red-Mud Supported Ni Catalysts for Ammonia Decomposition to Hydrogen. *Int. J. Hydrogen Energy* **2014**, *39* (11), 5747−5755.
(288) Lu, A.-H.; Nitz, J.-J.; Comotti, M.; Weidenthaler, C.; Schlichte, K.; Lehmann, C. W.; Terasaki, O.; Schüth, F. Spatially and Size Selective Synthesis of Fe-Based Nanoparticles on Ordered Mesoporous Supports as Highly Active and Stable Catalysts for Ammonia Decomposition. *J. Am. Chem. Soc.* **2010**, *132* (40), 14152−14162.
(289) Tüysüz, H.; Schüth, F.; Zhi, L.; Müllen, K.; Comotti, M. Ammonia Decomposition over Iron Phthalocyanine-Based Materials. *ChemCatChem* **2015**, *7* (9), 1453−1459.
(290) Liang, C.; Li, W.; Wei, Z.; Xin, Q.; Li, C. Catalytic Decomposition of Ammonia over Nitrided MoN_x/Alfa-Al_2O_3 and $NiMoN_y$/Alfa-Al_2O_3 Catalysts. *Ind. Eng. Chem. Res.* **2000**, *39*, 3694−3697.
(291) Han, X.; Chu, W.; Ni, P.; Luo, S. Z.; Zhang, T. Promoting Effects of Iridium on Nickel Based Catalyst in Ammonia Decomposition. *J. Fuel Chem. Technol.* **2007**, *35* (6), 691−695.
(292) Huang, C.; Li, H.; Yang, J.; Wang, C.; Hu, F.; Wang, X.; Lu, Z. H.; Feng, G.; Zhang, R. $Ce_{0.6}Zr_{0.3}Y_{0.1}O_2$ Solid Solutions-Supported Ni−Co Bimetal Nanocatalysts for NH_3 Decomposition. *Appl. Surf. Sci.* **2019**, *478*, 708−716.
(293) Hu, Z.-P.; Weng, C.-C.; Chen, C.; Yuan, Z.-Y. Catalytic Decomposition of Ammonia to CO_x-Free Hydrogen over Ni/ZSM-5 Catalysts: A Comparative Study of the Preparation Methods. *Appl. Catal., A* **2018**, *562*, 49−57.
(294) Kunsman, C. H. The Decomposition of Ammonia on Iron Catalysts. *Science (Washington, DC, U. S.)* **1927**, *65* (1691), 527−528.
(295) Kowalczyk, Z.; Sentek, J.; Jodzis, S.; Muhler, M.; Hinrichsen, O. Effect of Potassium on the Kinetics of Ammonia Synthesis and Decomposition over Fused Iron Catalyst at Atmospheric Pressure. *J. Catal.* **1997**, *169*, 407−414.
(296) Arabczyk, W.; Pelka, R. Studies of the Kinetics of Two Parallel Reactions: Ammonia Decomposition and Nitriding of Iron Catalyst. *J. Phys. Chem. A* **2009**, *113* (2), 411−416.
(297) Othman, N. E. F.; Salleh, H. M.; Purwanto, H. Utilization of Low-Grade Iron Ore in Ammonia Decomposition. *Procedia Chem.* **2016**, *19*, 119−124.
(298) Tseng, J.-C.; Gu, D.; Pistidda, C.; Horstmann, C.; Dornheim, M.; Ternieden, J.; Weidenthaler, C. Tracking the Active Catalyst for Iron-Based Ammonia Decomposition by In Situ Synchrotron Diffraction Studies. *ChemCatChem* **2018**, *10* (19), 4465.
(299) Pelka, R.; Moszyńska, I.; Arabczyk, W. Catalytic Ammonia Decomposition over Fe/Fe_4N. *Catal. Lett.* **2009**, *128* (1−2), 72−76.
(300) Pelka, R.; Arabczyk, W. Studies of the Kinetics of Reaction between Iron Catalysts and Ammonia-Nitriding of Nanocrystalline Iron with Parallel Catalytic Ammonia Decomposition. *Top. Catal.* **2009**, *52* (11), 1506−1516.
(301) Pelka, R.; Kiełbasa, K.; Arabczyk, W. Catalytic Ammonia Decomposition during Nanocrystalline Iron Nitriding at 475°C with NH_3/H_2 Mixtures of Different Nitriding Potentials. *J. Phys. Chem. C* **2014**, *118* (12), 6178−6185.
(302) Kiełbasa, K.; Pelka, R.; Arabczyk, W. Studies of the Kinetics of Ammonia Decomposition on Promoted Nanocrystalline Iron Using Gas Phases of Different Nitriding Degree. *J. Phys. Chem. A* **2010**, *114* (13), 4531−4534.
(303) Pelka, R.; Kiełbasa, K.; Arabczyk, W. The Effect of Iron Nanocrystallites' Size in Catalysts for Ammonia Synthesis on Nitriding Reaction and Catalytic Ammonia Decomposition. *Cent. Eur. J. Chem.* **2011**, *9* (2), 240−244.
(304) Pelka, R.; Arabczyk, W. Influence of Chemical Composition of Nanocrystalline Iron's Surface on the Rates of Two Parallel Reactions:

https://doi.org/10.1021/acs.iecr.1c00843
Ind. Eng. Chem. Res. 2021, 60, 18560−18611

Nitriding and Catalytic Decomposition of Ammonia. *Chem. Pap.* **2012**, *66* (1), 18−25.
(305) Feyen, M.; Weidenthaler, C.; Guttel, R.; Schlichte, K.; Holle, U.; Lu, A.-H.; Schuth, F. Schüth, F. High-Temperature Stable, Iron-Based Core-Shell Catalysts for Ammonia Decomposition. *Chem. - Eur. J.* **2011**, *17* (2), 598−605.
(306) Li, Y.; Yao, L.; Liu, S.; Zhao, J.; Ji, W.; Au, C.-T. Cs-Modified Iron Nanoparticles Encapsulated in Microporous and Mesoporous SiO_2 for CO_x-Free H_2 Production via Ammonia Decomposition. *Catal. Today* **2011**, *160* (1), 79−86.
(307) Hu, Z.-P.; Chen, L.; Chen, C.; Yuan, Z.-Y. Fe/ZSM-5 Catalysts for Ammonia Decomposition to CO_x-Free Hydrogen: Effect of SiO_2/Al_2O_3 Ratio. *Mol. Catal.* **2018**, *455*, 14−22.
(308) Cui, H.-Z.; Gu, Y.-Q.; He, X.-X.; Wei, S.; Jin, Z.; Jia, C.-J.; Song, Q.-S. Iron-Based Composite Nanostructure Catalysts Used to Produce CO_x-Free Hydrogen from Ammonia. *Sci. Bull.* **2016**, *61* (3), 220−226.
(309) Tsubouchi, N.; Hashimoto, H.; Ohtsuka, Y. High Catalytic Performance of Fine Particles of Metallic Iron Formed from Limonite in the Decomposition of a Low Concentration of Ammonia. *Catal. Lett.* **2005**, *105* (3−4), 203−208.
(310) Rein, D.; Friedel Ortega, K.; Weidenthaler, C.; Bill, E.; Behrens, M. The Roles of Co-Precipitation PH, Phase-Purity and Alloy Formation for the Ammonia Decomposition Activity of Ga-Promoted Fe/MgO Catalysts. *Appl. Catal., A* **2017**, *548*, 52−61.
(311) Ortega, K. F.; Rein, D.; Lüttmann, C.; Heese, J.; Özcan, F.; Heidelmann, M.; Folke, J.; Kähler, K.; Schlögl, R.; Behrens, M. Ammonia Decomposition and Synthesis over Multinary Magnesio-ferrites: Promotional Effect of Ga on Fe Catalysts for the Decomposition Reaction. *ChemCatChem* **2017**, *9* (4), 659−671.
(312) Itoh, M.; Masuda, M.; Machida, K. Hydrogen Generation by Ammonia Cracking with Iron Metal-Rare Earth Oxide Composite Catalyst. *Mater. Trans.* **2002**, *43* (11), 2763−2767.
(313) Li, L.; Meng, Q.; Ji, W.; Shao, J.; Xu, Q.; Yan, J. Embedded Iron Nanoparticles by Graphitized Carbon as Highly Active yet Stable Catalyst for Ammonia Decomposition. *Mol. Catal.* **2017**, *442*, 147−153.
(314) Jedynak, A.; Kowalczyk, Z.; Szmigiel, D.; Rarog, W.; Zielinski, J. Ammonia Decomposition over the Carbon-Based Iron Catalyst Promoted with Potassium. *Appl. Catal., A* **2002**, *237*, 223−226.
(315) Ji, J.; Duan, X.; Qian, G.; Li, P.; Zhou, X.; Chen, D.; Yuan, W. Fe Particles on the Tops of Carbon Nanofibers Immobilized on Structured Carbon Microfibers for Ammonia Decomposition. *Catal. Today* **2013**, *216*, 254−260.
(316) Ji, J.; Yan, X.; Qian, G.; Peng, C.; Duan, X.; Zhou, X. Morphology and Location Manipulation of Fe Nanoparticles on Carbon Nanofibers as Catalysts for Ammonia Decomposition to Generate Hydrogen. *Int. J. Hydrogen Energy* **2017**, *42* (27), 17466−17475.
(317) Duan, X.; Qian, G.; Zhou, X.; Sui, Z.; Chen, D.; Yuan, W. Tuning the Size and Shape of Fe Nanoparticles on Carbon Nanofibers for Catalytic Ammonia Decomposition. *Appl. Catal., B* **2011**, *101* (3−4), 189−196.
(318) Wang, Y.; Ross Kunz, M.; Siebers, S.; Rollins, H. W.; Gleaves, J.; Yablonsky, G.; Fushimi, R. Transient Kinetic Experiments within the High Conversion Domain: The Case of Ammonia Decomposition. *Catalysts* **2019**, *9* (1), 1−19.
(319) Otremba, T.; Frenzel, N.; Lerch, M.; Ressler, T.; Schomäcker, R. Kinetic Studies on Ammonia Decomposition over Zirconium Oxynitride. *Appl. Catal., A* **2011**, *392* (1−2), 103−110.
(320) Vilekar, S. a.; Fishtik, I.; Datta, R. The Peculiar Catalytic Sequence of the Ammonia Decomposition Reaction and Its Steady-State Kinetics. *Chem. Eng. Sci.* **2012**, *71*, 333−344.
(321) Arabczyk, W.; Zamłynny, J. Study of the Ammonia Decomposition over Iron Catalysts. *Catal. Lett.* **1999**, *60*, 167−171.
(322) Zhang, J.; Muller, J.-O.; Zheng, W.; Wang, D.; Su, D.; Schlogl, R. Individual Fe-Co Alloy Nanoparticles on Carbon Nanotubes: Structural and Catalytic Properties. *Nano Lett.* **2008**, *8* (9), 2738−2743.
(323) Lorenzut, B.; Montini, T.; Bevilacqua, M.; Fornasiero, P. FeMo-Based Catalysts for H_2 Production by NH_3 Decomposition. *Appl. Catal., B* **2012**, *125*, 409−417.
(324) Lendzion-Bieluń, Z.; Pelka, R.; Arabczyk, W. Study of the Kinetics of Ammonia Synthesis and Decomposition on Iron and Cobalt Catalysts. *Catal. Lett.* **2009**, *129* (1−2), 119−123.
(325) Zhang, Z.-S.; Fu, X. P.; Wang, W.-W.; Jin, Z.; Song, Q.-S.; Jia, C.-J. Promoted Porous Co_3O_4-Al_2O_3 Catalysts for Ammonia Decomposition. *Sci. China: Chem.* **2018**, *61* (11), 1389−1398.
(326) Czekajło, Ł.; Lendzion-Bieluń, Z. Effect of Preparation Conditions and Promoters on the Structure and Activity of the Ammonia Decomposition Reaction Catalyst Based on Nanocrystalline Cobalt. *Chem. Eng. J.* **2016**, *289*, 254−260.
(327) Gu, Y.-Q.; Fu, X.-P.; Du, P.-P.; Gu, D.; Jin, Z.; Huang, Y.-Y.; Si, R.; Zheng, L.-Q.; Song, Q.-S.; Jia, C.-J.; Weidenthaler, C. *In Situ* X-Ray Diffraction Study of Co-Al Nanocomposites as Catalysts for Ammonia Decomposition. *J. Phys. Chem. C* **2015**, *119* (30), 17102−17110.
(328) Zhang, H.; Alhamed, Y. A.; Chu, W.; Ye, Z.; Alzahrani, A.; Petrov, L. Controlling Co-Support Interaction in Co/MWCNTs Catalysts and Catalytic Performance for Hydrogen Production via NH_3 Decomposition. *Appl. Catal., A* **2013**, *464*−*465*, 156−164.
(329) Zhang, H.; Alhamed, Y. A.; Al-Zahrani, A.; Daous, M.; Inokawa, H.; Kojima, Y.; Petrov, L. A. Tuning Catalytic Performances of Cobalt Catalysts for Clean Hydrogen Generation via Variation of the Type of Carbon Support and Catalyst Post-Treatment Temperature. *Int. J. Hydrogen Energy* **2014**, *39* (31), 17573−17582.
(330) Lara-García, H. A.; Mendoza-Nieto, J. A.; Pfeiffer, H.; Torrente-Murciano, L. CO_x-Free Hydrogen Production from Ammonia on Novel Cobalt Catalysts Supported on 1D Titanate Nanotubes. *Int. J. Hydrogen Energy* **2019**, *44* (57), 30062−30074.
(331) Podila, S.; Alhamed, Y. A.; Alzahrani, A. A.; Petrov, L. A. Hydrogen Production by Ammonia Decomposition Using Co Catalyst Supported on Mg Mixed Oxide Systems. *Int. J. Hydrogen Energy* **2015**, *40* (45), 15411−15422.
(332) Podila, S.; Driss, H.; Zaman, S. F.; Alhamed, Y. A.; Alzahrani, A. A.; Daous, M. A.; Petrov, L. A. Hydrogen Generation by Ammonia Decomposition Using Co/MgO-La_2O_3 Catalyst: Influence of Support Calcination Atmosphere. *J. Mol. Catal. A: Chem.* **2016**, *414*, 130−139.
(333) Podila, S.; Driss, H.; Zaman, S. F.; Ali, A. M.; Al-Zahrani, A. A.; Daous, M. A.; Petrov, L. A. Effect of Preparation Methods on the Catalyst Performance of Co/Mg−La Mixed Oxide Catalyst for CO_x-Free Hydrogen Production by Ammonia Decomposition. *Int. J. Hydrogen Energy* **2017**, *42* (38), 24213−24221.
(334) Hu, X.-C.; Wang, W.-W.; Gu, Y.-Q.; Jin, Z.; Song, Q.-S.; Jia, C.-J. Co-SiO_2 Nanocomposite Catalysts for CO_x-Free Hydrogen Production by Ammonia Decomposition. *ChemPlusChem* **2017**, *82* (3), 368−375.
(335) Varisli, D.; Kaykac, N. G. CO_x Free Hydrogen Production over Cobalt Incorporated Silicate Structured Mesoporous Catalysts. *Appl. Catal., B* **2012**, *127*, 389−398.
(336) Varışlı, D.; Kaykac, N. G. Hydrogen from Ammonia over Cobalt Incorporated Silicate Structured Catalysts Prepared Using Different Cobalt Salts. *Int. J. Hydrogen Energy* **2016**, *41* (14), 5955−5968.
(337) Lendzion-Bieluń, Z.; Narkiewicz, U.; Arabczyk, W. Cobalt-Based Catalysts for Ammonia Decomposition. *Materials* **2013**, *6* (6), 2400−2409.
(338) Ji, J.; Duan, X.; Qian, G.; Zhou, X.; Tong, G.; Yuan, W. Towards an Efficient CoMo/γ-Al_2O_3 Catalyst Using Metal Amine Metallate as an Active Phase Precursor: Enhanced Hydrogen Production by Ammonia Decomposition. *Int. J. Hydrogen Energy* **2014**, *39* (24), 12490−12498.
(339) Duan, X.; Qian, G.; Zhou, X.; Chen, D.; Yuan, W. MCM-41 Supported Co-Mo Bimetallic Catalysts for Enhanced Hydrogen Production by Ammonia Decomposition. *Chem. Eng. J.* **2012**, *207*−*208*, 103−108.
(340) Tagliazucca, V.; Schlichte, K.; Schüth, F.; Weidenthaler, C. Molybdenum-Based Catalysts for the Decomposition of Ammonia: In Situ X-Ray Diffraction Studies, Microstructure, and Catalytic Properties. *J. Catal.* **2013**, *305*, 277−289.

https://doi.org/10.1021/acs.iecr.1c00843
Ind. Eng. Chem. Res. 2021, 60, 18560−18611

(341) Santhana Krishnan, P.; Neelaveni, M.; Tamizhdurai, P.; Mythily, M.; Krishna Mohan, S.; Mangesh, V. L.; Shanthi, K. CO_x-Free Hydrogen Generation via Decomposition of Ammonia over Al, Ti and Zr−Laponite Supported MoS_2 Catalysts. *Int. J. Hydrogen Energy* **2020**, *45* (15), 8568−8583.
(342) Xu, J.; Yan, H.; Jin, Z.; Jia, C.-J. Facile Synthesis of Stable MO_2N Nanobelts with High Catalytic Activity for Ammonia Decomposition. *Chin. J. Chem.* **2019**, *37* (4), 364−372.
(343) Liu, H.; Wang, H.; Shen, J.; Sun, Y.; Liu, Z. Influence of Preparation Conditions on the Catalytic Performance of MoNx/SBA-15 for Ammonia Decomposition. *J. Nat. Gas Chem.* **2006**, *15* (3), 178−180.
(344) Li, L.; Chu, W.; Ding, C.; Xi, X.; Jiang, R.; Yan, J. Embedded MoN@C Nanocomposites as an Advanced Catalyst for Ammonia Decomposition to CO_x-Free Hydrogen. *Int. J. Hydrogen Energy* **2017**, *42* (52), 30630−30638.
(345) Wise, R. S.; Markel, E. J. Catalytic NH_3 Decomposition by Topotactic Molybdenum Oxides and Nitrides: Effect on Temperature Programmed γ-Mo_2N Synthesis. *J. Catal.* **1994**, *145* (2), 335−343.
(346) Tagliazucca, V.; Leoni, M.; Weidenthaler, C. Crystal Structure and Microstructural Changes of Molybdenum Nitrides Traced during Catalytic Reaction by in Situ X-Ray Diffraction Studies. *Phys. Chem. Chem. Phys.* **2014**, *16* (13), 6182−6188.
(347) Podila, S.; Zaman, S. F.; Driss, H.; Alhamed, Y. A.; Al-Zahrani, A. A.; Petrov, L. A. Hydrogen Production by Ammonia Decomposition Using High Surface Area Mo_2N and Co_3Mo_3N Catalysts. *Catal. Sci. Technol.* **2016**, *6* (5), 1496−1506.
(348) Jolaoso, L. A.; Zaman, S. F.; Podila, S.; Driss, H.; Al-Zahrani, A. A.; Daous, M. A.; Petrov, L. Ammonia Decomposition over Citric Acid Induced γ-Mo_2N and Co_3Mo_3N Catalysts. *Int. J. Hydrogen Energy* **2018**, *43* (10), 4839−4844.
(349) Zaman, S. F.; Jolaloso, L. A.; Al-Zahrani, A. A.; Alhamed, Y. A.; Podila, S.; Driss, H.; Daous, M. A.; Petrov, L. A. Study of Fe_3Mo_3N Catalyst for Ammonia Decomposition. *Bulg. Chem. Commun.* **2018**, *50* (H), 181−188.
(350) Srifa, A.; Okura, K.; Okanishi, T.; Muroyama, H.; Matsui, T.; Eguchi, K. CO_X-Free Hydrogen Production via Ammonia Decomposition over Molybdenum Nitride-Based Catalysts. *Catal. Sci. Technol.* **2016**, *6* (20), 7495−7504.
(351) Zaman, S. F.; Jolaloso, L. A.; Podila, S.; Al-Zahrani, A. A.; Alhamed, Y. A.; Driss, H.; Daous, M. M.; Petrov, L. A. Ammonia Decomposition over Citric Acid Chelated γ-Mo_2N and Ni_2Mo_3N Catalysts. *Int. J. Hydrogen Energy* **2018**, *43*, 17252−17258.
(352) Choi, J.-G.; Ha, J.; Hong, J.-W. Synthesis and Catalytic Properties of Vanadium Interstitial Compounds. *Appl. Catal., A* **1998**, *168* (1), 47−56.
(353) Choi, J.-G.; Jung, M.-K.; Choi, S.; Park, T.-K.; Kuk, I. H.; Yoo, J. H.; Park, H. S.; Lee, H.-S.; Ahn, D.-H.; Chung, H. Synthesis and Catalytic Properties of Vanadium Nitrides. *Bull. Chem. Soc. Jpn.* **1997**, *70* (5), 993−996.
(354) Choi, J.-G.; Oh, H.-G.; Back, Y.-S. Tantalum Carbide Hydrodenitrogenation Catalysts. *J. Ind. Eng. Chem.* **1998**, *4* (2), 94−98.
(355) Kraupner, A.; Antonietti, M.; Palkovits, R.; Schlicht, K.; Giordano, C. Mesoporous Fe_3C Sponges as Magnetic Supports and as Heterogeneous Catalyst. *J. Mater. Chem.* **2010**, *20* (29), 6019−6022.
(356) Pansare, S. S.; Torres, W.; Goodwin, J. G., Jr. Ammonia Decomposition on Tungsten Carbide. *Catal. Commun.* **2007**, *8* (4), 649−654.
(357) Cui, X.; Li, H.; Guo, L.; He, D.; Chen, H.; Shi, J. Synthesis of Mesoporous Tungsten Carbide by an Impregnation−Compaction Route, and Its NH_3 Decomposition Catalytic Activity. *Dalt. Trans.* **2008**, No. 45, 6435−6440.
(358) Soerijanto, H.; Rödel, C.; Wild, U.; Lerch, M.; Schomäcker, R.; Schlögl, R.; Ressler, T. The Impact of Nitrogen Mobility on the Activity of Zirconium Oxynitride Catalysts for Ammonia Decomposition. *J. Catal.* **2007**, *250* (1), 19−24.
(359) Wang, P.; Guo, J.; Xiong, Z.; Wu, G.; Wang, J.; Chen, P. The Interactions of Li_3FeN_2 with H_2 and NH_3. *Int. J. Hydrogen Energy* **2016**, *41* (32), 14171−14177.
(360) Cao, H.; Guo, J.; Chang, F.; Pistidda, C.; Zhou, W.; Zhang, X.; Santoru, A.; Wu, H.; Schell, N.; Niewa, R.; Chen, P.; Klassen, T.; Dornheim, M. Transition and Alkali Metal Complex Ternary Amides for Ammonia Synthesis and Decomposition. *Chem. - Eur. J.* **2017**, *23* (41), 9766−9771.
(361) Duan, X.; Ji, J.; Yan, X.; Qian, G.; Chen, D.; Zhou, X. Understanding Co-Mo Catalyzed Ammonia Decomposition: Influence of Calcination Atmosphere and Identification of Active Phase. *ChemCatChem* **2016**, *8* (5), 938−945.
(362) Zhao, Z.; Zou, H.; Lin, W. Effect of Rare Earth and Other Cationic Promoters on Properties of $CoMoN_x$/CNTs Catalysts for Ammonia Decomposition. *J. Rare Earths* **2013**, *31* (3), 247−250.
(363) Srifa, A.; Okura, K.; Okanishi, T.; Muroyama, H.; Matsui, T.; Eguchi, K. Hydrogen Production by Ammonia Decomposition over Cs-Modified Co_3Mo_3N Catalysts. *Appl. Catal., B* **2017**, *218*, 1−8.
(364) Leybo, D. V.; Baiguzhina, A. N.; Muratov, D. S.; Arkhipov, D. I.; Kolesnikov, E. A.; Levina, V. V.; Kosova, N. I.; Kuznetsov, D. V. Effects of Composition and Production Route on Structure and Catalytic Activity for Ammonia Decomposition Reaction of Ternary Ni-Mo Nitride Catalysts. *Int. J. Hydrogen Energy* **2016**, *41* (6), 3854−3860.
(365) Ehiro, T.; Katagiri, K.; Yamaguchi, S.; Nishimura, T.; Saito, M.; Yoshioka, Y. The Effects of the Addition of Calcium Phosphate on Catalytic Activities for Ammonia Decomposition on CoMo-Based Catalysts. *J. Ceram. Soc. Jpn.* **2019**, *127* (11), 802−809.
(366) Egawa, C. Ammonia Decomposition on Co/Mo(112) Model Surface. *e-J. Surf. Sci. Nanotechnol.* **2018**, *16*, 115−118.
(367) Lendzion-Bielun, Z.; Pelka, R.ł; Czekajło, Łu. Characterization of FeCo Based Catalyst for Ammonia Decomposition. The Effect of Potassium Oxide. *Pol. J. Chem. Technol.* **2014**, *16* (4), 111−116.
(368) Lendzion-Bieluń, Z.; Arabczyk, W. Fused Fe-Co Catalysts for Hydrogen Production by Means of the Ammonia Decomposition Reaction. *Catal. Today* **2013**, *212*, 215−219.
(369) Podila, S.; Driss, H.; Zaman, S. F.; Ali, A. M.; Al-Zahrani, A. A.; Daous, M. A.; Petrov, L. A. MgFe and Mg−Co−Fe Mixed Oxides Derived from Hydrotalcites: Highly Efficient Catalysts for CO_x Free Hydrogen Production from NH_3. *Int. J. Hydrogen Energy* **2020**, *45* (1), 873−890.
(370) Chellappa, A. S.; Fischer, C. M.; Thomson, W. J. Ammonia Decomposition Kinetics over Ni-Pt/Al_2O_3 for PEM Fuel Cell Applications. *Appl. Catal., A* **2002**, *227*, 231−240.
(371) Hajduk, S.; Dasireddy, V. D. B. C.; Likozar, B.; Dražić, G.; Crnjak Orel, Z. CO_x-Free Hydrogen Production via Decomposition of Ammonia over Cu−Zn-Based Heterogeneous Catalysts and Their Activity/Stability. *Appl. Catal., B* **2017**, *211*, 57−67.
(372) Lucentini, I.; Colli, G. G.; Luzi, C. D.; Serrano, I.; Martínez, O. M.; Llorca, J. Catalytic Ammonia Decomposition over Ni-Ru Supported on CeO_2 for Hydrogen Production: Effect of Metal Loading and Kinetic Analysis. *Appl. Catal., B* **2021**, *286*, 1−10.
(373) David, W. I. F.; Makepeace, J. W.; Callear, S. K.; Hunter, H. M. A.; Taylor, J. D.; Wood, T. J.; Jones, M. O. Hydrogen Production from Ammonia Using Sodium Amide. *J. Am. Chem. Soc.* **2014**, *136* (38), 13082−13085.
(374) Makepeace, J. W.; Hunter, H. M. A.; Wood, T. J.; Smith, R. I.; Murray, C. A.; David, W. I. F. Ammonia Decomposition Catalysis Using Lithium-Calcium Imide. *Faraday Discuss.* **2016**, *188*, 525−544.
(375) Wood, T. J.; Makepeace, J. W. Assessing Potential Supports for Lithium Amide-Imide Ammonia Decomposition Catalysts. *ACS Appl. Energy Mater.* **2018**, *1* (6), 2657−2663.
(376) Makepeace, J. W.; Wood, T. J.; Marks, P. L.; Smith, R. I.; Murray, C. A.; David, W. I. F. Bulk Phase Behavior of Lithium Imide-Metal Nitride Ammonia Decomposition Catalysts. *Phys. Chem. Chem. Phys.* **2018**, *20* (35), 22689−22697.
(377) Wood, T. J.; Makepeace, J. W.; David, W. I. F. Neutron Diffraction and Gravimetric Study of the Manganese Nitriding Reaction under Ammonia Decomposition Conditions. *Phys. Chem. Chem. Phys.* **2018**, *20* (13), 8547−8553.
(378) Chang, F.; Guo, J.; Wu, G.; Wang, P.; Yu, P.; Chen, P. Influence of Alkali Metal Amides on the Catalytic Activity of Manganese Nitride for Ammonia Decomposition. *Catal. Today* **2017**, *286*, 141−146.

https://doi.org/10.1021/acs.iecr.1c00843
Ind. Eng. Chem. Res. 2021, 60, 18560−18611

(379) Guo, J.; Chang, F.; Wang, P.; Hu, D.; Yu, P.; Wu, G.; Xiong, Z.; Chen, P. Highly Active MnN-Li_2NH Composite Catalyst for Producing CO_x-Free Hydrogen. *ACS Catal.* **2015**, *5* (5), 2708−2713.
(380) Yu, P.; Guo, J.; Liu, L.; Wang, P.; Wu, G.; Chang, F.; Chen, P. Ammonia Decomposition with Manganese Nitride-Calcium Imide Composites as Efficient Catalysts. *ChemSusChem* **2016**, *9* (4), 364−369.
(381) Chiuta, S.; Everson, R. C.; Neomagus, H. W. J. P.; Le Grange, L. A.; Bessarabov, D. G. A Modelling Evaluation of an Ammonia-Fuelled Microchannel Reformer for Hydrogen Generation. *Int. J. Hydrogen Energy* **2014**, *39* (22), 11390−11402.
(382) Tsai, W.; Weinberg, W. H. Steady-State Decomposition of Ammonia on the Ruthenium(001) Surface. *J. Phys. Chem.* **1987**, *91* (20), 5302−5307.
(383) McCabe, R. W. Kinetics of Ammonia Decomposition on Nickel. *J. Catal.* **1983**, *79*, 445−450.
(384) Oyama, S. T. Kinetics of Ammonia Decomposition on Vanadium Nitride. *J. Catal.* **1992**, *133*, 358−369.
(385) Armenise, S.; Cazaña, F.; Monzón, A.; García-Bordejé, E. In Situ Generation of COx-Free H_2 by Catalytic Ammonia Decomposition over Ru-Al-Monoliths. *Fuel* **2018**, *233*, 851−859.
(386) Armenise, S.; García-Bordejé, E.; Valverde, J. L.; Romeo, E.; Monzón, A. A Langmuir−Hinshelwood Approach to the Kinetic Modelling of Catalytic Ammonia Decomposition in an Integral Reactor. *Phys. Chem. Chem. Phys.* **2013**, *15*, 12104−12117.
(387) Abashar, M. E. E. Multi-Stage Membrane Reactors for Hydrogen Production by Ammonia Decomposition. *Int. J. Petrochemistry Res.* **2018**, *2* (1), 109−115.
(388) Deshmukh, S. R.; Mhadeshwar, A. B.; Vlachos, D. G. Microreactor Modeling for Hydrogen Production from Ammonia Decomposition on Ruthenium. *Ind. Eng. Chem. Res.* **2004**, *43* (12), 2986−2999.
(389) Itoh, N.; Oshima, A.; Suga, E.; Sato, T. Kinetic Enhancement of Ammonia Decomposition as a Chemical Hydrogen Carrier in Palladium Membrane Reactor. *Catal. Today* **2014**, *236*, 70−76.
(390) Kim, S.; Song, J.; Lim, H. Conceptual Feasibility Studies of a CO_x-Free Hydrogen Production from Ammonia Decomposition in a Membrane Reactor for PEM Fuel Cells. *Korean J. Chem. Eng.* **2018**, *35* (3), 1−8.
(391) Zhang, Z.; Liguori, S.; Fuerst, T. F.; Way, J. D.; Wolden, C. A. Efficient Ammonia Decomposition in a Catalytic Membrane Reactor to Enable Hydrogen Storage and Utilization. *ACS Sustainable Chem. Eng.* **2019**, *7* (6), 5975−5985.
(392) Abashar, M. E. E. Ultra-Clean Hydrogen Production by Ammonia Decomposition. *J. King Saud Univ., Eng. Sci.* **2018**, *30*, 2−11.
(393) Ganley, J. C. A Heterogeneous Chemical Reactor Analysis and Design Laboratory: The Kinetics of Ammonia Decomposition. *Educ. Chem. Eng.* **2017**, *21*, 11−16.
(394) Djéga-Mariadassou, G.; Shin, C.-H.; Bugli, G. Tamaru's Model for Ammonia Decomposition over Titanium Oxynitride. *J. Mol. Catal. A: Chem.* **1999**, *141*, 263−267.
(395) Shindo, H.; Egawa, C.; Onishi, T.; Tamaru, K. Mechanism of Ammonia Decomposition on Tungsten; NH_3 and ND_3 Isotope Effect. *Z. Naturforsch., A: Phys. Sci.* **1979**, *34a* (1), 96−98.
(396) Shindo, H.; Egawa, C.; Onishi, T.; Tamaru, K. Reaction Mechanism of Ammonia Decomposition on Tungsten. *J. Chem. Soc., Faraday Trans. 1* **1980**, *76*, 280−290.
(397) Tamaru, K. Adsorption Measurements during the Decomposition of Ammonia on a Tungsten Catalyst. *Trans. Faraday Soc.* **1961**, *57*, 1410−1415.
(398) Tamaru, K. A "New" General Mechanism of Ammonia Synthesis and Decomposition on Transition Metals. *Acc. Chem. Res.* **1988**, *21* (2), 88−94.
(399) De La Osa, A. R.; De Lucas, A.; Romero, A.; Valverde, J. L.; Sánchez, P. Kinetic Models Discrimination for the High Pressure WGS Reaction over a Commercial CoMo Catalyst. *Int. J. Hydrogen Energy* **2011**, *36* (16), 9673−9684.
(400) Wang, Y.; Kunz, M. R.; Fang, Z.; Yablonsky, G.; Fushimi, R. Accumulation Dynamics as a New Tool for Catalyst Discrimination: An Example from Ammonia Decomposition. *Ind. Eng. Chem. Res.* **2019**, *58* (24), 10238−10248.
(401) Logan, S. R.; Kemball, C. The Catalytic Decomposition of Ammonia on Evaporated Metal Films. *Trans. Faraday Soc.* **1960**, *56*, 144−153.
(402) Hansgen, D. A.; Vlachos, D. G.; Chen, J. G. Using First Principles to Predict Bimetallic Catalysts for the Ammonia Decomposition Reaction. *Nat. Chem.* **2010**, *2* (6), 484−489.
(403) Hansgen, D. A.; Thomanek, L. M.; Chen, J. G.; Vlachos, D. G. Experimental and Theoretical Studies of Ammonia Decomposition Activity on Fe-Pt, Co-Pt, and Cu-Pt Bimetallic Surfaces. *J. Chem. Phys.* **2011**, *134* (18), 184701−184707.
(404) Duan, X.; Ji, J.; Qian, G.; Fan, C.; Zhu, Y.; Zhou, X.; Chen, D.; Yuan, W. Ammonia Decomposition on Fe(1 1 0), Co(1 1 1) and Ni(1 1 1) Surfaces: A Density Functional Theory Study. *J. Mol. Catal. A: Chem.* **2012**, *357*, 81−86.
(405) Hansgen, D. A.; Vlachos, D. G.; Chen, J. G. Ammonia Decomposition Activity on Monolayer Ni Supported on Ru, Pt and WC Substrates. *Surf. Sci.* **2011**, *605* (23−24), 2055−2060.
(406) Zhong, J.-Q.; Zhou, X.; Yuan, K.; Wright, C. A.; Tadich, A.; Qi, D.; Li, H. X.; Wu, K.; Xu, G. Q.; Chen, W. Probing the Effect of the Pt-Ni-Pt(111) Bimetallic Surface Electronic Structures on the Ammonia Decomposition Reaction. *Nanoscale* **2017**, *9* (2), 666−672.
(407) Love, K. S.; Emmett, P. H. The Catalytic Decomposition of Ammonia Over Iron Synthetic Ammonia Catalysts. *J. Am. Chem. Soc.* **1941**, *63* (12), 3297−3308.
(408) Takezawa, N.; Toyoshima, I. The Change of the Rate-Determining Step of the Ammonia Decomposition over an Ammonia Synthetic Iron Catalyst. *J. Phys. Chem.* **1966**, *70* (2), 594−595.
(409) Takezawa, N.; Toyoshima, I. The Rate-Determining Step of Ammonia Decomposition over a Well-Reduced Doubly Promoted Iron Catalyst. *J. Res. Inst. Catal. Hokkaido Univ.* **1966**, *14* (1), 41−58.
(410) Ertl, G.; Huber, M. Mechanism and Kinetics of Ammonia Decomposition on Iron. *J. Catal.* **1980**, *61* (2), 537−539.
(411) Kunsman, C. H. The Thermal Decomposition of Ammonia on Iron Catalysts. II. *J. Am. Chem. Soc.* **1929**, *51* (3), 688−695.
(412) Kunsman, C. H. The Thermal Decomposition of Ammonia on Tungsten, Molybdenum and Nickel. I. *J. Am. Chem. Soc.* **1928**, *50* (8), 2100−2113.
(413) Rasim, K.; Bobeth, M.; Pompe, W.; Seriani, N. A Microkinetic Model of Ammonia Decomposition on a Pt Overlayer on Au(111). *J. Mol. Catal. A: Chem.* **2010**, *325* (1−2), 15−24.
(414) Vajo, J. J.; Tsai, W.; Weinberg, W. H. Mechanistic Details of the Heterogeneous Decomposition of Ammonia on Platinum. *J. Phys. Chem.* **1985**, *89* (15), 3243−3251.
(415) Egawa, C.; Nishida, T.; Naito, S.; Tamaru, K. Ammonia Decomposition on (1 1 10) and (0 0 1) Surfaces of Ruthenium. *J. Chem. Soc., Faraday Trans. 1* **1984**, *80* (6), 1595−1604.
(416) Huang, W.; Lai, W.; Xie, D. First-Principles Study of Decomposition of NH_3 on Ir(1 0 0). *Surf. Sci.* **2008**, *602* (6), 1288−1294.
(417) Zhou, S.; Lin, S.; Guo, H. First-Principles Insights into Ammonia Decomposition Catalyzed by Ru Clusters Anchored on Carbon Nanotubes: Size Dependence and Interfacial Effects. *J. Phys. Chem. C* **2018**, *122* (16), 9091−9100.
(418) Roy, S. K.; Ray, N.; Mukherjee, D. K.; Sen, S. P. Kinetics and Mechanism of Ammonia Decomposition over Alumina Supported Nickel Catalysts. *Proceedings of Indian National Science Academy.* **1975**, 485−495.
(419) Tsai, W.; Vajo, J. J.; Weinberg, W. H. Inhibition by Hydrogen of the Heterogeneous Decomposition of Ammonia on Platinum. *J. Phys. Chem.* **1985**, *89* (23), 4926−4932.
(420) Löffler, D. G.; Schmidt, L. D. Kinetics of NH_3 Decomposition on Polycrystalline Pt. *J. Catal.* **1976**, *41*, 440−454.
(421) Löffler, D. G.; Schmidt, L. D. Kinetics of NH_3 Decomposition on Iron at High Temperatures. *J. Catal.* **1976**, *44*, 244−258.
(422) Hashimoto, K.; Toukai, N. Decomposition of Ammonia over a Catalyst Consisting of Rutheniurn Metal and Cerium Oxides

https://doi.org/10.1021/acs.iecr.1c00843
Ind. Eng. Chem. Res. 2021, 60, 18560−18611

Supported on Y-Form Zeolite. *J. Mol. Catal. A: Chem.* **2000**, *161* (1−2), 171−178.
(423) Prasad, V.; Vlachos, D. G. Multiscale Model and Informatics-Based Optimal Design of Experiments: Application to the Catalytic Decomposition of Ammonia on Ruthenium. *Ind. Eng. Chem. Res.* **2008**, *47* (17), 6555−6567.
(424) Bradford, M. C. J.; Fanning, P. E.; Vannice, M. A. Kinetics of NH_3 Decomposition over Well Dispersed Ru. *J. Catal.* **1997**, *172* (2), 479−484.
(425) Mortensen, H.; Diekhöner, L.; Baurichter, A.; Jensen, E.; Luntz, A. C. Dynamics of Ammonia Decomposition on Ru(0001). *J. Chem. Phys.* **2000**, *113* (16), 6882−6887.
(426) Novell-Leruth, G.; Valcárcel, A.; Pérez-Ramírez, J.; Ricart, J. M. Ammonia Dehydrogenation over Platinum-Group Metal Surfaces. Structure, Stability, and Reactivity of Adsorbed NH_x Species. *J. Phys. Chem. C* **2007**, *111* (2), 860−868.
(427) Stolbov, S.; Rahman, T. S. First-Principles Study of Some Factors Controlling the Rate of Ammonia Decomposition on Ni and Pd Surfaces. *J. Chem. Phys.* **2005**, *123*, 204716.
(428) Guo, W.; Vlachos, D. G. Patched Bimetallic Surfaces Are Active Catalysts for Ammonia Decomposition. *Nat. Commun.* **2015**, *6* (8619), 1−7.
(429) Wu, H.; Sutton, J. E.; Guo, W.; Vlachos, D. G. Volcano Curves for in Silico Prediction of Mono- And Bifunctional Catalysts: Application to Ammonia Decomposition. *J. Phys. Chem. C* **2019**, *123* (44), 27097−27104.
(430) Shustorovich, E.; Bell, A. T. Synthesis and Decomposition of Ammonia on Transition Metal Surfaces: Bond-Order-Conservation-Morse-Potential Analysis. *Surf. Sci.* **1991**, *259* (3), L791−L796.
(431) Jiang, Z.; Qin, P.; Fang, T. Theoretical Study of NH_3 Decomposition on Pd-Cu (1 1 1) and Cu-Pd (1 1 1) Surfaces: A Comparison with Clean Pd (1 1 1) and Cu (1 1 1). *Appl. Surf. Sci.* **2016**, *371*, 337−342.
(432) Mianowski, A.; Siudyga, T.; Polański, J. Szarawara−Kozik's Temperature Criterion in the Context of Three-Parameter Equation for Modeling Ammonia or Methanol Decomposition during Heterogenous Catalysis. *React. Kinet., Mech. Catal.* **2018**, *125* (2), 493−504.
(433) Zaman, S. F. A DFT Study of Ammonia Dissociation over Mo_3N_2 Cluster. *Bulg. Chem. Commun.* **2018**, *50* (H), 201−208.
(434) Wood, T. J.; Makepeace, J. W.; Hunter, H. M. A.; Jones, M. O.; David, W. I. F. Isotopic Studies of the Ammonia Decomposition Reaction Mediated by Sodium Amide. *Phys. Chem. Chem. Phys.* **2015**, *17* (35), 22999−23006.
(435) Offermans, W. K.; Jansen, A. P. J.; Van Santen, R. A.; Novell-Leruth, G.; Ricart, J. M.; Pérez-Ramírez, J. Ammonia Dissociation on Pt{100}, Pt{111}, and Pt{211}: A Comparative Density Functional Theory Study. *J. Phys. Chem. C* **2007**, *111* (47), 17551−17557.
(436) Popa, C.; Offermans, W. K.; Van Santen, R. A.; Jansen, A. P. J. Ab Initio Density-Functional Theory Study of NH_x Dehydrogenation and Reverse Reactions on the Rh(111) Surface. *Phys. Rev. B: Condens. Matter Mater. Phys.* **2006**, *74*, 155428.
(437) Gundry, P. M.; Haber, J.; Tompkins, F. C. Surface Potential Measurements on Nickel and Iron Films during the Chemisorption of Ammonia, Nitrogen, and Hydrogen. *J. Catal.* **1962**, *1* (4), 363−371.
(438) Ertl, G.; Rüstig, J. Decomposition of NH_3 on Nickel: Absence of a Magneto-Catalytic Effect. *Surf. Sci.* **1982**, *119* (1), 314−318.
(439) Tamaru, K.; Tanaka, K.-I.; Fukasaku, S.; Ishida, S. Decomposition of Ammonia on a Nickel Catalyst. *Trans. Faraday Soc.* **1965**, *61*, 765−772.
(440) Hüttinger, M.; Küppers, J. Intermediate Product Identification for Ammonia Decomposition at Ni (110). *Surf. Sci. Lett.* **1983**, *130* (1), L277−L282.
(441) Chrysostomou, D.; Flowers, J.; Zaera, F. Thermal Chemistry of Ammonia on Ni(110). *Surf. Sci.* **1999**, *439* (1−3), 34−48.
(442) Grunze, M.; Golze, M.; Driscoll, R. K.; Dowben, P. A. Ammonia Adsorption and Decomposition on a Ni(110) Surface. *J. Vac. Sci. Technol.* **1981**, *18* (2), 611−615.
(443) Bassignana, I. C.; Wagemann, K.; Küppers, J.; Ertl, G. Adsorption and Thermal Decomposition of Ammonia on a Ni(110) Surface: Isolation and Identification of Adsorbed NH_2 and NH. *Surf. Sci.* **1986**, *175* (1), 22−44.
(444) Duan, X.; Qian, G.; Fan, C.; Zhu, Y.; Zhou, X.; Chen, D.; Yuan, W. First-Principles Calculations of Ammonia Decomposition on Ni(110) Surface. *Surf. Sci.* **2012**, *606* (3−4), 549−553.
(445) Grosman, M.; Löffler, D. G. Kinetics of Ammonia Decomposition on Polycrystalline Tungsten. *J. Catal.* **1983**, *80* (1), 188−193.
(446) Reed, A. P. C.; Lambert, R. M. Mechanism of Ammonia Decomposition on (100) Oriented Polycrystalline Tungsten and Single-Crystal W(100). *J. Phys. Chem.* **1984**, *88* (10), 1954−1959.
(447) Grosman, M.; Löffler, D. G. Ammonia Decomposition on Ir and Pt Wires. *React. Kinet. Catal. Lett.* **1987**, *33* (1), 87−92.
(448) Santra, A. K.; Min, B. K.; Yi, C. W.; Luo, K.; Choudhary, T. V.; Goodman, D. W. Decomposition of NH_3 on Ir(100): A Temperature Programmed Desorption Study. *J. Phys. Chem. B* **2002**, *106* (2), 340−344.
(449) Amano, A.; Taylor, H. The Decomposition of Ammonia on Ruthenium, Rhodium and Palladium Catalysts Supported on Alumina. *J. Am. Chem. Soc.* **1954**, *76* (16), 4201−4204.
(450) Zhao, J.; Cui, C.; Wang, H.; Han, J.; Zhu, X.; Ge, Q. Insights into the Mechanism of Ammonia Decomposition on Molybdenum Nitrides Based on DFT Studies. *J. Phys. Chem. C* **2019**, *123* (1), 554−564.
(451) Lanzani, G.; Laasonen, K. NH_3 Adsorption and Dissociation on a Nanosized Iron Cluster. *Int. J. Hydrogen Energy* **2010**, *35* (13), 6571−6577.
(452) Hellman, A.; Honkala, K.; Remediakis, I. N.; Logadóttir, Á.; Carlsson, A.; Dahl, S.; Christensen, C. H.; Nørskov, J. K. Ammonia Synthesis and Decomposition on a Ru-Based Catalyst Modeled by First-Principles. *Surf. Sci.* **2009**, *603* (10−12), 1731−1739.
(453) Dietrich, H.; Jacobi, K.; Ertl, G. Decomposition of NH_3 on Ru(1121). *Surf. Sci.* **1996**, *352*−*354* (95), 138−141.
(454) McGill, W. J.; Sebba, F. The Kinetics of Ammonia Decomposition over Vanadium Nitride. *J. Catal.* **1963**, *2* (2), 104−108.
(455) McGeer, J. P.; Taylor, H. S. Ammonia Decomposition and Related Phenomena on Rhenium Catalysts. *J. Am. Chem. Soc.* **1951**, *73* (6), 2743−2751.
(456) Jiang, Z.; Qin, P.; Fang, T. Mechanism of Ammonia Decomposition on Clean and Oxygen-Covered Cu (1 1 1) Surface: A DFT Study. *Chem. Phys.* **2014**, *445*, 59−67.
(457) Bao, J. L.; Carter, E. A. Surface-Plasmon-Induced Ammonia Decomposition on Copper: Excited-State Reaction Pathways Revealed by Embedded Correlated Wavefunction Theory. *ACS Nano* **2019**, *13* (9), 9944−9957.
(458) Brunauer, S.; Love, K. S.; Keenan, R. G. Adsorption of Nitrogen and the Mechanism of Ammonia Decomposition Over Iron Catalysts. *J. Am. Chem. Soc.* **1942**, *64* (4), 751−758.
(459) Bui, K. M.; Iwata, J.-I.; Kangawa, Y.; Shiraishi, K.; Shigeta, Y.; Oshiyama, A. First-Principle Study of Ammonia Decomposition and Nitrogen Incorporation on the GaN Surface in Metal Organic Vapor Phase Epitaxy. *J. Cryst. Growth* **2019**, *507*, 421−424.
(460) García-García, F. R.; Guerrero-Ruiz, A.; Rodríguez-Ramos, I.; Goguet, A.; Shekhtman, S. O.; Hardacre, C. TAP Studies of Ammonia Decomposition over Ru and Ir Catalysts. *Phys. Chem. Chem. Phys.* **2011**, *13* (28), 12892−12899.
(461) Barbato, P. S.; Landi, G.; Lisi, L.; Di Benedetto, A. CFD Simulations of Copper-Ceria Based Microreactor for COPROX. *Int. J. Chem. React. Eng.* **2016**, *14* (6), 1301−1313.
(462) Gyak, K.; Vishwakarma, N. K.; Hwang, Y.; Kim, J.; Yun, H.; Kim, D. 3D-Printed Monolithic SiCN Ceramic Microreactors from a Photocurable Preceramic Resin for the High Temperature Ammonia Cracking Process. *React. Chem. Eng.* **2019**, *4*, 1393−1399.
(463) Lucentini, I.; Serrano, I.; Soler, L.; Divins, N. J.; Llorca, J. Ammonia Decomposition over 3D-Printed CeO_2 Structures Loaded with Ni. *Appl. Catal., A* **2020**, *591*, 117382.
(464) Ganley, J. C.; Seebauer, E. G.; Masel, R. I. Development of a Microreactor for the Production of Hydrogen from Ammonia. *J. Power Sources* **2004**, *137* (1), 53−61.

https://doi.org/10.1021/acs.iecr.1c00843
Ind. Eng. Chem. Res. 2021, 60, 18560−18611

(465) Christian; Mitchell, M.; Kim, D.-P.; Kenis, P. J. A. Ceramic Microreactors for On-Site Hydrogen Production. *J. Catal.* **2006**, *241* (2), 235−242.
(466) Chiuta, S.; Everson, R. C.; Neomagus, H. W. J. P.; Bessarabov, D. G. Experimental Performance Evaluation of an Ammonia-Fuelled Microchannel Reformer for Hydrogen Generation. *Int. J. Hydrogen Energy* **2014**, *39* (14), 7225−7235.
(467) Chiuta, S.; Everson, R. C.; Neomagus, H. W. J. P.; Bessarabov, D. G. Performance Evaluation of a High-Throughput Microchannel Reactor for Ammonia Decomposition over a Commercial Ru-Based Catalyst. *Int. J. Hydrogen Energy* **2015**, *40* (7), 2921−2926.
(468) Chiuta, S.; Everson, R. C.; Neomagus, H. W. J. P.; Bessarabov, D. G. Hydrogen Production from Ammonia Decomposition over a Commercial Ru/Al_2O_3 Catalyst in a Microchannel Reactor: Experimental Validation and CFD Simulation. *Int. J. Hydrogen Energy* **2016**, *41* (6), 3774−3785.
(469) Sørensen, R. Z.; Nielsen, L. J. E.; Jensen, S.; Hansen, O.; Johannessen, T.; Quaade, U.; Christensen, C. H. Catalytic Ammonia Decomposition: Miniaturized Production of CO_x-Free Hydrogen for Fuel Cells. *Catal. Commun.* **2005**, *6* (3), 229−232.
(470) Sørensen, R. Z.; Klerke, A.; Quaade, U.; Jensen, S.; Hansen, O.; Christensen, C. H. Promoted Ru on High-Surface Area Graphite for Efficient Miniaturized Production of Hydrogen from Ammonia. *Catal. Lett.* **2006**, *112* (1−2), 77−81.
(471) Plana, C.; Armenise, S.; Monzón, A.; García-Bordejé, E. Ni on Alumina-Coated Cordierite Monoliths for in Situ Generation of CO-Free H_2 from Ammonia. *J. Catal.* **2010**, *275* (2), 228−235.
(472) Armenise, S.; Roldán, L.; Marco, Y.; Monzón, A.; García-Bordejé, E. Elucidation of Catalyst Support Effect for NH_3 Decomposition Using Ru Nanoparticles on Nitrogen-Functionalized Carbon Nanofiber Monoliths. *J. Phys. Chem. C* **2012**, *116* (50), 26385−26395.
(473) Ismagilov, Z. R.; Khairulin, S. R.; Shkrabina, R. A.; Yashnik, S. A.; Ushakov, V. A.; Moulijn, J. A.; Van Langeveld, A. D. Deactivation of Manganese Oxide-Based Honeycomb Monolith Catalyst under Reaction Conditions of Ammonia Decomposition at High Temperature. *Catal. Today* **2001**, *69* (1−4), 253−257.
(474) Liu, Y.; Wang, H.; Li, J.; Lu, Y.; Xue, Q.; Chen, J. Microfibrous Entrapped Ni/Al_2O_3 Using SS-316 Fibers for H_2 Production from NH_3. *AIChE J.* **2007**, *53* (7), 1845−1849.
(475) Lu, Y.; Wang, H.; Liu, Y.; Xue, Q.; Chen, L.; He, M. Novel Microfibrous Composite Bed Reactor: High Efficiency H_2 Production from NH_3 with Potential for Portable Fuel Cell Power Supplies. *Lab Chip* **2007**, *7* (1), 133−140.
(476) Deshmukh, S. R.; Vlachos, D. G. CFD Simulations of Coupled, Countercurrent Combustor/Reformer Microdevices for Hydrogen Production. *Ind. Eng. Chem. Res.* **2005**, *44* (14), 4982−4992.
(477) Ganley, J. C.; Seebauer, E. G.; Masel, R. I. Porous Anodic Alumina Microreactors for Production of Hydrogen from Ammonia. *AIChE J.* **2004**, *50* (4), 829−834.
(478) Dillon, A. C.; Gupta, P.; Robinson, M. B.; Bracker, A. S.; George, S. M. FTIR Studies of Water and Ammonia Decomposition on Silicon Surfaces. *J. Electron Spectrosc. Relat. Phenom.* **1990**, *54*−*55* (C), 1085−1095.
(479) Plana, C.; Armenise, S.; Monzón, A.; García-Bordejé, E. Process Optimisation of in Situ H_2 Generation from Ammonia Using Ni on Alumina Coated Cordierite Monoliths. *Top. Catal.* **2011**, *54* (13−15), 914−921.
(480) Wang, M.; Li, J.; Chen, L.; Lu, Y. Miniature NH_3 Cracker Based on Microfibrous Entrapped $Ni\text{-}CeO_2/Al_2O_3$ Catalyst Monolith for Portable Fuel Cell Power Supplies. *Int. J. Hydrogen Energy* **2009**, *34* (4), 1710−1716.
(481) Zou, J.; Lu, D.-P.; Zhai, Q.-J. The Research on Ni-Based Ammonia Decomposition Catalyst. *Appl. Mech. Mater.* **2014**, *644*−*650*, 5364−5367.
(482) Pereira, S. I. Modeling of Fixed Bed Catalytic Reactors. *Comput. Chem. Eng.* **1985**, *1354* (December 2017), 535 DOI: 10.1016/0098-1354(85)80028-4.
(483) Chen, J.; Yang, H.; Wang, N.; Ring, Z.; Dabros, T. Mathematical Modeling of Monolith Catalysts and Reactors for Gas Phase Reactions. *Appl. Catal., A* **2008**, *345* (1), 1−11.
(484) Chen, L.; Kang, Q.; He, Y.-L.; Tao, W.-Q. Pore-Scale Simulation of Coupled Multiple Physicochemical Thermal Processes in Micro Reactor for Hydrogen Production Using Lattice Boltzmann Method. *Int. J. Hydrogen Energy* **2012**, *37* (19), 13943−13957.
(485) Molaeimanesh, G. R.; Sanati Davarani, M. H. A Pore-Scale Model for Microfibrous Ammonia Cracking Microreactors via Lattice Boltzmann Method. *Korean J. Chem. Eng.* **2016**, *33* (4), 1211−1219.
(486) Waghode, A. N.; Hanspal, N. S.; Shigidi, I. M. T. A.; Nassehi, V.; Hellgardt, K. Computer Modelling and Numerical Analysis of Hydrodynamics and Heat Transfer in Non-Porous Catalytic Reactor for the Decomposition of Ammonia. *Chem. Eng. Sci.* **2005**, *60* (21), 5862−5877.
(487) Qazi Zade, A.; Renksizbulut, M.; Friedman, J. Ammonia Decomposition for Hydrogen Production in Catalytic Microchannels with Slip/Jump Effects. *J. Appl. Fluid Mech.* **2015**, *8* (4), 703−712.
(488) Badescu, V. Optimal Design and Operation of Ammonia Decomposition Reactors. *Int. J. Energy Res.* **2020**, *44*, 5360−5384.
(489) Chein, R.-Y.; Chen, Y.-C.; Chang, C.-S.; Chung, J. N. Numerical Modeling of Hydrogen Production from Ammonia Decomposition for Fuel Cell Applications. *Int. J. Hydrogen Energy* **2010**, *35* (2), 589−597.
(490) Alagharu, V.; Palanki, S.; West, K. N. Analysis of Ammonia Decomposition Reactor to Generate Hydrogen for Fuel Cell Applications. *J. Power Sources* **2010**, *195* (3), 829−833.
(491) Gallucci, F.; Fernandez, E.; Corengia, P.; van Sint Annaland, M. Recent Advances on Membranes and Membrane Reactors for Hydrogen Production. *Chem. Eng. Sci.* **2013**, *92*, 40−66.
(492) López, E.; Divins, N. J.; Llorca, J. Hydrogen Production from Ethanol over $Pd\text{-}Rh/CeO_2$ with a Metallic Membrane Reactor. *Catal. Today* **2012**, *193* (1), 145−150.
(493) Rahimpour, M. R.; Asgari, A. Production of Hydrogen from Purge Gases of Ammonia Plants in a Catalytic Hydrogen-Permselective Membrane Reactor. *Int. J. Hydrogen Energy* **2009**, *34* (14), 5795−5802.
(494) Gómez-García, M. Á.; Dobrosz-Gómez, I.; Fontalvo, J.; Rynkowski, J. M. Membrane Reactor Design Guidelines for Ammonia Decomposition. *Catal. Today* **2012**, *191* (1), 165−168.
(495) Hedayati, A.; Llorca, J. Experimental Study of 2-Methoxyethanol Steam Reforming in a Membrane Reactor for Pure Hydrogen Production. *Fuel* **2017**, *190*, 312−317.
(496) Palo, E.; Salladini, A.; Morico, B.; Palma, V.; Ricca, A.; Iaquaniello, G. Application of Pd-Based Membrane Reactors: An Industrial Perspective. *Membranes (Basel, Switz.)* **2018**, *8* (101), 1−15.
(497) Lundin, S.-T. B.; Yamaguchi, T.; Wolden, C. A.; Oyama, S. T.; Way, J. D. The Role (or Lack Thereof) of Nitrogen or Ammonia Adsorption-Induced Hydrogen Flux Inhibition on Palladium Membrane Performance. *J. Membr. Sci.* **2016**, *514*, 65−72.
(498) Sakamoto, F.; Kinari, Y.; Chen, F. L.; Sakamoto, Y. Hydrogen Permeation through Palladium Alloy Membranes in Mixture Gases of 10% Nitrogen and Ammonia in the Hydrogen. *Int. J. Hydrogen Energy* **1997**, *22* (4), 369−375.
(499) Liu, J.; Ju, X.; Tang, C.; Liu, L.; Li, H.; Chen, P. High Performance Stainless-Steel Supported Pd Membranes with a Finger-like and Gap Structure and Its Application in NH_3 Decomposition Membrane Reactor. *Chem. Eng. J.* **2020**, *388*, 124245.
(500) Li, G.; Kanezashi, M.; Lee, H. R.; Maeda, M.; Yoshioka, T.; Tsuru, T. Preparation of a Novel Bimodal Catalytic Membrane Reactor and Its Application to Ammonia Decomposition for CO_x-Free Hydrogen Production. *Int. J. Hydrogen Energy* **2012**, *37* (17), 12105−12113.
(501) Li, G.; Kanezashi, M.; Tsuru, T. Highly Enhanced Amsmonia Decomposition in a Bimodal Catalytic Membrane Reactor for CO_x-Free Hydrogen Production. *Catal. Commun.* **2011**, *15* (1), 60−63.
(502) Li, G.; Kanezashi, M.; Yoshioka, T.; Tsuru, T. Ammonia Decomposition in Catalytic Membrane Reactors: Simulation and Experimental Studies. *AIChE J.* **2013**, *59* (1), 168−179.
(503) Cheng, H.; Meng, B.; Li, C.; Wang, X.; Meng, X.; Sunarso, J.; Tan, X.; Liu, S. Single-Step Synthesized Dual-Layer Hollow Fiber

Membrane Reactor for on-Site Hydrogen Production through Ammonia Decomposition. *Int. J. Hydrogen Energy* **2020**, *45* (12), 7423−7432.
(504) Zhang, J.; Xu, H.; Li, W. High-Purity CO_x-Free H_2 Generation from NH_3 via the Ultra Permeable and Highly Selective Pd Membranes. *J. Membr. Sci.* **2006**, *277* (1−2), 85−93.
(505) García-García, F. R.; Ma, Y. H.; Rodríguez-Ramos, I.; Guerrero-Ruiz, A. High Purity Hydrogen Production by Low Temperature Catalytic Ammonia Decomposition in a Multifunctional Membrane Reactor. *Catal. Commun.* **2008**, *9* (3), 482−486.
(506) Collins, J. P.; Way, J. D. Catalytic Decomposition of Ammonia in a Membrane Reactor. *J. Membr. Sci.* **1994**, *96* (3), 259−274.
(507) Rizzuto, E.; Palange, P.; Del Prete, Z. Characterization of an Ammonia Decomposition Process by Means of a Multifunctional Catalytic Membrane Reactor. *Int. J. Hydrogen Energy* **2014**, *39* (22), 11403−11410.
(508) Itoh, N.; Kikuchi, Y.; Furusawa, T.; Sato, T. Tube-Wall Catalytic Membrane Reactor for Hydrogen Production by Low-Temperature Ammonia Decomposition. *Int. J. Hydrogen Energy* **2020**, DOI: 10.1016/j.ijhydene.2020.03.162.
(509) Israni, S. H.; Nair, B. K. R.; Harold, M. P. Hydrogen Generation and Purification in a Composite Pd Hollow Fiber Membrane Reactor: Experiments and Modeling. *Catal. Today* **2009**, *139* (4), 299−311.
(510) Prasad, V.; Karim, A. M.; Ulissi, Z.; Zagrobelny, M.; Vlachos, D. G. High Throughput Multiscale Modeling for Design of Experiments, Catalysts, and Reactors: Application to Hydrogen Production from Ammonia. *Chem. Eng. Sci.* **2010**, *65* (1), 240−246.
(511) Di Carlo, A.; Dell'Era, A.; Del Prete, Z. 3D Simulation of Hydrogen Production by Ammonia Decomposition in a Catalytic Membrane Reactor. *Int. J. Hydrogen Energy* **2011**, *36* (18), 11815−11824.
(512) Cechetto, V.; Di Felice, L.; Medrano, J. A.; Makhloufi, C.; Zuniga, J.; Gallucci, F. H_2 Production via Ammonia Decomposition in a Catalytic Membrane Reactor. *Fuel Process. Technol.* **2021**, *216*, 106772.
(513) Shwe Hla, S.; Dolan, M. D. CFD Modelling of a Membrane Reactor for Hydrogen Production from Ammonia. *IOP Conf. Ser.: Mater. Sci. Eng.* **2018**, *297*, 012027.
(514) Divins, N. J.; Angurell, I.; Escudero, C.; Pérez-Dieste, V.; Llorca, J. Influence of the support on surface rearrangements of bimetallic nanoparticles in real catalysts. *Science* **2014**, *346*, 620−623.

https://doi.org/10.1021/acs.iecr.1c00843
Ind. Eng. Chem. Res. 2021, 60, 18560−18611